MEASURING INTRA-PARTICLE DIFFUSION COEFFICIENTS FOR MINE WASTE ROCK FRAGMENTS

RYAN MILLER

Thesis submitted to the University of Ottawa
in partial Fulfillment of the requirements for the Degree of Master of Science

Department of Earth and Environmental Sciences
Faculty of Science
University of Ottawa

Abstract

Sulfide mineral oxidation in mine waste materials is one of the principal contributors to poor quality drainage. The oxidation process is generally limited by the diffusion of O_2 into the pore space of waste piles and rock fragments. In this study, a non-destructive method that couples laboratory measurements and modelling techniques is developed to measure the diffusive properties of common sulfide-mineral-bearing waste rock fragments. X-ray imaging is used to acquire time-series images of iodide tracer diffusion through the oxidized rim and into the unaltered core of the rock fragments. The distribution of diffusion coefficients is determined by fitting results from two-dimensional numerical diffusion simulations to the measured spatial distribution of iodide tracer. In addition, one dimensional experiments were conducted to determine pore diffusion coefficients normal and parallel to waste rock foliation/bedding planes in the oxidized and unaltered domains. The average pore-diffusion coefficient (D_p) values measured parallel to foliation in the unaltered core and normal to foliation in the oxidized rim of quartz-sericite schist are $3.30 \times 10^{-10} \pm 5.00 \times 10^{-11}$ m^2/s and $8.27 \times 10^{-11} \pm 1.46 \times 10^{-11}$ m^2/s, respectively; $2.29 \times 10^{-10} \pm 3.07 \times 10^{-11}$ m^2/s and $1.89 \times 10^{-10} \pm 8.82 \times 10^{-11}$ m^2/s parallel to foliation in the unaltered core and oxidized rim of quartz-biotite schist, respectively; $2.34 \times 10^{-11} \pm 3.70 \times 10^{-12}$ m^2/s and $4.79 \times 10^{-11} \pm 1.89 \times 10^{-11}$ m^2/s in the unaltered core and oxidized rim of felsic meta-volcanic rock, respectively; and $6.75 \times 10^{-11} \pm 5.00 \times 10^{-12}$ m^2/s and $3.82 \times 10^{-11} \pm 3.72 \times 10^{-12}$ m^2/s parallel to foliation in the unaltered core and normal to foliation in the oxidized rim of quartz-muscovite schist, respectively. The D_p values for solutes such as O_2 and SO_4 are calculated using the known relationship between free-water diffusion coefficients for iodide and the solutes of interest. Coupled with inter-particle diffusion coefficient estimates, these data will aid in the development of numerical models that estimate oxidation rates and duration of hazardous leachate drainage from mine waste materials.

Acknowledgements

Tom Al, you lead by example. You inspire others explore, be curious, and pursue the mutual objectives freely through the lens of their passion. Your knowledge, ability to listen and discern, your even keel and ability to communicate difficult concepts with simplicity and clarity allows others to truly understand matters in a meaningful way. You have the perfect combination of patience and a knack of knowing when to keep information "in the holster" and when to share it that creates the perfect environment to learn long-lasting lessons and instill self-motivation, for those who seek it.

A Yellowknife term comes to mind; "you're good man in the bush, but a man at the black knight", the black knight is a bar...

The term means you're pretty reliable, when you can be.

I couldn't imagine a worse expression to describe you. The degree of scientific rigor and genuine compassion for others I know will not be found in anyone else. Your unwavering support is an institution. You are a true blessing to the Faculty and to all those who are graced by you.

Continue to foster research group cohesion. The friendships made and experiences had with the people in our research group made the University feel like a another home. Your leadership in this aspect is critical and must not waver.

Thank you Richard Amos and the rest of the TERRE-NET family for your guidance, support, and cooperation.

Thank you to the U of O staff and Faculty.

Thank you, Brien Cousins, Ian Clarke, Danielle Fortin, and Lorraine Houle for your efforts in my thesis presentation and defense process.

Thank you Ariel Greenblat for inspiring me to defend the thesis after I had been unwilling to finalise this work for over 3 years.

Bless you all.

Table of Contents

List of Figures

List of Tables

1 Introduction

Waste rock piles generated by mining sulfide-rich mineral deposits have a high potential for generating poor quality drainage (Brezina, Campbell, & Whitley, 1970; Ehrlich, 1963; Hodge, 1937). When partially saturated waste containing sulfide minerals is exposed to atmospheric O_2, sulfide minerals may oxidize and produce acid rock drainage (ARD) (Akcil & Koldas, 2006; Elberling & Nicholson, 1996; Evangelou & Zhang, 1995; Nordstrom & Southam, 1997). Drainage of this nature is characterized by elevated concentrations of SO_4, Fe, and other dissolved metals (Al et al., 1997; Pollio and Kunin, 1967; Smuda et al., 2007). Porewater acidification and generation of ARD have widespread negative impacts on ecosystems in receiving waterways (Deniseger and Kwong, 1996; Dyer, 1977; Ellis et al., 1995). Additionally, bioaccumulation and biomagnification may result in the dispersal of contaminants to ecosystems and human food networks at large distances from the source of contamination (Badsha and Sainsbury, 1977; McFarlane and Franzin, 1980).

The most common sulfide mineral phase contributing to ARD generation is pyrite. The solubility of sulfide minerals, including pyrite, increases in the presence of oxidants such as dissolved oxygen (DO) and ferric iron (Fe(III)) (Moses et al., 1987). Equations 1 and 2 illustrate oxidative dissolution reactions for pyrite:

$$FeS_{2(s)} + \frac{7}{2}O_{2(aq)} + H_2O \rightarrow Fe^{2+} + 2SO_4^{2-} + 2H^+ \qquad [1]$$

$$FeS_{2(s)} + 14Fe^{3+} + 8H_2O \rightarrow 15Fe^{2+} + 2SO_4^{2-} + 16H^+ \qquad [2]$$

As pH decreases, the acidity released into waste rock pore-water promotes dissolution of other primary mineral phases, mobilizing sulfur and metal species such as Bi, Co, Fe, As, Cu, Zn, and more. These species diffuse away from the mineral surface into the pore network and diffuse out of waste-rock fragments where they may be transported away from the waste impoundment, creating ARD (Lu et al., 2005).

The rate of sulfide oxidation and subsequent metal dissolution is controlled by the rate of O_2 ingress through the inter- and intra-particle pore spaces of the waste rock pile (Davis et al., 1986; Davis and Ritchie, 1986; Jaynes et al., 1984a, 1984b). The rate at which O_2 and contaminants are transported in or out of rock fragments via the intra-particle pore space, and in or out of the waste-rock pile via the inter-particle pore space, is controlled by the diffusive properties and permeability of the fragments and pile, respectively (Aachib et al, 2004; Lowson, 1982; Mbonimpa et al., 2003). Oxygen abundance and transport within the waste rock pile will vary with each waste-rock environment. Some waste settings may have pyrite rich zones which, due to the exothermic nature of sulfide oxidation, produce heat and create thermally driven gas and O_2 transport within the inter-particle pore-space. Daily and seasonal wetting and freezing effects also influence diffusion and permeability properties of the pore space (Amos et al., 2015; Lefebvre et al., 2001). Additionally, there may be external factors that influence gas transport such as wind direction and speed, and ambient temperature changes (Fig. 1a).

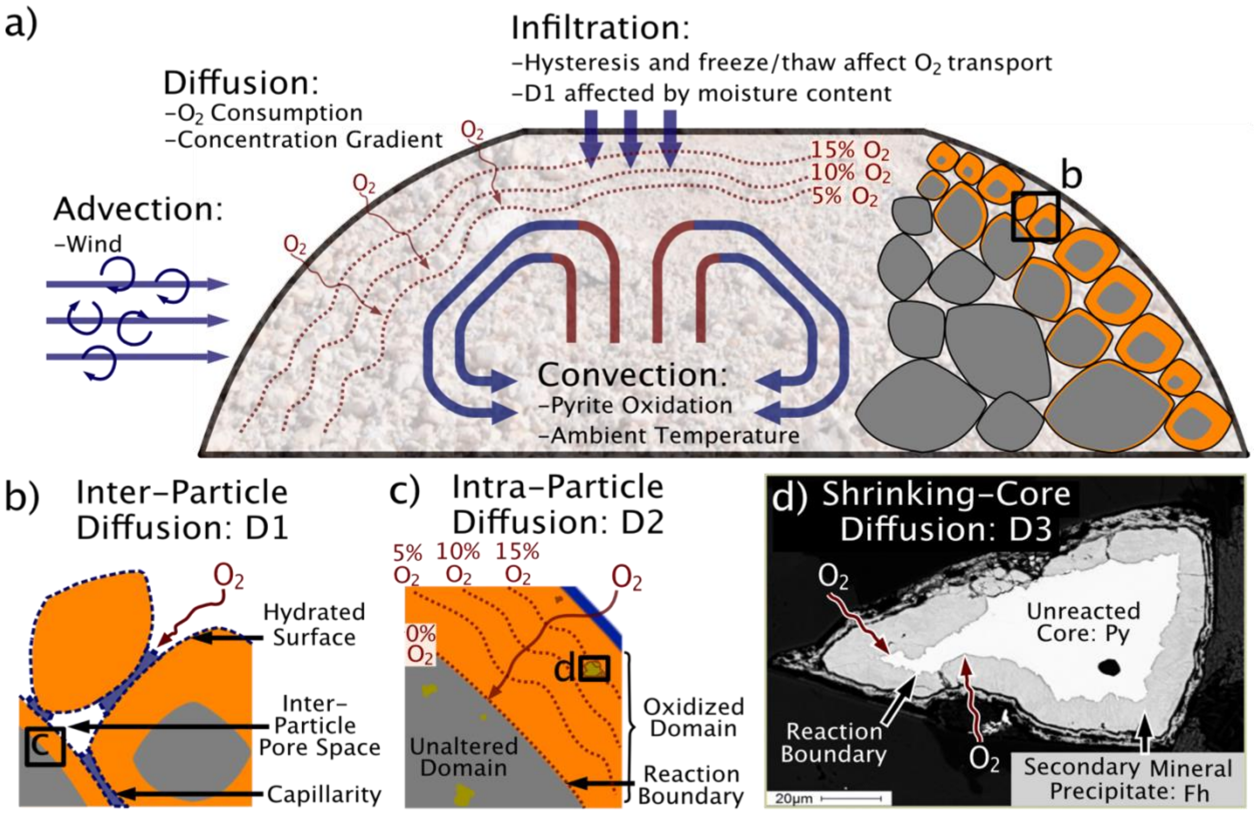

Figure 1. *Processes controlling O_2 transport from the periphery of waste rock piles to sulfide mineral grains.*

Oxygen diffusion in waste rock piles is of practical and scientific interest because it is the dominant control on sulfide oxidation in the waste via the coupled processes of inter-particle diffusion – this diffusion coefficient is here referred to as D1 - and intra-particle diffusion, referred to as D2. A third diffusion coefficient, D3, may be defined to represent O_2 transport through the secondary-mineral reaction coatings that commonly form around sulfide minerals (Fig. 1d), growing thicker with time (Davis and Ritchie, 1987; Jaynes et al., 1984a, 1984b; Nicholson et al., 1989). The inter- and intra-particle conceptualization and corresponding D1, D2, and by extension D3, terminology used here are similar to those described by Davis and Ritchie (1986a,b) for a shrinking-core model of sulfide oxidation. Single- and dual-porosity models are commonly used to describe gas transport in waste rock systems (Blackmore et al., 2018; Šimůnek et al., 2003; van Genuchten and Wierenga, 1976). Sophisticated numerical models have been developed to simulate the diffusion and reaction processes leading to ARD (Cheng and Yeh, 1998; Mayer, 1999; Parkhurst, 1995; Steefel and Lasaga, 1994; Xu et al., 2004), but current modelling efforts rely on estimates for diffusion coefficients that are developed by fitting model-generated O_2 concentrations to measured O_2 pore-gas concentrations (Aachib et al., 2004; Davis and Ritchie, 1986, 1987; Fala et al., 2006; Lefebvre et al., 2001; Puura and Neretnieks, 2000). Efforts to develop and apply these models for quantifying sulfide oxidation in waste rock will benefit from experimental measurements that constrain the range of values for these diffusion parameters (Drake and Le Bosquet, 1931; Harries and Ritchie, 1985; Hulshof and Macdonald, 1998; Miller et al., 1990).

Numerous investigations have been conducted to obtain estimates of diffusion rates in waste rock and other unconsolidated geologic material such as pyritic tailings (D1) (Elberling et al., 1994; Elberling et al., 2000; Gerke and van Genuchten, 1993; Harries and Ritchie, 1985; Lefebvre et al., 2001; Mbonimpa et al., 2003; Nicholson et al., 1989; Yanful, 1993) and on determining the diffusion coefficient of specific rock types (D2) (J. A. Nunn et al., 2018; Palut et al., 2003; Savoye et al., 2011; Van Loon et al., 2004; Wersin et al., 2004). However, few investigations have sought the quantification of diffusion coefficients within potentially acid generating (PAG) rocks (Biglari et al., 2008; Nicholson et al., 1989; Wunderly et al., 1996) and currently no analytical or numerical modeling data exists on intact PAG waste rock particles.

Many laboratory scale techniques have been successful in measuring the diffusive properties of intact rock fragments. Successful techniques include radial diffusion (Lakshminarasimha and Lucas, 1977; Van Der Kamp et al., 1996), in- diffusion (Cormenzana et al., 2003), out-diffusion (Appelo et al., 2008; Sardini et al., 2003); through diffusion (Tits et al., 2003; Van Loon et al., 2005; Van Loon et al., 2003) and the radiography methods used in this study (Cavé et al., 2009; Loomer et al., 2013; Tidwell et al., 2000; Xiang et al., 2013). Generally, these methods aim to measure diffusion coefficients, but the nomenclature in the literature is not consistent. Here we relate the terminology that is commonly used by researchers engaged in studying diffusion properties of porous geologic media to the D2 parameter used in the present work.

1. The pore diffusion coefficient (D_p) is defined as:
   $D_p = D_0 \cdot \tau_f$, where D_0 is the free-water diffusion coefficient and τ_f is the tortuosity factor ($0 < \tau_f \leq 1$) [3]
2. The effective diffusion coefficient (D_e), is defined as:
   $D_e = D_p \cdot \phi_w$, where ϕ_w is the water-accessible porosity of the rock fragment. [4]

The use of ϕ_w is relevant here because the porosity of rock fragments is expected to remain water saturated due to capillarity, even when larger inter-particle pore spaces drain.

The objectives of this research are to: 1) estimate diffusion coefficients (D2) in common acid-generating waste-rock lithologies, and 2) develop a method to define the spatial variability of diffusion coefficients (D2) in two-dimensions for anisotropic and heterogeneous geologic material.

2 Materials and methods

One-dimensional (1-D) diffusion experiments were conducted using 18 sample cores from waste rock obtained from volcanogenic massive sulfide (VMS) deposits, including felsic meta-volcanic, quartz-biotite schist, quartz-muscovite schist and quartz-sericite schist (Table 1). The samples were obtained from the LaRonde Mine in Québec and the Restigouche Mine in New Brunswick, Canada (Fig. 2).

Table 1 *A summary of the physical and mineralogical components of each rock sample used in 1-D diffusion experiments.*

Component	Quartz-sericite schist[1]	Quartz-biotite schist[2]	Meta-volcanic rock[2]	Quartz-muscovite schist[2]	Meta-sedimentary rock[3]
Unaltered Domain	quartz 35% sericite 30% pyrite 15% arsenopyrite 10% titanium oxide 5%	quartz 35% biotite 35% pyrite 15% eztlite anglesite	quartz 40% biotite 20% muscovite 10% pyrite 10% arsenopyrite 10% galena 5%	quartz 35% muscovite 30% pyrite 10% dolomite 5% arsenopyrite 5% titanium oxide 5%	quartz 30% dolomite 20% muscovite 10% albite 10% pyrite 10% apatite 5% titanium oxide 5%
Oxidized Domain		quartz 40% biotite 40% iron oxide 10% arsenich-iron oxide 5% walentaite epidote pb monzanite	quartz 45% biotite 15% iron oxide 15% muscovite 5% arsenic-iron oxide 5% xenotime monzanite	quartz 40% muscovite 35% iron oxide 15% anatase 5% barite ilsemannite	quartz 35% ferrihydrite 20% muscovite 16% albite 14% apatite 8% titanium oxide 7%
Horizontal Foliation Angle[4]	LR11a: 75-115 LR11b: 80-115 LR13: $x \leq 30$ and $x \geq 170$ LR14: $x \leq 15$ and $x \geq 165$	RM31: 110-165 RM33: 85-130 RM32a: 100-115 RM33a: 80-90	RM41: N/A RM42: N/A RM432: N/A RM41a: N/A RM44a: N/A	RM91: 70-120 RM91a: 70-100 RM94a: $x \leq 10$ and $x \geq 165$	N/A
Vertical Foliation Angle[5]	LR11a: 100-120 LR11b: 125-145 LR13: N/A LR14: N/A	RM31: 20-60 RM33: 20-40 RM32a: 70-110 RM33a: 120-150	RM41: N/A RM42: N/A RM432: N/A RM41a: N/A RM44a: N/A	RM91: 140-170 RM91a: $160 \leq x \geq 10$ RM94a: N/A	N/A
Weathering[6]	LR11a: 0:15, no oxidation LR11b: 0:12, slight oxidation shown by yellowing in foliation planes LR13: 0:15, slight oxidation shown by yellowing in foliation planes LR14: 0:15, no oxidation	RM31: 10:14, weathering gradient RM33: 12:14, weathering gradient RM32a: 0:14, no oxidation RM33a: 0:15, no oxidation	RM41: 15:15, weathering gradient RM42: 13:15, weathering gradient RM432: 13:15, weathering gradient RM41a: 0:14: no oxidation RM44a: 0:15, no oxidation	RM91: 0:13, strong oxidation oxidation at base, very little oxidation in foliation planes RM91a: 0:16, slight oxidation in minerals and foliation planes RM94a: 0:20, very little oxidation in minerals and foliation planes	N/A

[1]Sample collected at LaRonde mine.
[2]Sample Collected at Restigouche mine.
[3]Sample Collected from a road-side rock cut near Meductic, New Brunswick.
[4]Foliation angle parallel with diffusion direction. 90 degrees aligns with the detector, ranging from 0 to 180 increasing CCW.
[5]Foliation angle perpendicular to diffusion direction. Angle increases CCW to a maximum of 180 degrees.
[6]Ratio comparing mm of visually oxidized core to total core height.

2.1 Sample descriptions

The Au-rich VMS deposits in the Doyon-Bousquet-Laronde gold district of Abitibi-Témisquémingue are located approximately 45 km east of Rouyn-Noranda in the Abitibi greenstone belt, within the Superior province of the Canadian Shield (Mercier-Langevin et al., 2007). The LaRonde Penna deposit consists of four stacked massive sulfide lenses within the upper member of the Bousquet Formation (2698–2697 Ma) of the Blake River Group (Dubé et al., 2007; Mercier-Langevin et al., 2007). This member consists of basaltic to rhyolitic flows, domes, synvolcanic intrusions, volcaniclastic strata, and dacitic-rhyodacitic rock. Core samples extracted from these waste rock fragments (quartz-sericite schist) were drilled approximately normal and parallel to the foliation plane (Table 1).

The Restigouche deposit is a VMS deposit hosted by the Mount Brittain Formation located in the northern region of the Miramachi highlands and the western section of the Bathurst mining camp (Bein et al., 2006; Lentz et al., 1996; Whalen et al., 2004). The Mount Brittain Formation of the California Lake Group is a felsic volcanic succession composed dominantly of feldspar-quartz porphyritic dacitic to rhyolitic volcanic rocks (Bein et al., 2006; Gower and McCutcheon, 1997;

Sullivan and van Staal, 1990). Samples (quartz-biotite schist, quartz-muscovite schist and felsic meta-volcanic rocks) were drilled approximately normal and parallel to the dominant foliation plane in both oxidized and unaltered domains of the waste rock fragments.

Waste rock produced at the LaRonde and Restigouche VMS deposits typically contains elevated concentrations of metals such as Fe, Cu, Pb, Zn, Ni and Cd. Waste rock piles from these deposit types are potentially acid-generating which can lead to the mobilization of these metals in ARD.

The rock sample used for two-dimensional (2-D) analysis is a pyrite-bearing meta-sedimentary rock from the Baskahegan Lake Formation (Lutes et al., 2005) that was sampled from a rock cut along the Trans-Canada Highway near Meductic, New Brunswick, Canada (Fig. 2). The mineral phases appearing in the unaltered core are quartz, sheet silicates (muscovite), plagioclase, dolomite, and pyrite.

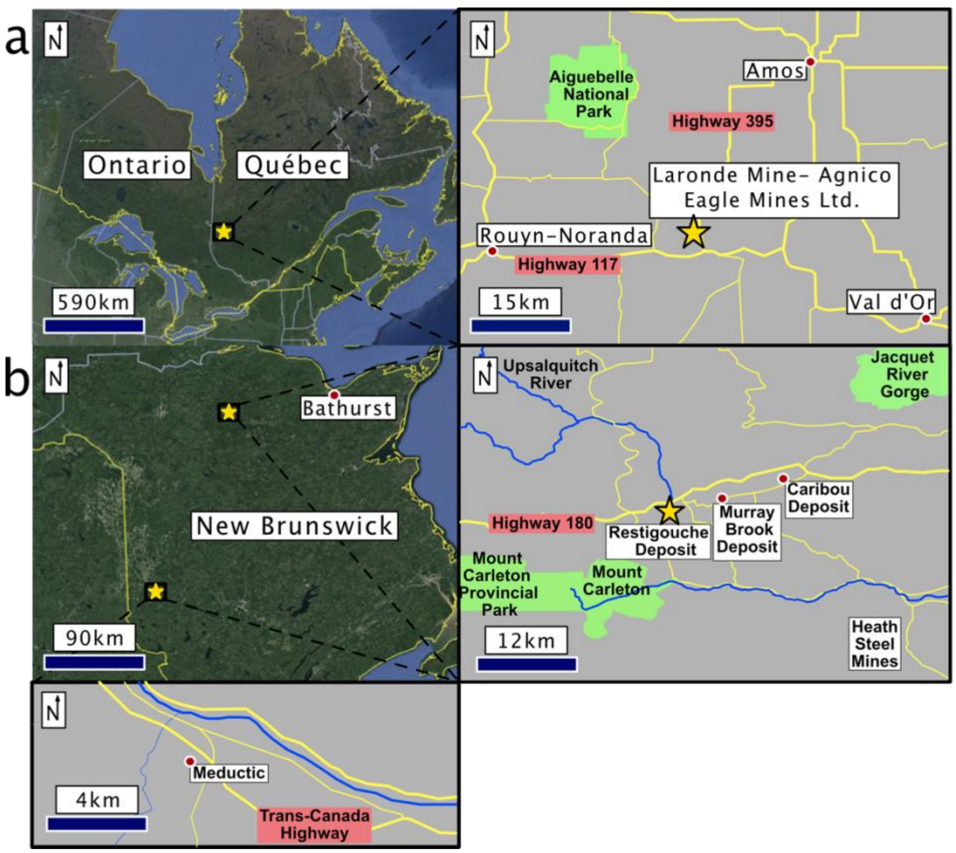

Figure 2. *Location maps for a) the LaRonde mine, b) the Restigouche mine and Meductic, NB.*

2.2 Measurement of tracer concentrations and porosity

2.2.1 Sample preparation

Samples prepared for 1-D analysis were drilled with a diamond coring bit 20 mm in internal-diameter, using water to cool the bit. Drilled cores range from 11 to 20 mm in length. Samples prepared for 2-D analysis were prepared using a water-cooled diamond saw by cutting a cross-sectional slab with a 15 mm thickness.

A 0.5 M $NaNO_3$ synthetic pore-water (SPW) was used to saturate the rock samples using the method described by Cavé et al. (2009) and Xiang et al. (2013), and a 0.5 M NaI solution was used as a tracer (T-SPW). Iodide is geochemically conservative and has strong X-ray attenuation properties that provide imaging contrast in most geologic media (Agbogun, Al, & Hussein, 2013; Cavé et al., 2009; Nakashima, 2000; Subudhi, Hussein, & Al, 2010; Tidwell et al., 2000).

2.2.2 Electron microscopy analysis

Polished thin sections for electron-microscopy observations were prepared at the University of Ottawa. The thin-sections were carbon coated under vacuum and investigations of mineralogy and porosity were conducted at the University of Ottawa using a JEOL 6610LV scanning electron microscope (SEM) equipped with a large-area silicon-drift detector (Oxford INCA) which allowed for qualitative energy-dispersive X-ray spectrometry (EDS) analysis.

2.2.3 Diffusion cell for 1-D measurements

The diffusion cell in Figure 3 is modified based on the designs found in Cavé et al. (2009) and Xiang et al. (2013). Felt pads 19 mm in diameter were placed in contact with the top and bottom surfaces of the sample, and an aluminum standard was placed on top of the sample. The peripheral surface of the sample was sealed using a thin layer of 100% silicone sealant and heat-shrink tubing. The sample was then mounted on the diffusion cell using a thin bead of West System epoxy (105 resin and 205 fast hardener). A heat-shrink clamp was placed around the sample to ensure a tight seal around the peripheral surface of the sample, eliminating the threat of preferential diffusive pathways forming. Finally, a lead ball (2 mm diameter) was fixed to the aluminum standard and used as a fiducial marker for image registration.

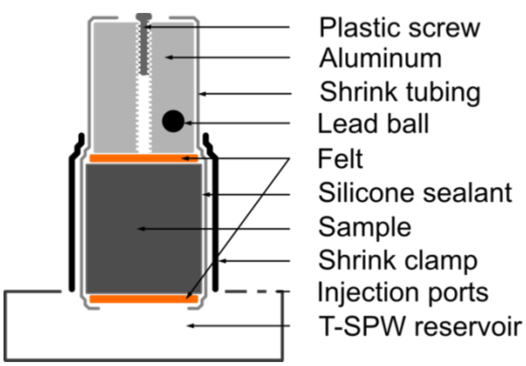

Figure 3. *One-dimensional diffusion cell showing rock core placement for radiography.*

2.2.4 Diffusion cell for 2-D measurements

A novel diffusion cell (Fig. 4) was designed to allow diffusive influx of the iodide tracer only around the peripheral-surface of a rock slab while diffusion was monitored using radiographic imaging. The 15 mm thick slab was cut from the center of a weathered sulfide-rich rock fragment, exposing a cross section of the oxidized rim and unaltered core. A thin coat of epoxy (West System 105) was applied on both exposed cross sectional faces. The sample was then saturated with SPW using the method described by Cavé et al. (2009). The sample was sandwiched between two acrylic plates, and the plates were sealed against the epoxy-coated faces of the sample with closed-pore silicone seals. A thin layer of silicone sealant was applied to both surfaces of the seals. The reservoir was then filled with the T-SPW and a triplicate series of reference images (REF) were collected.

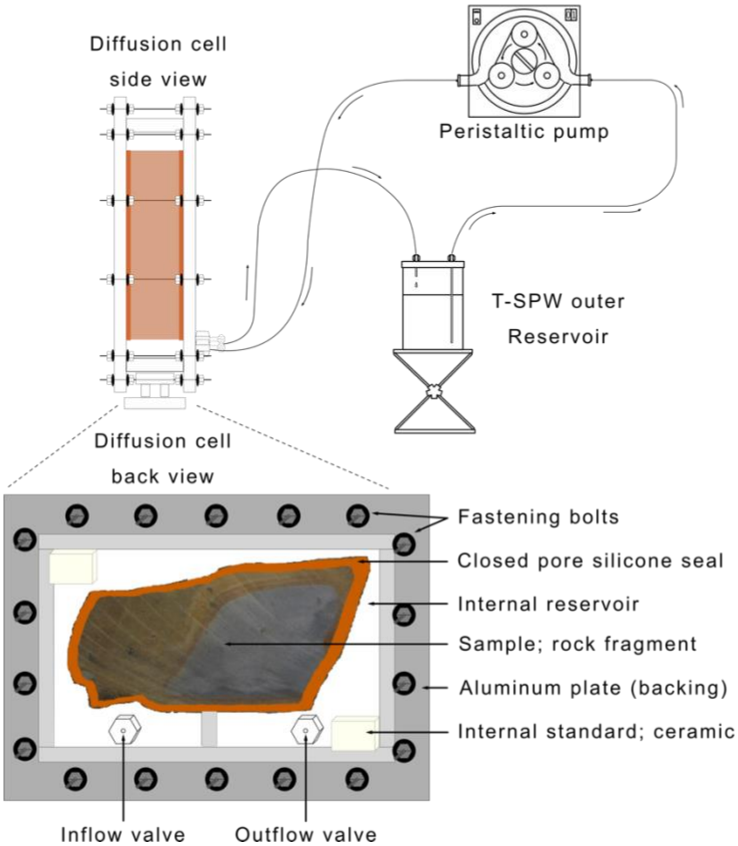

Figure 4. *2-D diffusion cell and pump system showing the rock sample cut to expose a cross section of the oxidized rim and unaltered core.*

2.2.5 X-ray Imaging

Solute diffusion was tracked using X-ray radiography as described by Cavé et al. (2009) based on the spatial and temporal changes in attenuation ($\Delta\mu$) due to the presence of aqueous iodide tracer. The $\Delta\mu$ measurements allow for the estimation of iodide-accessible porosity (ϕ_I) and D_p.

Radiographic imaging was conducted on an X-ray CT system (Pinnacle X-ray Systems, Atlanta, Georgia) equipped with a Varian® NDI-160/22 source, a Gulmay® CPL series (CP2-1402) 3000W generator and an amorphous-silicon flat-panel detector (Varian PaxScan® 1313DX). All images were acquired in 16-bit TIFF or 32-bit DICOM format.

Routine preparations included an instrument warm up time of 8 minutes, followed by flat-field and gain corrections (calibration) using the parameters found in Table 2. The source-object (SO) and object-detector (OD) distances used in 2D experiments were 869.99 mm and 116.01mm respectively, corresponding to an image magnification of 1.13 (Equation 5):

$$Mag. = \frac{SO+OD}{SO} \quad [5]$$

All experiments were initiated (t = 0) by replacing the SPW in the reservoir with T-SPW and immediately collecting three replicate 16-bit REF images which were averaged to obtain a single 32-bit REF image. In 1-D experiments, subsequent radiographs were acquired in time-series at approximately 4, 10, 24, 35 and 48 hours, and then daily until tracer breakthrough was observed at the top of the sample. Tracer was then introduced to the reservoirs at both the top and bottom of the samples to achieve complete iodide saturation faster, whereupon final tracer-saturated images were acquired. In 2-D experiments, reference and time-series radiographs were acquired at intervals similar to the 1-D experiment. The T-SPW was refreshed after each radiograph using a peristaltic pump in order to maintain a constant tracer concentration at the influx boundary. The 2-D experiments were terminated when there was no observable change in Δμ values in the oxidized rim region of the sample between weekly radiographs.

Table 2 *Calibration and radiograph acquisition parameters for 1-D and 2-D diffusion experiments.*

	Frame Averaging	Frame Rate (1/fps)	keV	mA	Source Filtration (mm)	Source to Object (cm)	Object to Detector (cm)
Calibration	32	15	50	10	3.3, Aluminum	350.00	900.00
One-dimensional	32	1	50	30	3.3, Aluminum	869.99	116.01
Two-dimensional	32	1	50	25	3.3, Aluminum	300	811.11

2.2.6 Radiograph data processing

Data from the 1-D diffusion experiments are processed according to the methods described by Cavé et al. (2009) to determine D_p values. 2-D image processing involved the following sequence of operations.

1. All time-series images and the final tracer-saturated image were manually registered to the REF image.
2. The radiographs were converted to 32-bit float format and GSVs were ln-transformed.
3. Drift in pixel intensities, due to slight fluctuations in X-ray source intensity over time and other factors were corrected using an internal standard included in each image (Fig. 4). The correction, or normalization factor (NF), was determined (Equation 6) from the average GSVs from a region of interest within the internal standard in the REF image ($ROI_{IS\text{-}REF}$) and the image requiring normalization – either a time-series image (ts) or the final tracer-saturated image (sat) ($ROI_{IS\text{-}ts/sat}$):

$$NF = \frac{\ln(ROI_{IS})_{REF}}{\ln(ROI_{IS})_{\frac{ts}{sat}}} \quad [6]$$

4. The GSVs for the time-series and the final saturated images were subtracted from corresponding GSVs in the REF image to obtain a $\Delta\mu_{x,y}$ image:

$$\ln\,(GSV_{x,y})_{REF} - \ln\,(GSV_{x,y})_{\frac{ts}{sat}} = (\Delta\mu_{\,x,y})_{\frac{ts}{sat}} \quad [7]$$

5. The time-series $\Delta\mu_{x,y}$ images were normalized to the tracer-saturated $\Delta\mu_{x,y}$ image to obtain relative concentration images reflecting spatially resolved, $C/C_{0x,y}$, values:

$$\left(\frac{C}{C_{0_{x,y}}}\right)_{ts} = \frac{(\Delta\mu_{\ x,y})_{ts}}{(\Delta\mu_{\ x,y})_{sat}} \qquad [8]$$

Any negative values, or those equal to ∞ or –∞, were replaced by a zero value.

6. The relative concentration images were cropped from 1024 × 1024 pixels to 966 × 966 pixels to remove borders of the diffusion cell. The image resolution was then binned to 161 × 161 using an arithmetic average interpolation method, with each pixel representing an area 715 × 715 µm.

2.2.7 Porosity measurements

The ϕ_w measurements were conducted on rock fragments weighing > 15 g using the gravimetric approach described by Xiang et al. (2013). Spatially resolved iodide-accessible porosity (ϕ_I) measurements were conducted in 1-D using the radiography technique described by Cavé et al. (2009). The same method was adapted for 2-D measurements (Equation 9):

$$\phi_{I_x} = \frac{(\Delta\mu_x)_{sat}}{(\Delta\mu_{avg})_{C_0}} \qquad [9]$$

where, $(\Delta\mu_{avg})_{C0}$ is the X-ray attenuation along a path length equal to the sample thickness, from an aqueous solution with a tracer concentration equal to C_0 – effectively a sample with 100% porosity. Measurements of $(\Delta\mu_{avg})_{C0}$ were made by replacing the rock-sample in the 2-D diffusion cell with tracer solution.

2.2.8 Detection limits

The $\Delta\mu_{x,y}$ values calculated from multiple images acquired with identical acquisition parameters should be zero. In practice, this approach yields non-zero values due to fluctuations in the X-ray source intensity, electronic noise in the detector, and random variations in X-ray attenuation mechanisms (Kaganer and Ostrovskii, 1991; Parker et al., 1982; Reed, 2001). In this study, triplicate $(\Delta\mu_{x,y})_{sat}$ measurements were used to estimate the detection limits for Δµ which can in turn be used to determine detection limits for $\phi_{Ix,y}$ and $C/C_{0x,y}$ measurements according to Equations 8 and 9 (Agbogun et al., 2013). The detection limit for Δµ was defined as the mean + 3σ ($\Delta\mu_{x,y}$ ẍ +3σ) and values less than this threshold were assigned a value of zero.

2.3 Estimating D_p

2.3.1 One-dimensional experiments

The 1-D diffusion experiments provide a single estimate of D_p for each sample. The value is obtained using a sum of squared weighted residuals approach to fit an analytical solution (Equation 10) to the measured 1-D profiles of C/C_0 values (Cavé et al., 2009; Xiang et al., 2013):

$$C_i(x,t) = C_0 erfc \frac{x}{2\sqrt{D_p t}} \qquad [10]$$

where, C_i is the tracer concentration at distance x from the influx boundary at time t; erfc is the complementary error function. The initial and boundary conditions of the analytical solution are as follows (Crank, 1975; Shackelford, 1991):

$$C_{(x,t)} = 0 \quad t = 0 \; x > 0$$

$$C_{(x,t)} = C_0 \quad t \geq 0 \; x = 0 \qquad [11]$$

$$C_{(x,t)} = 0 \quad t \geq 0 \; x = L$$

where, L is the sample length.

2.3.2 Two-dimensional experiments

To estimate the 2-D spatial distribution of D_p values, the multi-component reactive transport code MIN3P (ver. THCm_x64d_seq) was operated in conjunction with the parameter estimation code, PEST v16.0 (Doherty, 2018a, 2018b). A 2-D numerical grid was developed in MIN3P where the number and size of each voxel in the x and y dimensions correspond to the 161×161 area of pixels in the radiographs. MIN3P calculated the time-dependent tracer-concentrations at each voxel based on diffusive transport-rates according to Fick's second law:

$$\frac{\partial C}{\partial t} = \nabla \left(D_{p_{x,y}} \cdot \nabla \cdot \mathrm{C} \right) \qquad [12]$$

In the parameter estimation exercise, the PEST code adjusted the D_p values for each voxel iteratively until the simulated C/C_0 values match the measured values as closely as possible. Five ROIs were selected and oriented to have their long-dimension parallel to the direction of diffusion (Fig. 5). The difference between the laboratory measurements of $C/C_{0x,z}$ (observations) and simulated tracer concentrations of $C/C_{0x,z}$ in the ROIs was used to control model iterations toward convergence. It was necessary to work with these subsets of the measured $C/C_{0x,z}$ dataset because the PEST code is limited to 9,150 observations.

The simulated and measured distributions of C/C_0 were compared after total diffusion times of 22, 120, and 333 hours. The PEST code takes control of the MIN3P execution, calculating the sum of squared weighted residuals after each simulation to test for convergence, adjusts D_p accordingly, and continues this sequence until convergence is achieved. In practice, D_p is not an input parameter for MIN3P, so it cannot be adjusted directly. Instead, D_0 and τ_f are required input parameters and their product is equal to D_p (Equation 3). For aqueous iodide, a value for D_0 = 1.88×10^{-9} m^2s^{-1} was used in all model simulations (Hawlicka et al., 1990; Merchant et al., 1977; Mohammad et al., 2015; Ussing, 1949; Wang and Kennedy, 1950). D_0 is independent of the porous media properties, and voxel values for τ_f were adjusted iteratively by the PEST code to obtain convergence between the measured and modelled tracer concentrations, thereby controlling the spatial variability of D_p.

The simulations were conducted under fully saturated conditions. The voxel properties, hydraulic conductivity (K) and ϕ_I, and initial conditions for hydraulic head (H), τ_f and C were assigned in three zones within the model domain: the fluid reservoir, the oxidized rim and the unaltered core of the rock fragment (Table 3; Fig. 5). Very low K values (1.0×10^{-12} m/s) were assigned to all voxels in the model rock sample to ensure solute transport was dominated by diffusion, and a very high K value (0.1 m/s) was assigned to all voxels in the fluid reservoir to allow free circulation of the model tracer solution. To include the boundary conditions in model space, an additional column and row of nodes was added to the top, bottom and on either side of the 161x161 grid representing the diffusion cell reservoir and waste-rock fragment. This addition resulted in two columns and two rows of half cells between the sample and the domain boundary. The final model grid used to estimate diffusion rates was 162 x 162 cells. In these additional rows and columns, constant-head (H = 2 m) and constant-concentration (C_0 = 0.5 M) conditions were assigned at the fluid inflow boundaries, and the fluid outflow boundary was assigned a constant-head (H = 1 m) condition and a free-exit condition (Frind, 1988). All other cells along the perimeter of the grid were assigned a type-I boundary condition (q=0) to represent the impermeable reservoir.

To reduce the severity of conversion impacts on simulation output data in 2-D model grid space, two modifications were made on the geometric representation of the waste rock fragment. Cells along the slanted peripheral edge of the sample with ϕ_I measurements below 7% were re-assigned as fluid reservoir cells (K value of 0.1 m/s). Heterogeneous regions in the z dimension containing both large highly attenuating minerals, in addition to the fine porous matrix of the host rock were assigned a porosity value between that of their pure components.

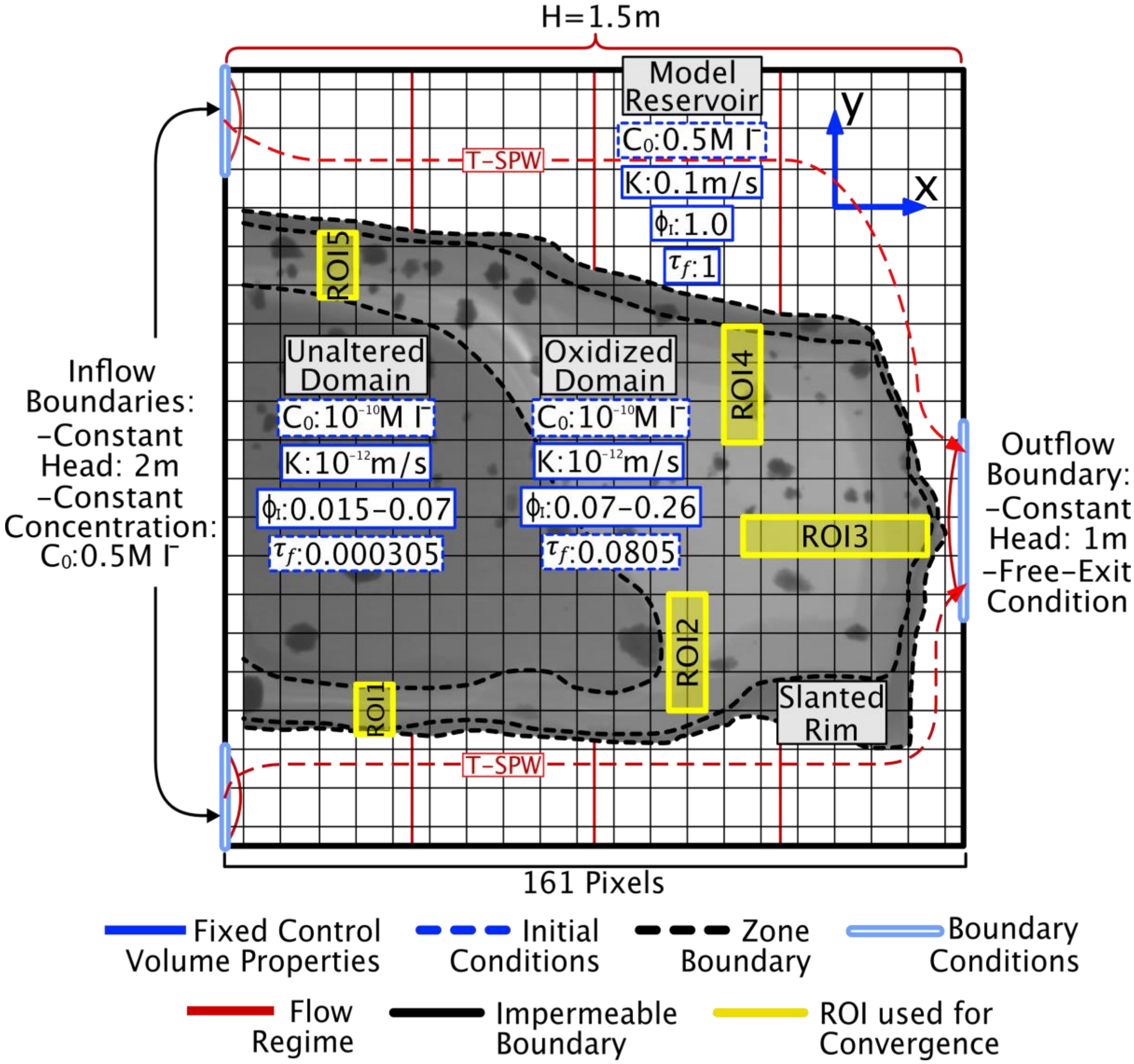

Figure 5. *Diagram of MIN3P model domain showing the three zones, initial and boundary conditions, voxel properties (blue), flow regime (red), and ROIs used to test for convergence (yellow).*

Table 3 *Initial model parameters.*

Domain	K (m/s)	C_0 (M)	τ_f (-)	ϕ_I (-)
Reservoir	1.0E10-1	5.0E10-1	1.0	1.0
Oxidized rim	1.0E10-12	1.0E10-10	8.05E10-2	0.07-0.26
Unaltered core	1.0E10-12	1.0E10-10	3.05E10-3	0.015-0.069

3 Results and discussion

3.1 Porosity

The gravimetric method for measuring ϕ_w (Emerson, 1990; Xiang et al., 2013) provides a single value, representing the whole sample. To complement this measurement, radiography was used to determine a sample-average ϕ_I value (Table 4; Fig. 6) obtained from spatially-resolved $\phi_{I\,(x)}$ profiles following the method of Cavé et al., (2009). The influence of weathering and mineralogical heterogeneity on porosity are investigated using SEM-BSEI imaging (Figs. 7-11). One-dimensional ϕ_I profiles from the meta-volcanic and quartz-sericite schist samples are presented in Figure 12 to demonstrate the sub-mm-scale changes in $\phi_{I\,(x)}$ caused by mineral heterogeneity and changes in physical properties along the length of the core. These 1-D profiles are complemented by 2-D $\Delta\mu_{(x,y)}$ distributions (Figs. 13, 14) from the same samples, in addition to cores from the quartz-biotite schist and the quartz-muscovite schist, to illustrate these features and assess their influence on tracer migration over time and on the final, saturated tracer distributions.

For all samples used in 1-D and 2-D diffusion experiments, the measured ϕ_w values for each sample compare well to their respective $\phi_{I(avg)}$ values, with the exception of the quartz-sericite schist from the LaRonde mine (Table 4; Fig. 6). Low ϕ_I values in sericite-containing cores may be caused by anion exclusion. In clay-mineral-rich rocks, narrow pore throats and overlapping diffuse double layers (DDLs) may prevent anionic solutes from accessing interlayer pore space between clay minerals (Celejewski et al., 2018; Gvirtzman and Gorelick, 1991). Employing the same measurement methods used in this study, Xiang et al., (2013) showed that ϕ_w values are generally larger than ϕ_I in illite-rich shale by a factor between one and two. If we assume that the quartz-sericite schist ϕ_I values are affected by anion exclusion and then adjust them by a factor of 2, the adjusted values are centered around the 1:1 line representing equivalence between ϕ_w and ϕ_I (Fig. 6).

Measurements of ϕ_w and ϕ_I from the oxidized domain of waste rock fragments were greater than their unaltered counterparts when carbonates were present in mineral assemblages. This is observed in the meta-sedimentary rock, which contains approximately 20% dolomite (Table 4). The inverse trend is observed when carbonates are not present or are present in low quantity. Measurements of ϕ_w and ϕ_I in the unaltered cores of felsic meta-volcanic rock and quartz-biotite schist, which do not contain carbonate minerals, were greater than values measured in the oxidized cores from their respective waste rock fragments. This was also observed in measurements of ϕ_w and ϕ_I in the unaltered cores of a quartz-muscovite schist, comprised of approximately 5% dolomite.

Table 4 *Porosity measurements for rock samples used in 1-D diffusion experiments.*

Domain	Quartz-sericite schist[1]				Quartz-biotite schist[2]			Meta-volcanic rock[2]			Quartz-muscovite schist[2]			Meta-sedimentary rock[3]		
	Sample ID	f_w	f_I	ϕ_I[4]	Sample ID	f_w	f_I	Sample ID	f_w	f_I	Sample ID	f_w	f_I	Sample ID	f_w	f_I
Oxidized					RM31		0.06	RM41		0.07						
					RM33	0.06	0.08	RM42	0.06	0.08	RM91	0.06	0.06	STB	0.18	0.20
								RM432		0.05						
Unaltered	LR11a		0.09	0.18												
	LR11b	0.24	0.11	0.22	RM32a	0.09	0.09	RM41a	0.08	0.08	RM91a	0.04	0.03	STB	0.01	0.01
	LR13		0.12	0.24	RM33a		0.09	RM42a		0.09	RM94a		0.04			
	LR14		0.15	0.3				RM44a		0.1	RM94b		0.04			

[1]Samples collected at LaRonde mine.
[2]Samples collected at Restigouche mine.
[3]Samples collected from rock-cut near Meductic, NB.
[4]Values adjusted to account for anion exclusion.

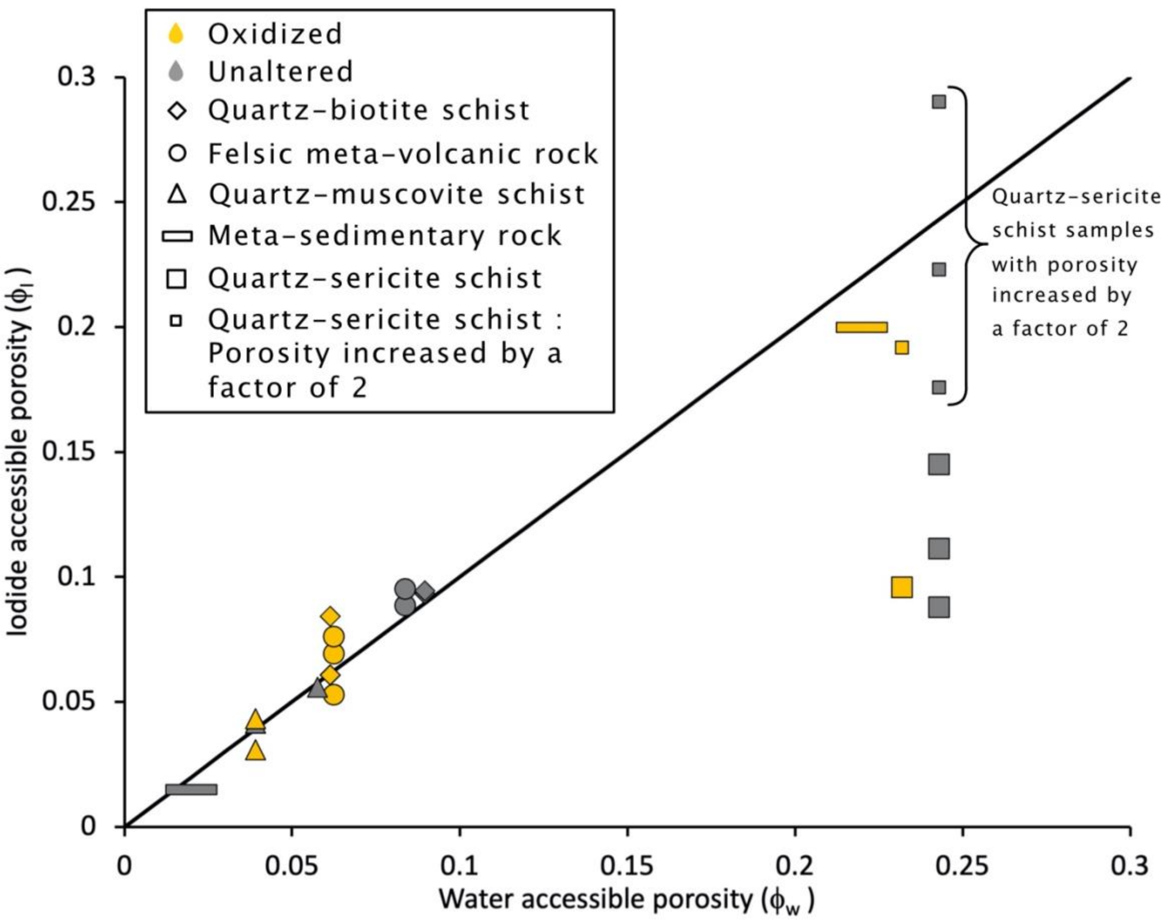

Figure 6. *Comparison of ϕ_I to ϕ_w from rocks used in 1-D and 2-D experiments. There is good agreement between methods with the exception of the quartz-sericite schist from the LaRonde mine. The comparison is improved by adjustment of the ϕ_I values in the quartz-sericite schist by a factor of 2 to correct for anion exclusion.*

Measurements of ϕ_w in the unaltered and oxidized zones of the weathered meta-sedimentary rock are 0.69% and 18.44%, respectively. The 2-D spatially resolved ϕ_I measurements obtained from radiography (Fig. 7a) compare well to the ϕ_w values. A comparison of the porosity-distribution image in Figure 7a to a photo of the rock surface in Figure 7b demonstrates that the weathered zone corresponds to the zone of elevated porosity. The maximum ϕ_I measured in the unaltered core is 2%, with an average of 20% (min 11% and max 30%) measured in the oxidized rim. Measurements of ϕ_I decrease to values less than 11% in heterogenous regions where high-density pyrite grains remain in the oxidized matrix.

The apparent, low ϕ_I values around the perimeter of the rock (Figure 7a) are an artifact of sample morphology. The outer edges of the rock slab are not normal to the image plane at all locations, resulting in localized decreases in the sample thickness parallel to the X-ray path. With reference to equation 9, a local decrease in sample thickness causes incorrect, low values for $(\Delta\mu_{x,y})_{sat}$ which, when compared to a constant value for $(\Delta\mu_{avg})_{C0}$, leads to incorrect, low values for $\phi_{Ix,y}$.

The nature of porosity in different rock samples is revealed by SEM investigations (Figs. 7 to 10). Back-scattered electron images (BSEI) from both the unaltered and oxidized domains within the same waste rock fragment suggest that oxidation reactions of primary sulfide minerals are followed by changes in porosity and pore volume distribution. Oxidation of samples that do not contain carbonate minerals may cause a decrease in pH which can lead to a local increase in porosity due to the dissolution of sulfide and aluminosilicate minerals (Figs. 8, 9), followed by transport of soluble Fe, Al and SO_4 from the system. Oxidation of samples composed of silicates, sulfides and carbonate minerals leads to a local increase in pore volume due to the dissolution of sulfide and carbonate minerals (Figs. 7, 10). In cases where the pH is buffered to near-neutral conditions, secondary ferric oxy-hydroxide minerals can precipitate as pseudomorphs after the primary sulfide minerals (Fig. 8), or they may precipitate in other pore spaces along the transport path. For example, Figures 7g illustrates ferric oxy-hydroxide precipitates in voids created by carbonate-mineral dissolution, and Figure 10f shows the infilling of pore channels by ferric oxy-hydroxides. The dominant source of ferric iron is likely to be oxidation of ferrous sulfide minerals. Such occlusion of pore channels may cause a decrease in the water- and tracer-accessible porosity that is consistent with the observed reduction of ϕ_w and ϕ_I in some of the altered samples. The reduction might also be explained by transformation of sheet silicates and feldspars to clay minerals. Sheet silicates such as muscovite and biotite are sensitive to changes in pH, and they weather to form iron and aluminum oxy-hydroxides and clay minerals (Taboada and García, 1999). Biotite weathering commonly results in the precipitation of ferric oxy-hydroxides between layers which may both reduce overall porosity and clog local pore throats (Goodfellow et al., 2016). The oxy-hydroxide and clay minerals commonly precipitated in these conditions are less dense than the primary silicates, potentially leading to decreased pore volume. These phenomena are observed in high and low mag. SEM-BSEI investigations of the felsic meta-volcanic rock, changes in physical and chemical mineral phase character are captured and illustrated in Figures 10 and 11.

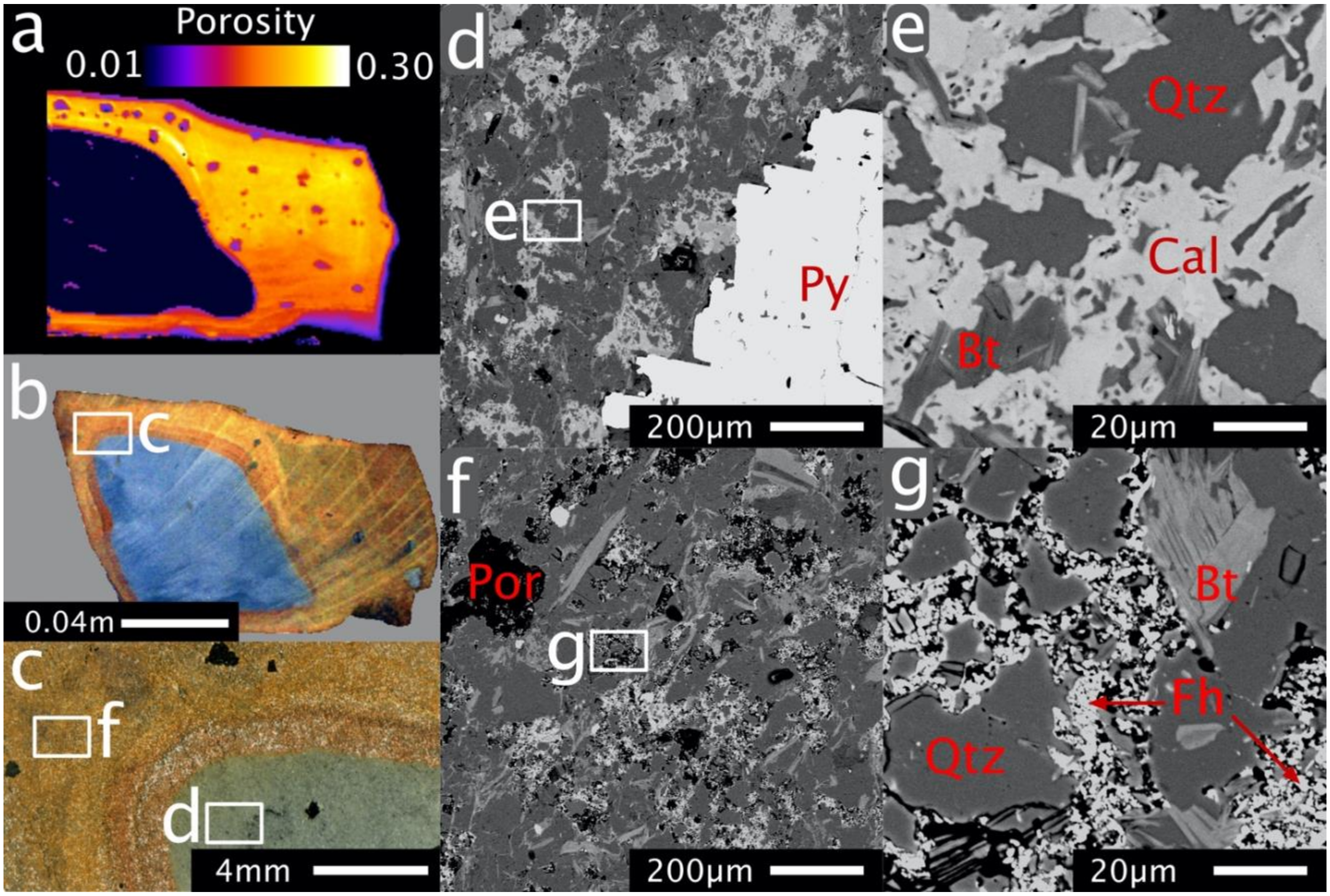

Figure 7. *a) The 2-D distribution of* ϕ_I *measured by X-ray radiography b) A cross sectional view of the waste rock fragment showing the unaltered core and oxidized rim. c) A region from a polished thin section at the boundary of the oxidized and unaltered domain. d) and e) BSEIs from the unaltered core where the dominant mineral phases are quartz, biotite, calcite and euhedral sulfides (mostly pyrite). f) and g) BSEIs from the oxidized rim where sulfide minerals such as pyrite have oxidized, leading to precipitation of iron oxy-hydroxides and generation of new porosity due to pyrite and carbonate dissolution. Black regions in 7d-g represent epoxy-filled pore space. Qtz = quartz, Bt = biotite, Cal = calcite, Py = pyrite, Fh = ferric oxy-hydroxide.*

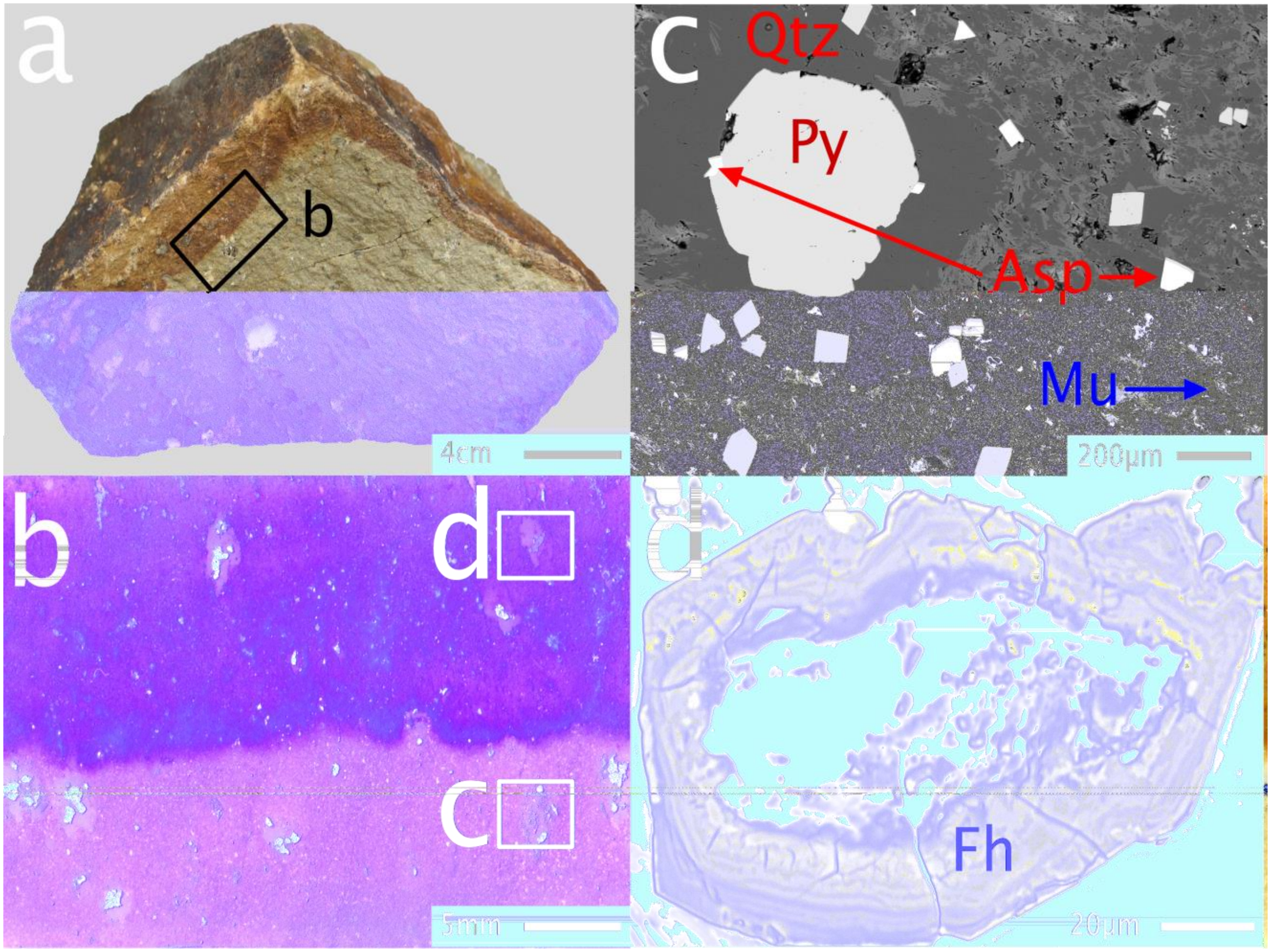

Figure 8. *Images illustrating the effects of sulfide-mineral oxidation in the meta-volcanic rock fragment (RM4). a) A view of the waste rock fragment highlighting the oxidized rim bordering the unaltered core. b) A region on a polished thin section showing the boundary of the oxidized and unaltered domain. c) An SEM-BSEI acquired in the unaltered core where the matrix is dominated by muscovite surrounding quartz and unaltered pyrite and arsenopyrite grains. d) An SEM-BSEI acquired in the oxidized rim showing a porous shell of ferric oxy-hydroxide precipitate that is a remnant pseudomorph from pyrite oxidation. Black regions in 8c,d represent epoxy-filled pore space. Qtz = quartz, Py = pyrite, Fh = ferric oxy-hydroxide, Asp = arsenopyrite, Mu = muscovite.*

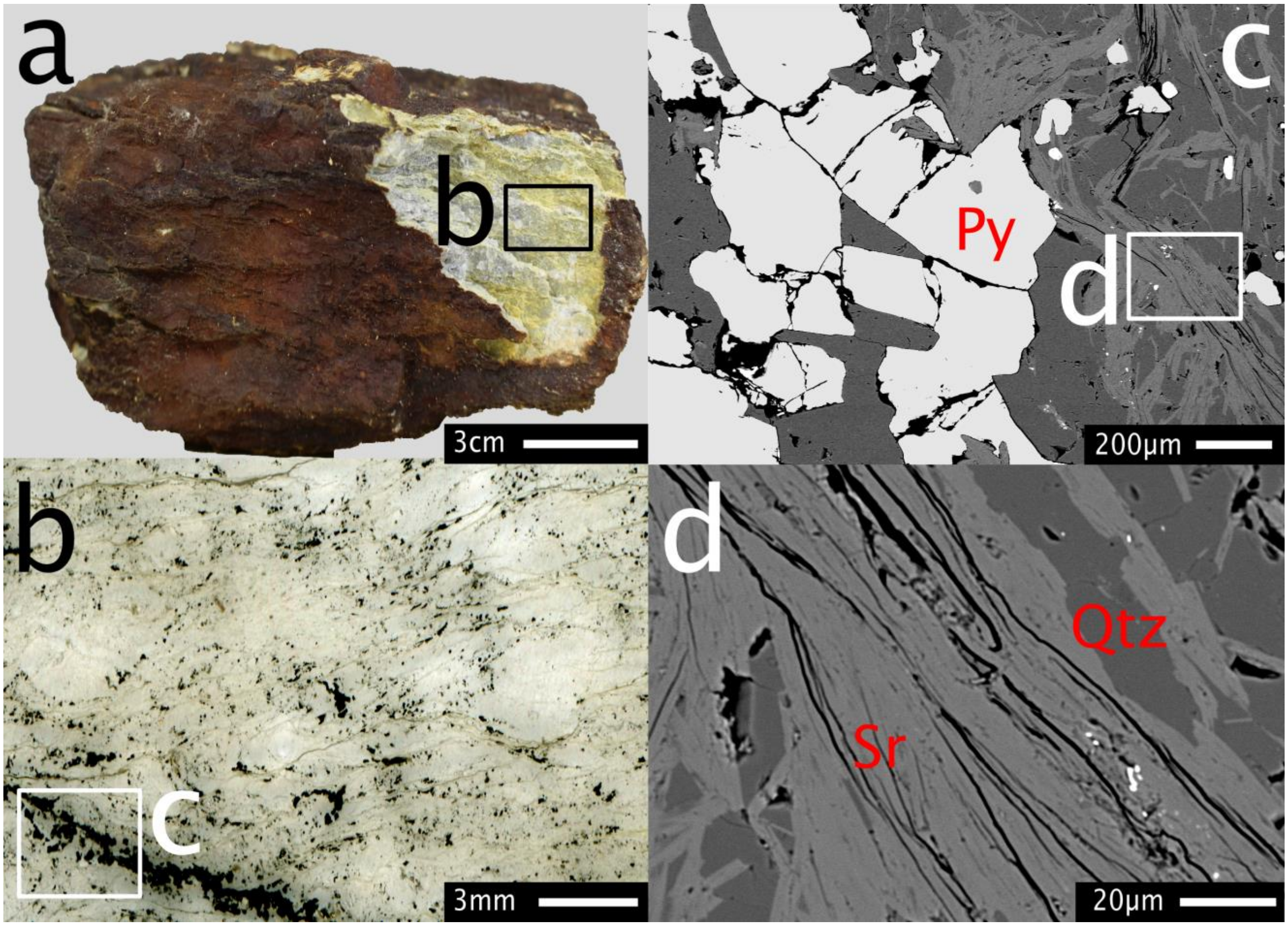

Figure 9. *Images highlighting the preferential solute transport pathways in a quartz-sericite schist (LR1). a) View of the waste rock fragment showing a thin oxidized rim and slight oxidation (discoloration) within the peripheral foliation. b) Thin section taken from the minimally oxidized core of the rock waste rock fragment. c) and d) SEM-BSEIs showing the interconnected pore space in a sulfide-mineral-rich vein. Black regions in 9c and d represent epoxy-filled pore space. Qtz = quartz, Py = pyrite, Sr = sericite.*

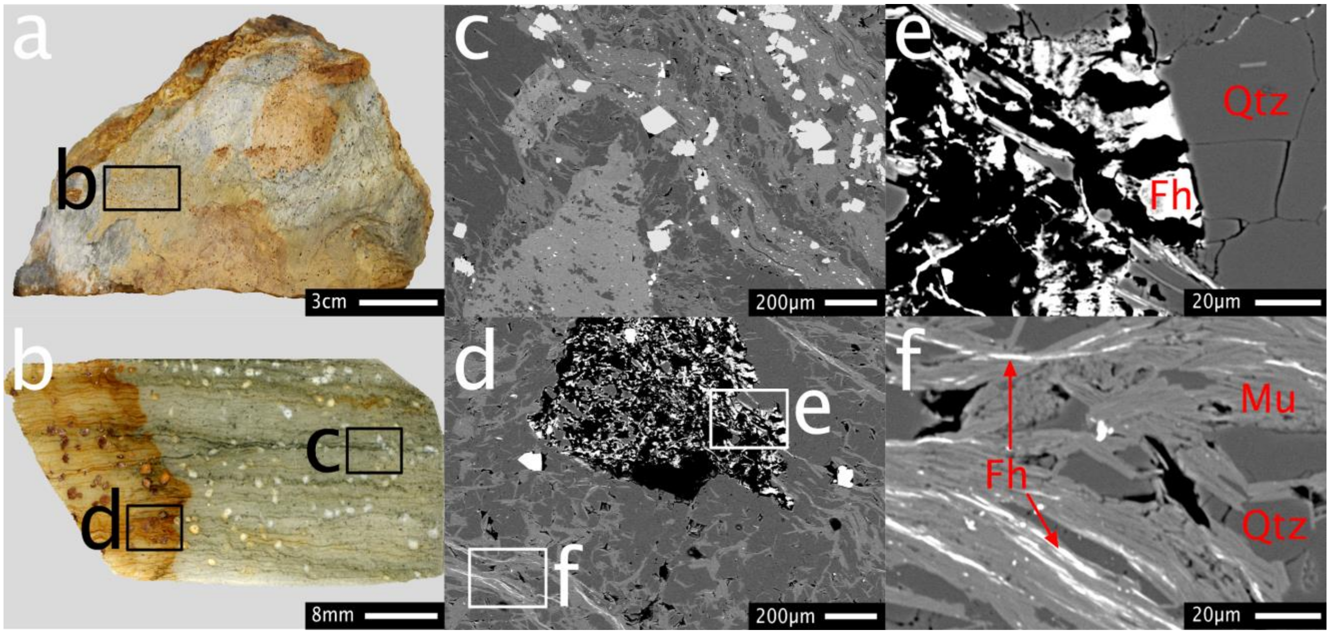

Figure 10. *Images illustrating the effects of sulfide mineral oxidation in a quartz-muscovite schist (RM9) and porous pathways for solute transport. a) A view of the waste rock fragment. b) A region of a polished thin section showing the boundary between oxidized and unaltered domains. c) An SEM-BSEI acquired in the unaltered region where the dominant mineral phases are quartz, muscovite, dolomite and unaltered sulfides. d) – f) SEM-BSEIs acquired in the oxidized rim, showing voids created by the dissolution of sulfide and carbonate minerals and secondary ferric oxy-hydroxide precipitation in the pore space (e and f). Black regions in 10c – f represent epoxy-filled pore space. Qtz = quartz, Fh = ferric oxy-hydroxide, Mu = muscovite.*

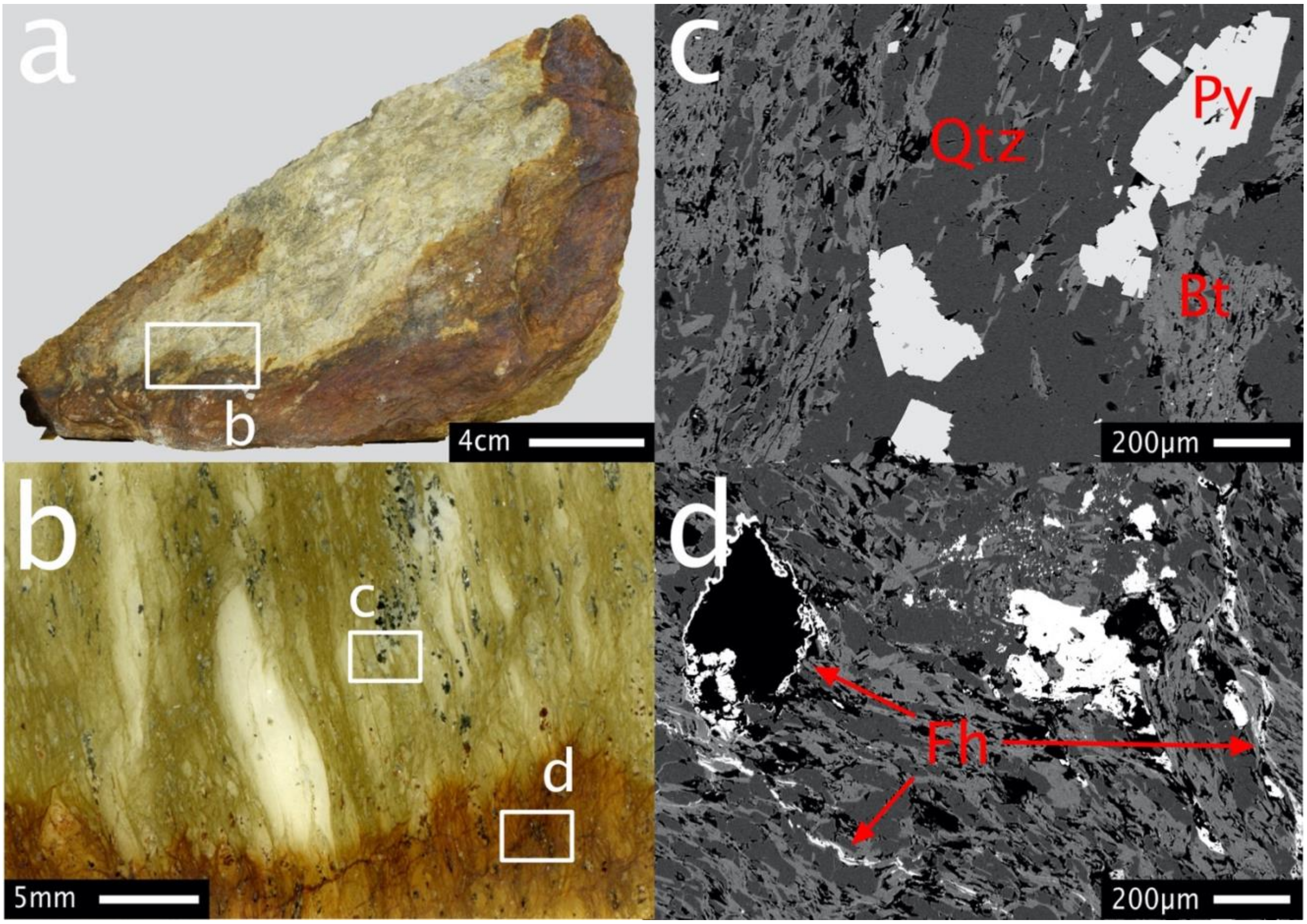

Figure 11. *Images illustrating the effects of sulfide mineral oxidation in a quartz-biotite schist (RM3) resulting in the precipitation of ferric oxy-hydroxides between layers and local pore throats. a) A view of the waste rock fragment. b) A region of a polished thin section showing the boundary between oxidized and unaltered domains. c) An SEM-BSEI acquired in the unaltered region where the dominant mineral phases are quartz, biotite, and unaltered sulfides. d) SEM-BSEI acquired in the oxidized rim, showing voids created by the dissolution of sulfides and biotite and secondary ferric oxy-hydroxide precipitation in the pore space. Black regions in 11c and d represent epoxy-filled pore space. Qtz = quartz, Fh = ferric oxy-hydroxide, Bt = biotite.*

The measured difference in ϕ_w and ϕ_I of the quartz-biotite schist, quartz-muscovite schist and the felsic meta-volcanic waste rock fragments used in 1-D diffusion experiments is less than ± 3% between their unaltered and oxidized domains. This minor variance in porosity suggests that the variability of porosity observed may be due to sample heterogeneity.

3.2 Diffusion Measurements 1-D

Spatially resolved 1-D profiles of C/C_0 values are plotted at discrete times to monitor diffusive tracer migration through the felsic meta-volcanic rock and quartz-sericite schist cores (Fig. 12). Modelled, best-fit D_p values for each time-series profile are indicated at chronologically ascending intervals. Diffusion measurements from the felsic meta-volcanic rock allow comparison between the unaltered (RM41a, Fig. 12a) and oxidized domain (RM41, Fig. 12b). The profiles illustrated in Figure 12 c and d capture the difference in diffusion rate between cores drilled parallel (LR1a) and normal (LR1-3) to foliation from the unaltered domain of the quartz-sericite schist waste rock sample.

The profiles from the unaltered domain of the felsic meta-volcanic rock display a reasonably good fit to the modelled profile, with D_p values average 2.22×10^{-11} m^2/s and ϕ_I values averaging 0.095 (Fig. 12a). Measured profiles from the oxidized domain fit the analytical solution well in the early-time data and at small distances from the influx boundary. As time and distance from the influx boundary increase, the fit becomes poor (Fig. 12b). A discontinuity at a distance of approximately 0.005 m is evident in the C/C_0 profiles after 26 hours (Fig. 12b), indicating that the sample material is heterogeneous. The raw data from radiography (Fig. 13) demonstrate that elevated tracer concentrations beyond 0.005 m correspond to concentrations of pyrite and/or ferric oxy-hydroxides, suggesting that regions with oxidized pyrite act as preferential diffusion pathways. This inference is supported by the SEM imaging that show increases in void space accompany pyrite oxidation (Figs. 7 – 11). The analytical model (Equation 10) requires homogeneous properties so it cannot be used to fit the full length of the profile. Instead, the analytical model was fit to a subset of the data from 0 to 0.006 m (see red curves in Figure 12b). In this region of the sample, the ϕ_I values from the oxidized region average 0.06 and D_p values measured in sample RM41 average 3.83×10^{-11}. Similar to, and slightly higher than the D_p values for the unaltered material from sample RM44a. This small difference in D_p values between the oxidized and altered domains cannot be attributed to weathering effects with certainty. However, the limits of the 1-D analytical model are apparent. In the oxidized region, tracer mas migrated the length of the sample after before 26 hours of diffusion. In the unaltered zone, tracer has not migrated the length of the sample after 260 hours. This data supports oxidation reactions creating localized voids, preferential diffusion pathways, and reduced pore throat size and connectivity.

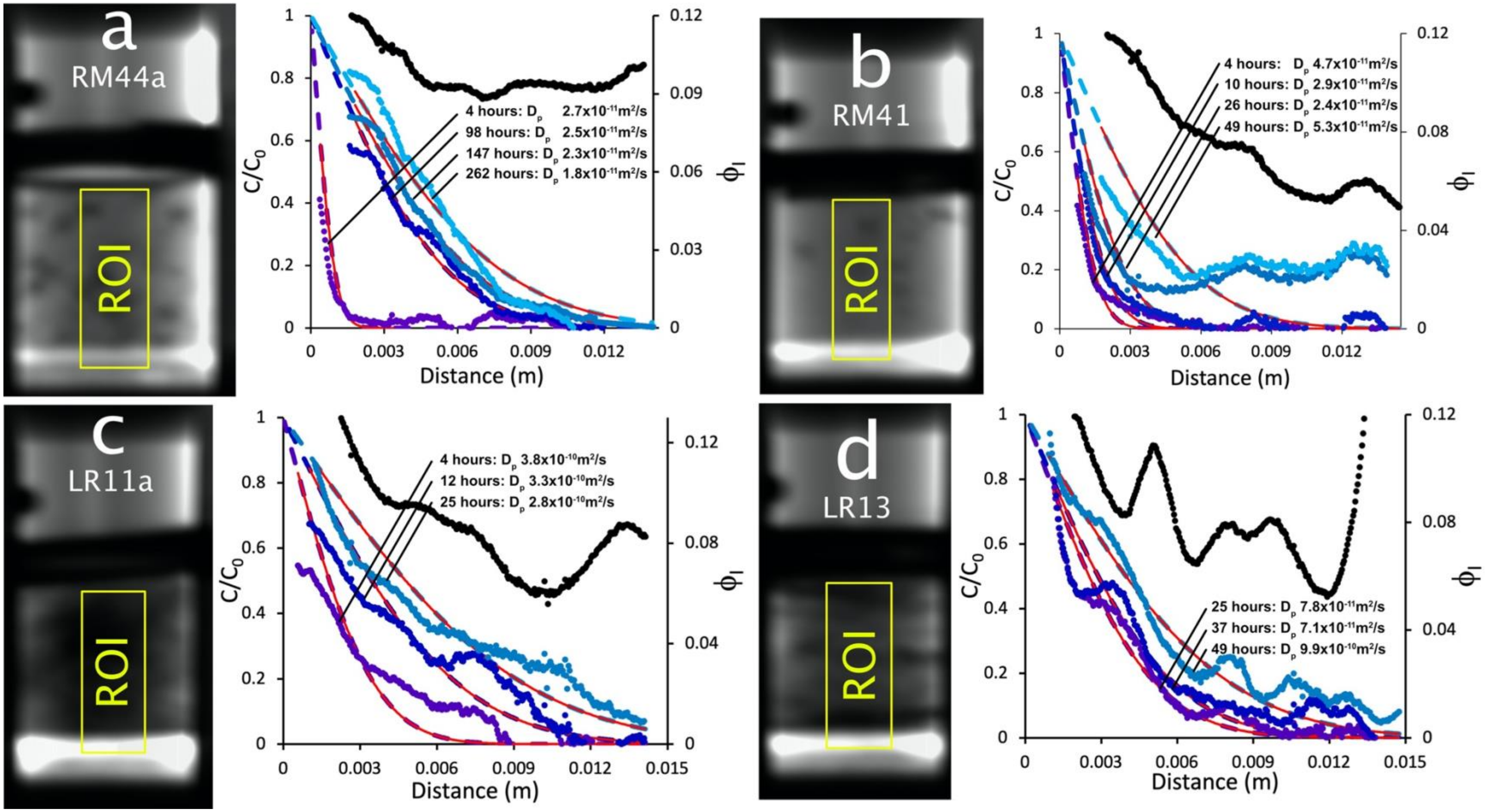

Figure 12. *One dimensional profiles of relative tracer concentration (C/C_0; blue profiles) and ϕ_I (black profiles). The C/C_0 data were collected at discrete times during the 1-D diffusion experiments. The dashed profiles are modelled lines that were fit to the section of the sample indicated by the red lines. a) Unaltered rock sample RM44a, b) Oxidized sample RM41, c) Unaltered sample LR11a drilled parallel to foliation, d) Unaltered sample LR13 drilled normal to foliation.*

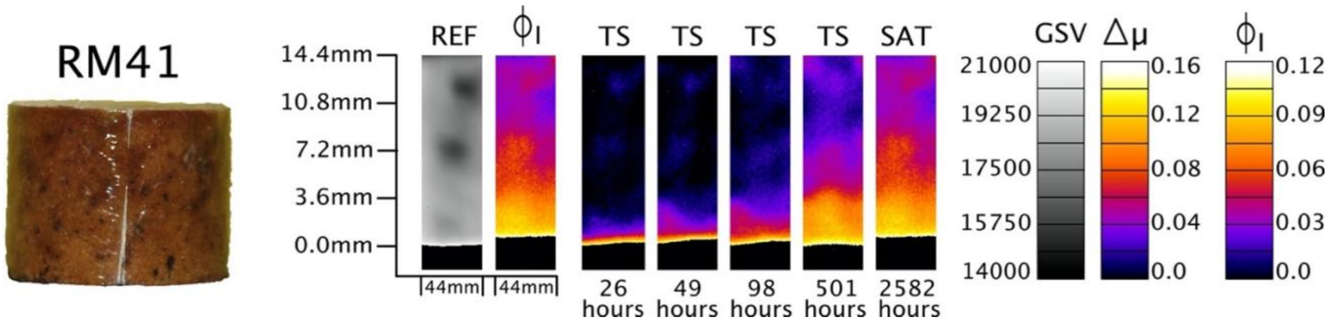

Figure 13. *RM41 drill core from the oxidized portion of sample, 2-D reference radiograph (REF), ϕ_I distribution within the ROI, and five time-series $\Delta\mu$ images, along with legends for the grey-scale values (gsv), $\Delta\mu$ and ϕ_I. The dark regions in the upper half of the radiograph represent pyrite and/or ferric oxy-hydroxides. Elevated $\Delta\mu$ values correspond with the presence of the pyrite and/or ferric oxy-hydroxides, suggesting regions of oxidized pyrite represent preferential pathways.*

The D_p values measured normal to foliation (Fig. 12c) in quartz-sericite schist average 8.27×10^{-11} m^2/s and the D_p values measured parrallel to the foliation (Fig. 12d) average 3.3×10^{-10} m^2/s, indicating that the mineral foliation orientation exerts anisotropy in diffusive transport. The anisotropy ratio in diffusion coefficients ($D_{p\ parallel}$: $D_{p\ normal}$) observed in the available cores is greater than 3, which is consistent with ratios from 1.4 to 11 and 1.1 to 7.0 measured in sedimentary rocks by Schaefer et al., (2012) and Xiang et al., (2013), respectively. The orientation of pores observed in SEM-BSEIs (Fig. 10) further suggests that solute transport occurs dominantly parallel to foliation defined by sheet silicates (biotite, muscovite, and sericite).

Many of the samples prepared for 1-D measurements displayed significant heterogeneity and could not be used for estimation of D_p. Examples are manifest in radiography data from quartz-sericite and quartz-muscovite schist samples (Fig. 14). For the samples with lower degrees of heterogeneity, the estimated D_p values are compiled in Tables 5, 6, and 7. The data are sorted by rock type, degree of weathering/oxidation and alignment of foliation relative to the direction of tracer diffusion.

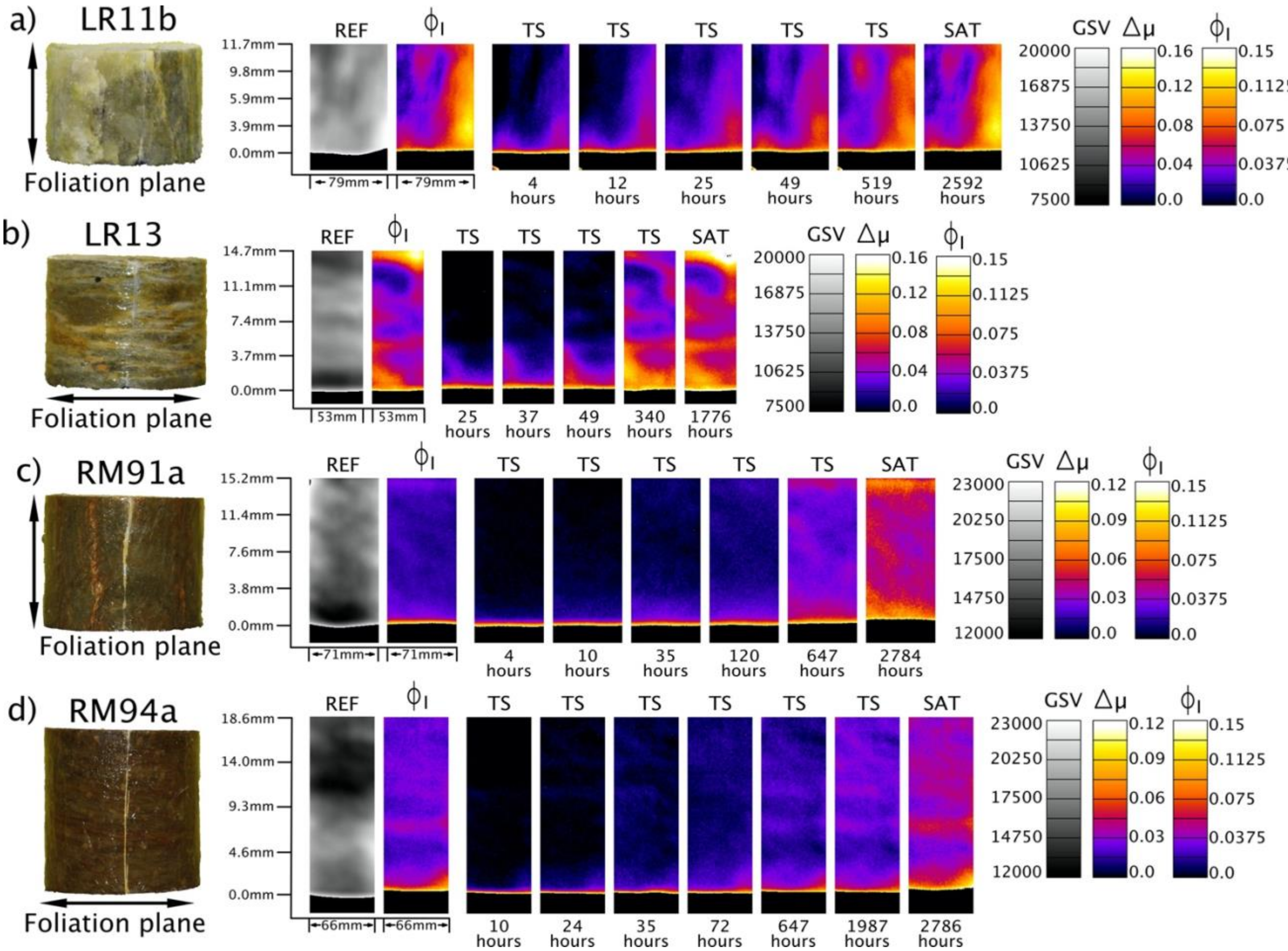

Figure 14. *Radiography data presented to illustrate heterogeneity in porosity and diffusion properties. Images of the drill cores are shown in the column on the left side. To the right of each drill core are shown 2-D reference radiographs (REF), 2-D ϕ_I distributions, and time-series $\Delta\mu$ distributions. a) Quartz-sericite schist core (LR11b) drilled parallel to foliation. The $\Delta\mu$ images illustrate heterogeneity with preferential pathways parallel to the core axis within sericite-rich regions (high gsv). b) Quartz-sericite schist core (LR11b) drilled normal to foliation; the $\Delta\mu$ images illustrate heterogeneity and demonstrate that tracer migration is retarded when connectivity between preferred transport pathways is limited. c) Quartz-muscovite schist (RM91a) drilled parallel to foliation; the $\Delta\mu$ images illustrate heterogeneity normal to the core axis and demonstrates the effect of low ϕ_I in slowing diffusion . d) Quartz-muscovite schist (RM94a) drilled normal to foliation. The $\Delta\mu$ images illustrate heterogeneity associated with the foliation.*

Table 5 *The D_P, ϕ_I, and τ_f values for common waste rock types within the unaltered and oxidized domains, measured both parallel and normal to foliation when possible.*

Domain	LaRonde Mine - quartz –sericite schist							
	Sample ID	ϕ_I	τ_f	Normal to foliation Measured D_p	Sample ID	ϕ_I	τ_f	Parallel to foliation Measured D_p
Oxidized	LR13	0.096	4.40E-02 ± 7.75E-03	8.27E-11 ± 1.46E-11 m2/s, n=3				
Unaltered					LR11a	0.088	1.76E-01 ± 2.66E-02	3.30E-10 ± 5.00E-11 m^2/s, n=3

Domain	Restigouche Mine - quartz-biotite schist				Domain	Restigouche Mine - meta-volcanic rock[1]			
	Sample ID	ϕ_I	τ_f	Parallel to foliation Measured D_p		Sample ID	ϕ_I	τ_f	No foliation D_p
Oxidized	RM31	0.061	9.04E-02 ± 3.10E-02	1.70E-10 ± 5.83E-11 m^2/s , n=4	Oxidized	RM41	0.060	2.04E-02 ± 7.39E-03	3.83E-11 ± 1.39E-11 m^2/s, n=4
	RM33	0.076	1.11E-01 ± 6.28E-02	2.08E-10 ± 1.18E-10 m^2/s, n=3		RM432	0.053	3.06E-02 ± 1.27E-02	5.75E-11 ± 2.39E-11 m^2/s, n=3
	AVG	0.069	1.01E-01 ± 4.69E-02	1.89E-10 ± 8.82E-11		AVG	0.057	2.55E-02 ± 1.01E-02	4.79E-11 ± 1.89E-11
Unaltered	RM32a	0.083	1.12E-01 ± 5.32E-03	2.10E-10 ± 1.00E-11 m^2/s, n=3	Unaltered	RM41a	0.095	1.31E-02 ± 2.02E-03	2.47E-11 ± 3.79E-12 m^2/s, n=4
	RM33a	0.097	1.31E-01 ± 2.73E-02	2.47E-10 ± 5.13E-11 m^2/s, n=3		RM44a	0.095	1.17E-02 ± 1.92E-03	2.20E-11 ± 3.61E-12 m^2/s, n=4
	AVG	0.090	1.22E-01 ± 1.63E-02	2.29E-10 ± 3.07E-11		AVG	0.095	1.24E-02 ± 1.97E-03	2.34E-11 ± 3.70E-12

[1]*The Meta-volcanic rock has no dominant foliation.*

Resitgouche Mine - quartz-muscovite schist								
Domain	Sample ID	f_I	τ_f	Normal to foliation D_p	Sample ID	f_I	τ_f	Parallel to foliation Measured D_p
Oxidized	RM94a	0.041	2.10E-02 ± 2.68E-03	5.87E-11 ± 5.86E-12 m2/s, n=4				
	RM94b	0.036	1.96E-02 ± 1.28E-03	2.80E-11 ± 1.26E-11 m2/s, n=3				
	AVG	0.039	2.03E-02 ± 1.98E-03	3.82E-11 ± 3.72E-12				
Unaltered					RM91	0.048	3.59E-02 ± 2.66E-03	6.75E-11 ± 5.00E-12 m2/s, n=4

The distinction between D_p and D_e is noted in Equations 3 and 4, demonstrating that D_e for iodide can be calculated from the D_p and ϕ_I values determined in this study. In addition, given D_0 values for iodide from the literature (Vanysek, 1993) and D_p values measured with radiography, Equation 3 allows calculation of τ_f for iodide. If it can be assumed that τ_f is independent of the solute, then the experimentally derived values allow for estimation of D_p for any solute for which a D_0 value is known. This approach has been used here to estimate D_e for other solutes relevant to the study of sulfide oxidation in mine waste with the view that it could assist with parameter input for model predictions of oxidation rates in reactive transport modelling. The D_e values for each species (Table 8) were derived according to Equation 13:

$$D_e = D_0 \times \tau_{f\_iodide} \times \phi_I \qquad [13]$$

Where ϕ_I represents the average of the spatially resolved values determined experimentally (Tables, 4 and 5). The D_0 values for all inorganic cations and anions in Table 8 are from Vanysek (1993) and the D_0 value for dissolved oxygen is from Wise and Houghton (1966). This approach to estimating D_e values for a wide variety of species is subject to two key assumptions: i) pore space in the rock fragments is saturated with porewater, and ii) the experimentally determined values for τ_{f_iodide} are representative for all aqueous species. However, the diffusive transport of anionic species such as I^- is commonly affected by anion exclusion, as observed for iodide with the quartz-sericite schist (Fig. 6), resulting in lower values for τ_f compared to neutral or cationic species (Loomer et al., 2013; Xiang et al., 2013). In addition, most cationic species and some anions and gases exhibit non-conservative transport behavior due to reactions with mineral surfaces in the host rock. The estimated D_e values in Table 6 do not account for retardation of transport due to reaction processes.

***Table 6** Estimated D_e values for aqueous species Fe^{2+}, Fe^{3+}, Cl^- and SO_4^{2-}; the D_0 values are from Vanysek (1992), and estimated D_e values for dissolved O_2; the D_0 value is from Wise and Houghton (1966).*

Inorganic ion (Tracer)	Ion Charge (z)	Free-water diffusion coefficient (m^2/s)	Quartz-sericite schist: Oxidized normal to foliation	Quartz-sericite schist: Unaltered parallel to foliation	Quartz-biotite schist: Oxidized parallel to foliation	Quartz-biotite schist: Unaltered parallel to foliation	Meta-volcanic rock: Oxidized no dominant foliation plane	Meta-volcanic rock: Unaltered no dominant foliation plane	Quartz-muscovite schist: Oxidized normal to foliation	Quartz-muscovite schist: Unaltered parallel to foliation
		τ_f (-)	τ_f (-)	τ_f (-)	τ_f (-)	τ_f (-)	τ_f (-)	τ_f (-)	τ_f (-)	τ_f (-)
I-	1	1.88E-09	4.4E-02 ± 7.8E-03	1.8E-01 ± 2.7E-02	1.0E-01 ± 4.7E-02	1.2E-01 ± 1.6E-02	2.5E-02 ± 1.0E-02	1.2E-02 ± 2.0E-03	2.0E-02 ± 2.0E-03	3.6E-02 ± 2.7E-03
			ϕ_I (-)	ϕ_I (-)	ϕ_I (-)	ϕ_I (-)	ϕ_I (-)	ϕ_I (-)	ϕ_I (-)	ϕ_I (-)
			0.096	0.088	0.068	0.09	0.057	0.095	0.039	0.049
		D_0 (m^2/s)	D_e (m^2/s)	D_e (m^2/s)	D_e (m^2/s)	D_e (m^2/s)	D_e (m^2/s)	D_e (m^2/s)	D_e (m^2/s)	D_e (m^2/s)
Inorganic Cations										
Fe+2	2	7.2E-10	3.0E-12 ± 5.3E-13	1.1E-11 ± 1.7E-12	4.9E-12 ± 2.3E-12	7.9E-12 ± 1.1E-12	1.0E-12 ± 4.1E-13	8.5E-13 ± 1.3E-13	5.7E-13 ± 5.6E-14	1.3E-12 ± 9.4E-14
Fe+3	3	6.0E-10	2.5E-12 ± 4.5E-13	9.3E-12 ± 1.4E-12	4.9E-12 ± 1.9E-12	6.6E-12 ± 8.9E-13	8.8E-13 ± 3.5E-13	7.1E-13 ± 1.1E-13	4.8E-13 ± 4.7E-14	1.1E-12 ± 7.9E-14
Inorganic Anions										
Cl-	1	2.0E-09	8.6E-12 ± 1.5E-12	3.1E-11 ± 4.8E-12	4.9E-12 ± 6.5E-12	2.2E-11 ± 3.0E-12	2.9E-12 ± 1.2E-12	2.4E-12 ± 3.8E-13	1.6E-12 ± 1.6E-13	3.6E-12 ± 2.6E-13
SO4-2	2	1.1E-09	4.5E-12 ± 8.0E-13	1.7E-11 ± 2.5E-12	4.9E-12 ± 3.4E-12	1.2E-11 ± 1.6E-12	1.6E-12 ± 6.1E-13	1.3E-12 ± 2.0E-13	8.5E-13 ± 8.3E-14	1.9E-12 ± 1.4E-13
Systems										
	10	1.7E-09	7.2E-12 ± 1.3E-12	2.6E-11 ± 4.0E-12	4.9E-12 ± 5.4E-12	1.9E-11 ± 2.5E-12	2.5E-12 ± 9.7E-13	2.0E-12 ± 3.2E-13	1.3E-12 ± 1.3E-13	3.0E-12 ± 2.2E-13
O2/H20	20	2.3E-09	9.7E-12 ± 1.7E-12	3.6E-11 ± 5.4E-12	4.9E-12 ± 7.3E-12	2.5E-11 ± 3.4E-12	3.3E-12 ± 1.3E-12	2.7E-12 ± 4.3E-13	1.8E-12 ± 1.8E-13	4.0E-12 ± 3.0E-13
	30	2.8E-09	1.2E-11 ± 2.1E-12	4.3E-11 ± 6.6E-12	4.9E-12 ± 8.9E-12	3.1E-11 ± 4.1E-12	4.1E-12 ± 1.6E-12	3.3E-12 ± 5.2E-13	2.2E-12 ± 2.2E-13	4.9E-12 ± 3.6E-13

3.3 Diffusion measurements in 2D

The 2-D diffusion experiments provide images of the iodide tracer distribution, $C/C_{0x,y}$, in the sample after 22, 120 and 333 hours of diffusion (Fig. 15). The data illustrate the transport of NaI tracer through the oxidized domain by diffusion, starting at the boundary around the slab's uneven peripheral edge. As tracer is transported through the oxidized domain, the diffusion rate decreases when it approaches and is greatly retarded at and within the unaltered domain. The large contrast in tracer diffusion rates at this inner boundary coincides with a similarly abrupt change in porosity (Fig. 7a), the elevated porosity in the oxidized region resulting from dissolution of calcite cements from the pore space in response to sulfide oxidation.

Comparison of measured versus simulated concentration distributions in (Figs. 15b, f and j) and (Figs. 15a, e and i), respectively, suggests good correspondence, but the quality of fit between measured and simulated tracer concentrations is evaluated in more detail at five spatially distributed regions of interest (ROIs) located as shown in Figure 15d. At each of the output times (22, 120 and 333 hours), the simulated concentrations at ROI 2, 3 and 4 fit the measured values reasonably well (Figs. 16-18) but the fit quality is relatively poor throughout the duration of the model along the top-left and bottom-left boundaries at ROI 5 and ROI 1. In general, the fit quality declines with time as indicated by the sum of squared weighted residuals which increase from 1.176, to 2.444 to 3.124 at 22, 120 and 333 hours, respectively (Table 7). This degradation of the fit is caused by an oversight during assembly of the model domain, resulting in the inclusion of a column of half cells at the left-side boundary which were erroneously assigned the same properties (K, τ and ϕ_I) as the solution reservoir (Table 3). In the simulations, this allows tracer access, and therefore diffusion into the sample, along the left side of the domain – effectively a numerical artifact. As a result, the simulations show excessive tracer penetration into the left side of the sample.

The D_p values in the oxidized zone estimated by the 2-D numerical fitting range from 1.16 x 10^{-11} m^2/s to 3.06 x 10^{-10} m^2/s, with mean values (1.48 × 10^{-10} to 1.53 × 10^{-10} m^2/s) at each time increment that are identical within error (Figs. 15c, g, k; Table 7). The narrow range of D_p values indicates that sulfide oxidation, followed by calcite dissolution, creates nearly homogeneous porosity and pore structure that is likely an inherited characteristic of the uncemented precursor to the sandstone. The 2-D representation of the experimental data and model output are difficult to examine and confirm that concentration trends in time and space are consistent with expectations for diffusive transport. For this reason, an alternative method of examining the data is presented in Figures 19 and 20. These figures present 1-D profiles for data that have been extracted from ROI 1 and ROI 3, including the normalized grey-scale values (NGSV), $\Delta\mu$ and C/C_0 to demonstrate that characteristic diffusion curves underpin the 2-D datasets. The portions of these profiles that occur in the oxidized zone have been fit with a diffusion model and the resulting estimates for D_p (1.31 × 10^{-10} to 2.30 × 10^{-10} m^2/s) are consistent with the results of the 2-D analysis.

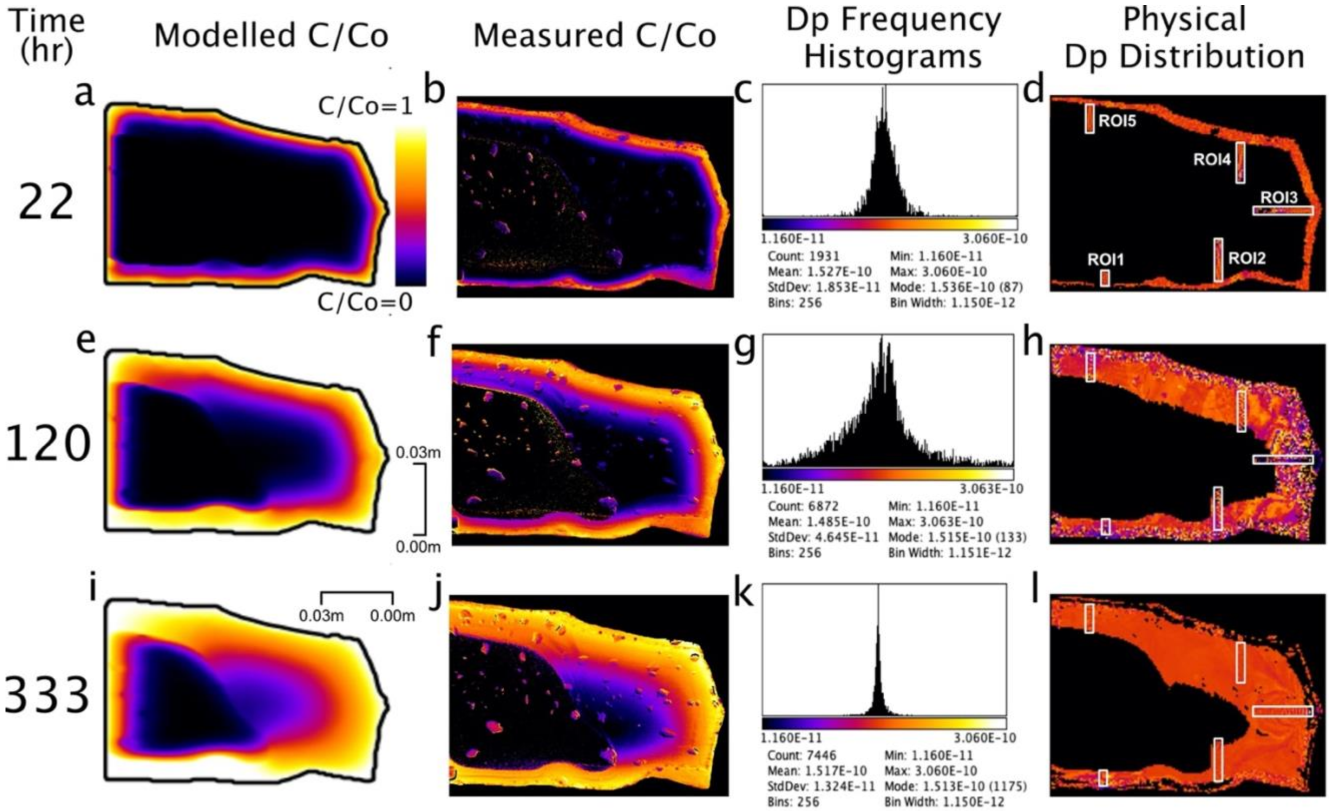

Figure 15. *Comparison of experimental measurements and modelled output after 22 (a-d), 120 (e-h) and 333 (i-l) hours of tracer diffusion. The black outline included in the model-output images indicates the location of the tracer influx boundary. Sections c, g, and k are frequency histograms for the best-fit D_p values calculated by the model. Sections d, h, l illustrate the 2-D distribution of estimated D_p values in the oxidized domain where measured C/C_0 values > 0.1 . This constraint was necessary to improve simulation time and efficiency.*

Table 7 *Estimated D_p values from model fit to experimental data.*

Hours	Voxel count	Mean D_P (m^2/s)	Min D_P (m^2/s) (- 2s)	Max D_P (m^2/s) (+2s)	St.Dev (m^2/s) (s)	Sum of squared weighed residuals (F)	Correlation coefficient (r)
22	1946	1.53E-10	1.17E-10	1.89.e-10	1.85E-10	1.176	0.76787
120	6872	1.48E-10	1.16E-11	3.06E-10	4.64E-11	2.444	0.83901
333	7446	1.52E-10	1.25E-10	1.79E-10	1.33E-11	3.124	0.77893

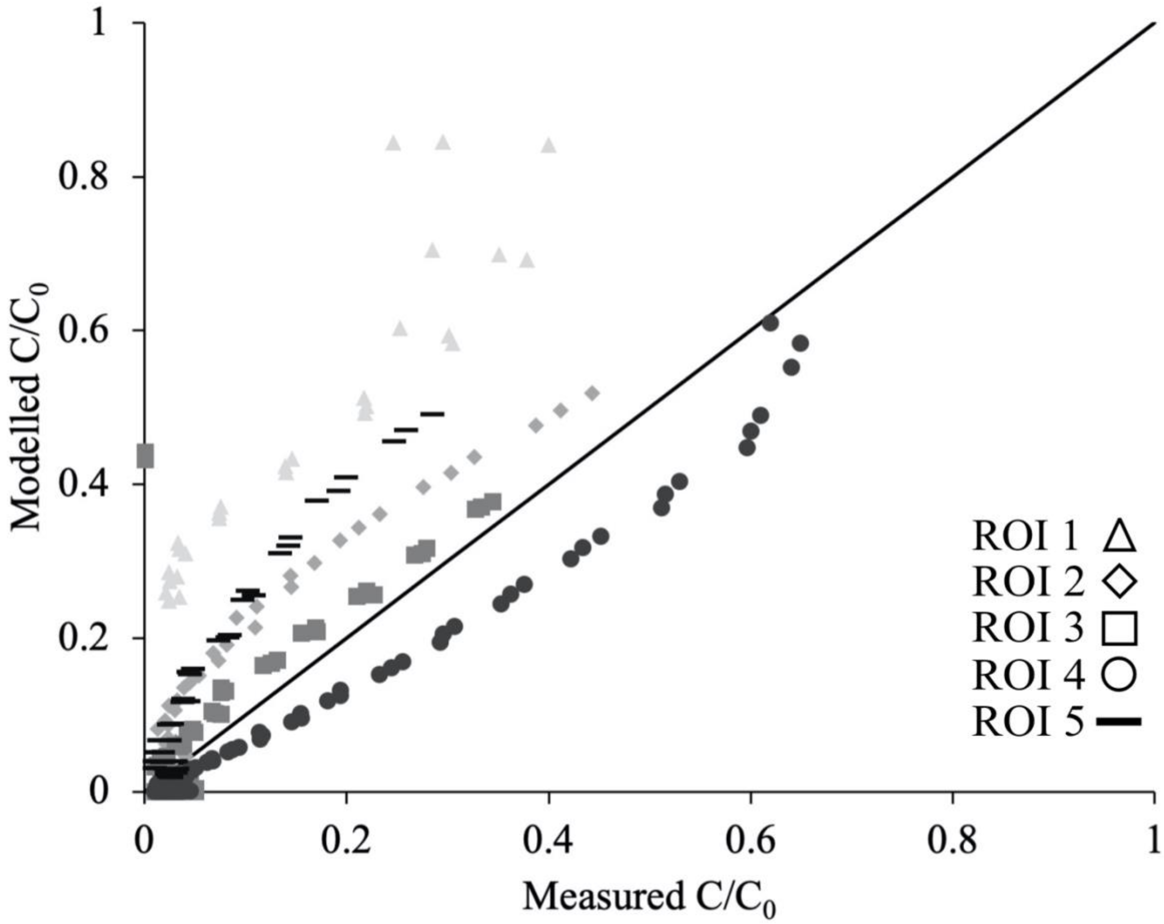

Figure 16. *Measured and modelled C/C_0 values representing ROIs 1-5 at the 22 hour time snapshot.*

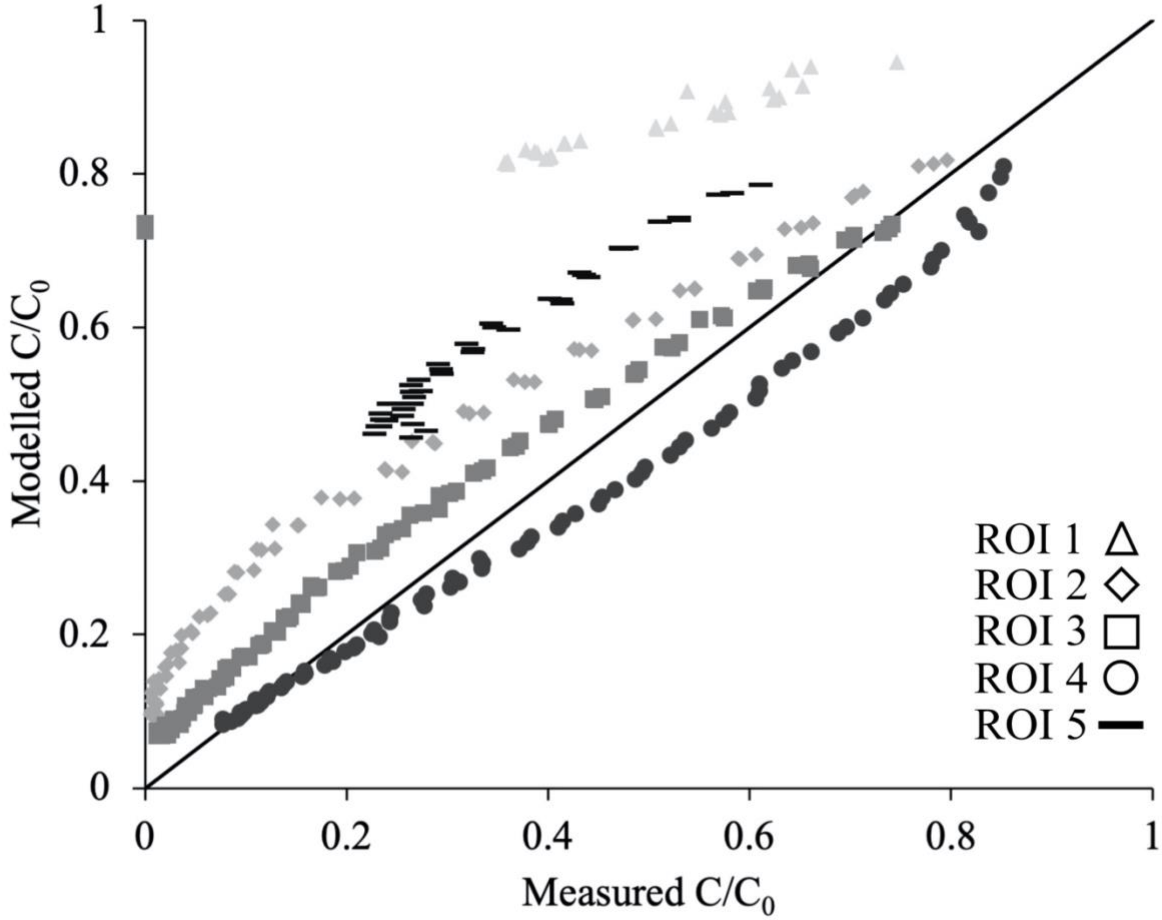

Figure 17. *Measured and modelled C/C_0 values representing ROIs 1-5 at the 120 hour time snapshot.*

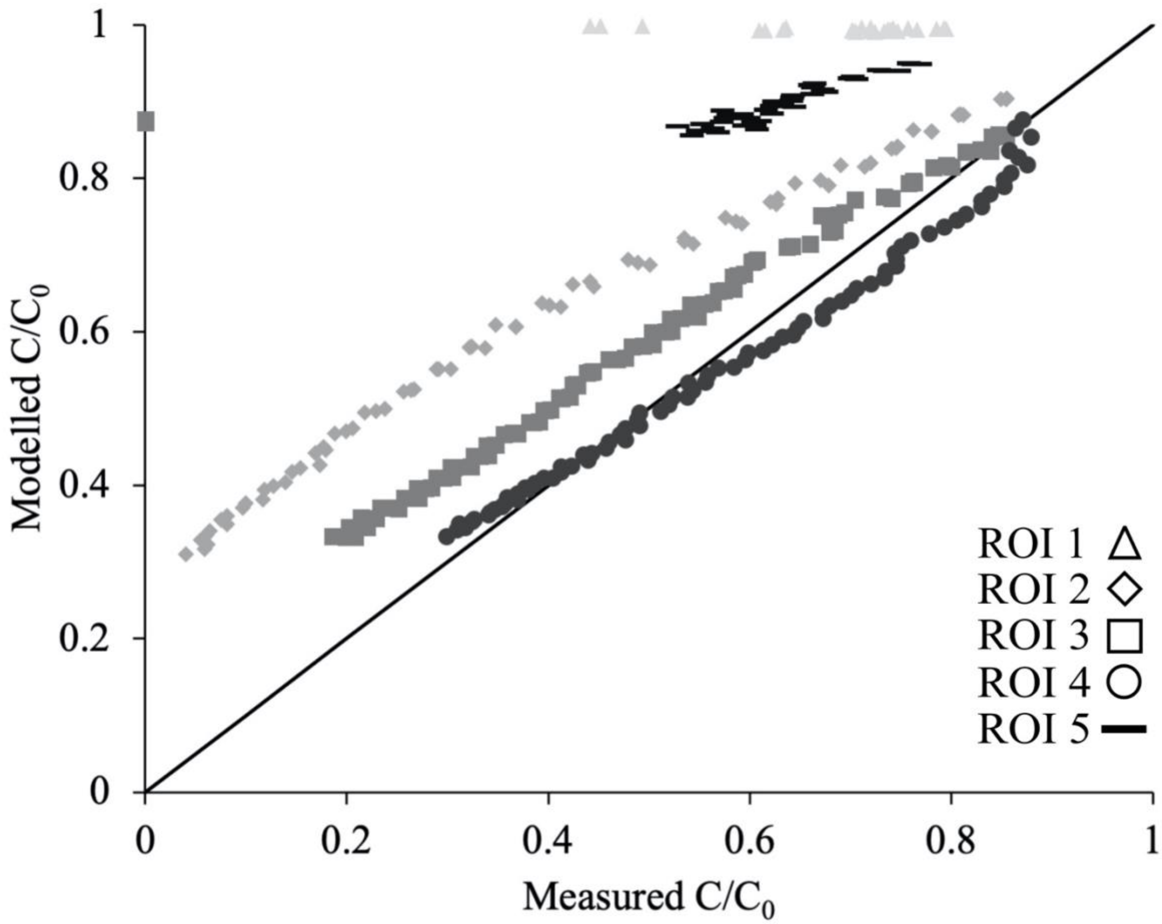

Figure 18. *Measured and modelled C/C_0 values representing ROIs 1-5 at the 333 hour time snapshot.*

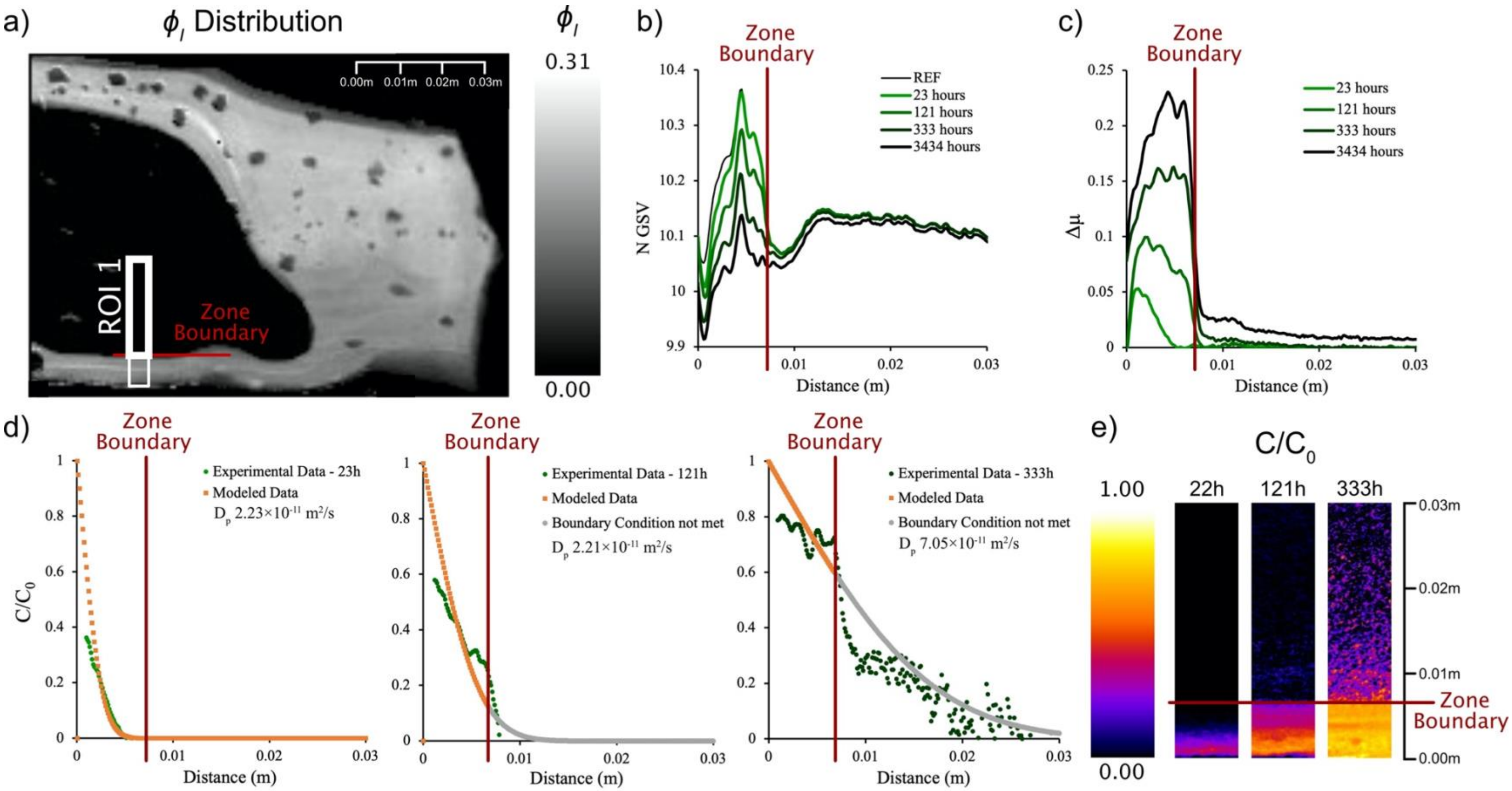

Figure 19. *1-D and 2-D diffusion measurement snapshots in ROI 1 after 22, 120, and 333 hours. a) 2-D distribution of ϕ_I measured by X-ray radiography. ROI 1 is extended to include both the oxidized and unaltered zone of the rock sample. b) 1-D normalized grey-scale value (NGSV) distribution transitioning from the oxidized zone into the unaltered core. c) 1-D $\Delta\mu$ distribution transitioning from the oxidized zone into the unaltered core. d) Modeled 1-D C/C_0 profile (orange) fit to measured 1-D C/C_0 values to estimate D_P in the oxidized zone. The analytical model used to calculate D_p is not applicable to heterogeneous material. The grey line is an extension of the valid model fit line projected into the unaltered zone and does not contribute to the calculated model fit and D_p value. e) 2-D distribution of C/C_0 values in both the oxidized and unaltered zone.*

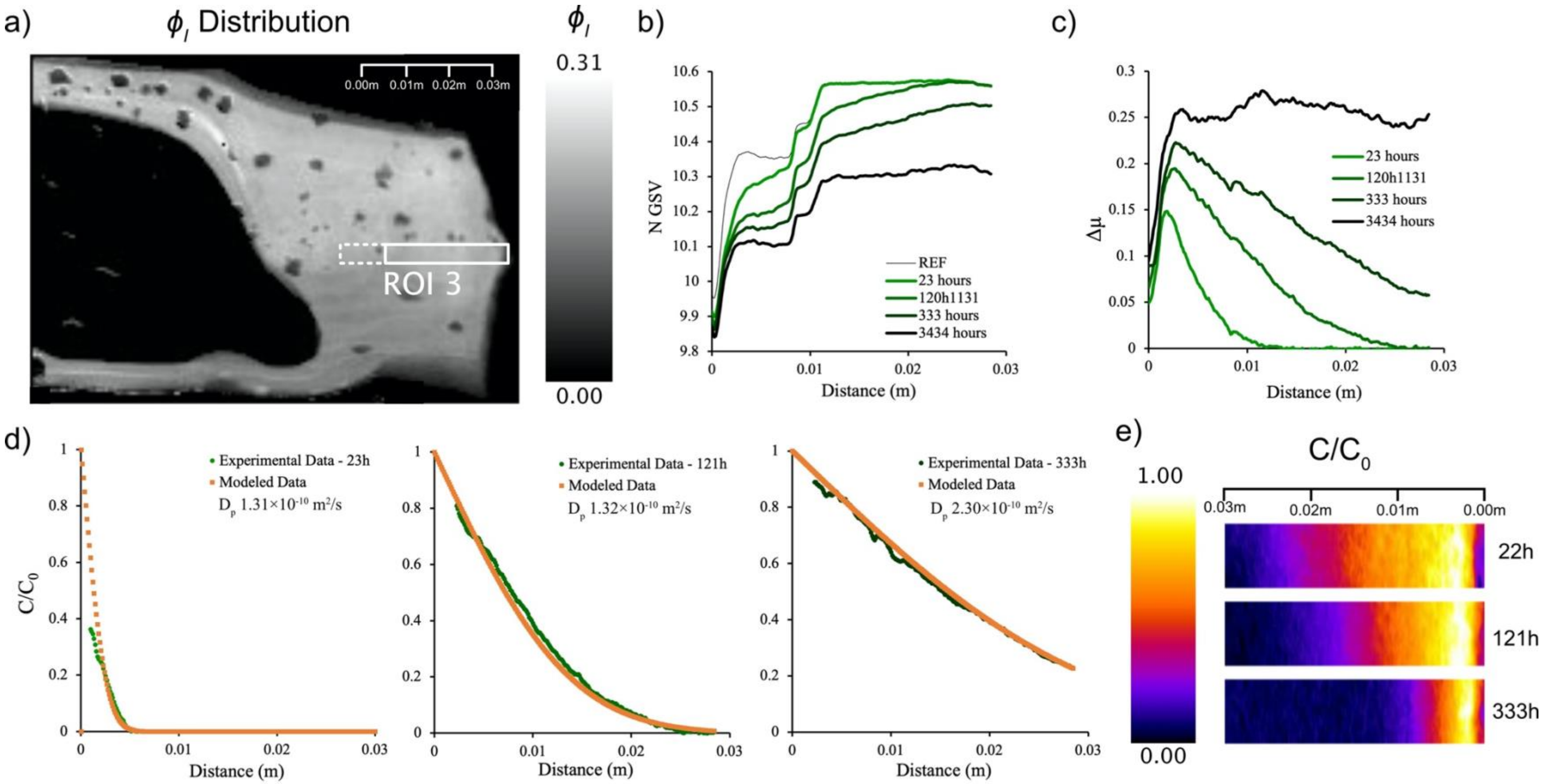

Figure 20. 1-D and 2-D diffusion measurement snapshots in ROI 1 after 22, 120, and 333 hours. a) 2-D distribution of ϕ_I measured by X-ray radiography. ROI 1 is extended to include both the oxidized and unaltered zone of the rock sample. b) 1-D normalized grey-scale value (NGSV) distribution transitioning from the oxidized zone into the unaltered core. c) 1-D $\Delta\mu$ distribution transitioning from the oxidized zone into the unaltered core. d) Modeled 1-D C/C_0 profile fitted with measured 1-D C/C_0 values to estimate D_P in the oxidized zone. e) 2-D distribution of C/C_0 values in both the oxidized and unaltered zone.

3.5 Suggestions for Improvements to Experimental Design

Some modifications could be made to the experimental methods in order to improve the outcome from this novel technique to measure diffusion coefficients that are spatially resolved in 2-D.

Radiography experiments were conducted using a method that promoted tracer diffusion through the height and width dimensions of a waste-rock slab. The rock slab is 1.5 cm thick and although transport rates are affected by heterogeneity in the depth dimension, the methods did not account for the influence of heterogeneity in the depth dimension. Increasing model complexity to account for 3-D material variation in 2-D space will result in more accurate Dp distributions and relative concentration outputs.

Achieving rotational alignment is not possible using the image processing techniques available in ImageJ. This study aligned the rock sample in the depth dimension at each time increment by calibrating the instrument motion axes and fixing them at identical settings. However, the positioning system is not perfect and axis positioning drift caused radiographs to vary in magnification making alignment of the reference and time-series images difficult to achieve using image processing techniques. Future studies would be able to reduce $\Delta\mu$ artifacts from positioning errors by improving the accuracy of the positioning system. In addition, placement of fiduciary markers on the rock sample would improve alignment on all axes.

Future studies may achieve this by capturing the entire diffusion cell and waste rock fragment in each radiograph and ensuring both components are aligned in all three dimensions with the reference image before acquiring time-series radiographs.

The time required for the 2-D modelling is related to the size of the model domain and the number of observations used to control the parameter estimation process. This study used the maximum number of observations allowed by the PEST code (9,000) with a significant cost to simulation efficiency. The simulation time required to achieve convergence ranged from 1 to 3 months. Optimizing the method in future studies will require a scaled approach, beginning with a smaller model domain and fewer observations before increasing scale and complexity.

Instead of defining all observations in just a few ROIs distributed at the perimeter of the rock domain, future studies may benefit from strategically distributing observations in a larger number of small ROIs.

Model sophistication and parameter optimization efforts are required to improve fit quality. Future work to improve this novel technique could focus on program development to resolve the current model limitations by reducing parameter optimization time and streamlining the data preparation process by developing a graphical user interface. Increasing accessibility by these means will encourage use and broaden the applicability of this technique.

4 Conclusions

This study successfully demonstrated methods that couple laboratory measurements and modelling techniques to quantify the diffusive properties of rock fragments both in one and two dimensions. X-ray radiography was used to assess the influence of sulfide-mineral oxidation and rock fabric orientation on solute distributions and transport rates. Data indicate that heterogeneity and mineral assemblages cause variation in tracer accessible porosities and diffusion rates. Results demonstrating the effects of these properties in 1-D were consistent with expectations. Porosity and diffusion rate measured in rocks composed of silicates, sulfides, and carbonates were sensitive to oxidation, observed as an increase in both parameters. Waste rock fragments without carbonates were less sensitive to oxidation, experiencing minimal change in both parameters. Variation in porosity and diffusion properties appear to be related to local changes in inter-connected pore-space and between sheet silicates where secondary mineral precipitates and silicate alterations clog pore throats. However, measured differences in water and tracer-accessible porosity were less than natural variations due to heterogeneity. The diffusion rate measured parallel to foliation was two-fold greater than rates measured normal to foliation. The novel technique used to measure diffusion coefficients in 2-D was successful. Coupled diffusion modelling and parameter estimation was used, with output at three discrete times through the diffusion experiment. The 2-D analysis provided estimates of D_p that are consistent with estimates from a simple 1-D estimation method.

5 References

Aachib, M., Mbonimpa, M., & Aubertin, M. (2004). Measurement and prediction of the oxygen diffusion coefficient in unsaturated media, with applications to soil covers. *Water, Air, and Soil Pollution*, *156*(1–4), 163–193. https://doi.org/10.1023/B:WATE.0000036803.84061.e5

Agbogun, H. M. D., Al, T. A., & Hussein, E. M. A. (2013). Three dimensional imaging of porosity and tracer concentration distributions in a dolostone sample during diffusion experiments using X-ray micro-CT. *Journal of Contaminant Hydrology*, *145*, 44–53. https://doi.org/10.1016/j.jconhyd.2012.11.008

Akcil, A., & Koldas, S. (2006). Acid Mine Drainage (AMD): causes, treatment and case studies. *Journal of Cleaner Production*, *14*(12-13 SPEC. ISS.), 1139–1145. https://doi.org/10.1016/j.jclepro.2004.09.006

Al, T. A., Blowes, D. W., Martin, C. J., Cabri, L. J., & Jambor, J. L. (1997). Aqueous geochemistry and analysis of pyrite surfaces in suifide-rich mine tailings. *Geochimica et Cosmochimica Acta*, *61*(12), 2353–2366. https://doi.org/10.1016/s0016-7037(97)00113-0

Altman, S. J., Uchida, M., Tidwell, V. C., Boney, C. M., & Chambers, B. P. (2004). Use of X-ray absorption imaging to examine heterogeneous diffusion in fractured crystalline rocks. *Journal of Contaminant Hydrology*, *69*(1–2), 1–26. https://doi.org/10.1016/S0169-7722(03)00153-0

Amos, R. T., Blowes, D. W., Bailey, B. L., Sego, D. C., Smith, L., & Ritchie, A. I. M. (2015). Waste-rock hydrogeology and geochemistry. *Applied Geochemistry*, *57*, 140–156. https://doi.org/10.1016/j.apgeochem.2014.06.020

Appelo, C. A. J., Vinsot, A., Mettler, S., & Wechner, S. (2008). Obtaining the porewater composition of a clay rock by modeling the in- and out-diffusion of anions and cations from an in-situ experiment. *Journal of Contaminant Hydrology*, *101*(1–4), 67–76. https://doi.org/10.1016/j.jconhyd.2008.07.009

Badsha, K. S., & Sainsbury, M. (1977). Uptake of zinc, lead and cadmium by young whiting in the Severn Estuary. *Marine Pollution Bulletin*, *8*(7), 164–166. https://doi.org/10.1016/0025-326X(77)90270-3

Banwart, S. A., & Malmström, M. E. (2001). Hydrochemical modelling for preliminary assessment of minewater pollution. *Journal of Geochemical Exploration*, *74*(1–3), 73–97. https://doi.org/10.1016/S0375-6742(01)00176-5

Bein, A., Lentz, D., Walker, J., & Piercey, S. (2006). *Volcanic Stratigraphy, Chemostratigraphy, and Hydrothermal Alteration of Felsic Volcanic Rocks of the Mount Brittain Formation that Host the Restigouche VMS Deposit, Bathurst Mining Camp, Northern New Brunswick*.

Biglari, M., Nicholson, R. V., Reilly, P. M., & Scharer, J. M. (2008). Model Development and Parameter Estimation for the Oxidation of Pyrrhotite-Containing Rock Surfaces. *The Canadian Journal of Chemical Engineering*, *84*(1), 116–124. https://doi.org/10.1002/cjce.5450840115

Blackmore, S., Vriens, B., Sorensen, M., Power, I. M., Smith, L., Hallam, S. J., … Beckie, R. D. (2018). Microbial and geochemical controls on waste rock weathering and drainage quality. *Science of the Total Environment*, *640–641*(2018), 1004–1014. https://doi.org/10.1016/j.scitotenv.2018.05.374

Bolt, G. H. (1979). The ionic distribution in the diffuse double layer. *Developments in Soil Science*, *5*, 1–26.

Boone, J. M., & Seibert, J. A. (1997). An accurate method for computer-generating tungsten anode x-ray spectra from 30 to 140 kV. *Medical Physics*, *24*(11), 1661–1670.

https://doi.org/10.1118/1.597953
Boving, T. B., & Grathwohl, P. (2001). Tracer diffusion coefficients in sedimentary rocks: correlation to porosity and hydraulic conductivity. *Journal of Contaminant Hydrology*, *53*(1), 85–100. https://doi.org/10.1016/j.apgeochem.2007.07.008
Brezina, E. R., Campbell, R. S., & Whitley, R. (1970). Effects of Acid Mine Drainage on Water Quality of a Reservoir. *Journal of the Water Pollution Control Federation*, *42*(8 pt 1), 1429–1436.
Cavé, L., Al, T., Xiang, Y., & Vilks, P. (2009). A technique for estimating one-dimensional diffusion coefficients in low-permeability sedimentary rock using X-ray radiography: Comparison with through-diffusion measurements. *Journal of Contaminant Hydrology*, *103*(1–2), 1–12. https://doi.org/10.1016/j.jconhyd.2008.08.001
Celejewski, M., Barton, D., & Al, T. (2018). Measurement of Cl-: Br- Ratios in the Porewater of Clay-Rich Rocks-A comparison of the Crush-and-Leach and the Paper-Absorption methods. *Geofluids*, *2018*(Ddl), 1–14. https://doi.org/10.1155/2018/9682042
Cheng, H. P., & Yeh, G. T. (1998). Development and demonstrative application of a 3-D numerical model of subsurface flow, heat transfer, and reactive chemical transport: 3DHYDROGEOCHEM. *Journal of Contaminant Hydrology*, *34*(1–2), 47–83. https://doi.org/10.1016/S0169-7722(98)00084-9
Clausnitzer, V., & Hopmans, J. W. (2000). Pore-scale measurements of solute breakthrough using microfocus X-ray computed tomography. *Water Resources Research*, *36*(8), 2067–2079. https://doi.org/10.1029/2000WR900076
Cormenzana, J. L., Garcıa-Gutierrez, M., Missana, T., & Junghanns, A. (2003). Simultaneous estimation of effective and apparent diffusion coefficients in compacted bentonite. *Contaminant Hydrogeology*, *61*, 63–72.
Crank, J. (1975). *The Mathematics of Diffusion*. *Journal of the American Chemical Society*. https://doi.org/10.1021/ja01562a072
Davis, G. B., Doherty, G., & Ritchie, A. I. M. (1986). A model of oxidation in pyritic mine wastes: part 2: comparison of numerical and approximate solutions. *Applied Mathematical Modelling*, *10*(5), 323–329. https://doi.org/10.1016/0307-904X(86)90091-0
Davis, G. B., & Ritchie, A. I. M. (1986). A model of oxidation in pyritic mine wastes: part 1 equations and approximate solution. *Applied Mathematical Modelling*, *10*(5), 314–322. https://doi.org/10.1016/0307-904X(86)90090-9
Davis, G. B., & Ritchie, A. I. M. (1987). A model of oxidation in pyritic mine wastes: part 3: import of particle size distribution. *Applied Mathematical Modelling*, *11*(6), 417–422. https://doi.org/10.1016/0307-904X(87)90166-1
Deniseger, J., & Kwong, Y. T. J. (1996). Risk Assessment of Copper-Contaminated Sediments in the Tsolum River near Courtenay, British Columbia. *Water Quality Resources Journal Canada*, *31*(4), 725–740.
Deslattes, R. D. (1969). Estimates of X-ray attenuation coefficients for the elements and their compounds. *Acta Crystallographica Section A: Crystal Physics, Diffraction, Theoretical and General Crystallography*, *25*(1), 89–93. https://doi.org/10.1107/S0567739469000118
Desponds, L., Depeursinge, C., Grecescu, M., Hessler, C., Samiri, A., & Valley, J. F. (1991). Influence of anode and filter material on image quality and glandular dose for screen-film mammography. *Physics in Medicine and Biology*, *36*(9), 1165–1182. https://doi.org/10.1088/0031-9155/36/9/002
Doherty, J. (2018a). *Model-Independent Parameter Estimation User Manual Part I: PEST*,

SENSAN and Global Optimisers.
Doherty, J. (2018b). *Model-Independent Parameter Estimation User Manual Part II: PEST Utility Support Software*.
Drake, C. F., & Le Bosquet, M. (1931). EFFECT OF ACID MINE DRAINAGE ON RIVER WATER SUPPLY [with DISCUSSION] Author (s): C . F . Drake , M . Le Bosquet and Jr . Published by : Wiley Stable URL : https://www.jstor.org/stable/41228258. *American Water Works Association*, *23*(10), 1474–1494.
Dubé, B., Mercier-Langevin, P., Hannington, M., Lafrance, B., Gosselin, G., & Gosselin, P. (2007). The LaRonde Penna world-class Au-rich volcanogenic massive sulfide deposit, Abitibi, Québec: Mineralogy and geochemistry of alteration and implications for genesis and exploration. *Economic Geology*, *102*(4), 633–666. https://doi.org/10.2113/gsecongeo.102.4.633
Dyer, R. (1977). The Effects of Mine Acid on the Pond River Watershed in Western Kentucky. *Journal of the American Water Resources Association*, *13*(5), 1069–1081. https://doi.org/10.1111/j.1752-1688.1977.tb03871.x
Ehrlich, H. L. (1963). MICROORGANISMS IN ACID DRAINAGE FROM A COPPER MINE. *Journal of Bacteriology*, *86*(2), 350–352.
Elberling, B., & Nicholson, R. V. (1996). Field determination of sulphide oxidation rates in mine tailings. *WATER RESOURCES RESEARCH*, *32*(6), 1773–1784.
Elberling, B., Nicholson, R. V., & Scharer, J. M. (1994). A combined kinetic and diffusion model for pyrite oxidation in tailings: a change in controls with time. *Journal of Hydrology*, *157*(1–4), 47–60. https://doi.org/10.1016/0022-1694(94)90098-1
Elberling, B., Schippers, A., & Sand, W. (2000). Bacterial and chemical oxidation of pyritic mine tailings at low temperatures. *Journal of Contaminant Hydrology*, *41*(3–4), 225–238. https://doi.org/10.1016/S0169-7722(99)00085-6
Ellis, D. V., Pedersen, T. F., Poling, G. W., Pelletier, C., & Horne, I. (1995). Review of 23 years of std: Island copper mine, Canada. *Marine Georesources and Geotechnology*, *13*(1–2), 59–99. https://doi.org/10.1080/10641199509388279
Emerson, D. W. (1990). Notes on mass properties of rocks? density, porosity, permeability. *Exploration Geophysics*, *21*(4), 209–216.
Eriksson, N., & Destouni, G. (1997). Combined effects of dissolution kinetics, secondary mineral precipitation, and preferential flow on copper leaching from mining waste rock. *Water Resources Research*, *33*(3), 471–483. https://doi.org/10.1029/96WR03466
Evangelou, V. P., & Zhang, Y. L. (1995). A review: Pyrite oxidation mechanisms and acid mine drainage prevention. *Critical Reviews in Environmental Science and Technology*, *25*(2), 141–199. https://doi.org/10.1080/10643389509388477
Fala, O., Molson, J., Aubertin, M., Bussière, B., & Chapuis, R. P. (2006). Numerical simulations of long term unsaturated flow and acid mine drainage at waste rock piles. *7th International Conference on Acid Rock Drainage 2006, ICARD - Also Serves as the 23rd Annual Meetings of the American Society of Mining and Reclamation*, *1*, 582–597. https://doi.org/10.21000/jasmr06020582
Frind, E. O. (1988). Solution of the advection-dispersion equation with free exit boundary. *Numerical Methods for Partial Differential Equations*, *4*(4), 301–313. https://doi.org/10.1002/num.1690040403
Gerke, H. H., & van Genuchten, M. T. (1993). A dual-porosity model for simulating the preferential movement of water and solutes in structured porous media. *Water Resources*

Research, *29*(2), 305–319. https://doi.org/10.1029/92WR02339

Giger, M. L., Ohara, K., & Doi, K. (1986). Effect of Quantization on Digitized Noise and Detection of Low -Contrast Objects. *Application of Optical Instrumentation in Medicine XIV and Picture Archiving and Communication Systems*, *626*, 214–224.

Goodfellow, B. W., Hilley, G. E., Webb, S. M., Leonard, S. S., Moon, S., & Olson, C. A. (2016). Journal of Geophysical Research : Earth Surface modeling study. *American Geophysical Union*, 1410–1435. https://doi.org/10.1002/2016JF003822.Received

Gower, S. J., & McCutcheon, S. R. (1997). Siluro-Devonian tectonostratigraphic relationships in the Portage Brook area, northern New Brunswick: Implications for timing of deformational events in the Bathurst Mining Camp. *Atlantic Geology*, *33*(1), 19–29. https://doi.org/10.4138/2056

Gvirtzman, H., & Gorelick, S. M. (1991). Dispersion and advection in unsaturated porous media enhanced by anion exclusion. *Nature*, *352*(6338), 793–795. https://doi.org/10.1038/352793a0

Harries, J. R., & Ritchie, A. I. M. (1985). Pore gas composition in waste rock dumps undergoing pyritic oxidation. *Soil Science*, *140*(2), 143–152. https://doi.org/10.1097/00010694-198508000-00010

Hawlicka, E., Grabowski, R., & Reimschuessel, W. (1990). Self-diffusion and conductance studies of acetonitrile. Water solutions of tetraethylammonium iodide. *Physical Chemistry Chemical Physics*, *94*(2), 158–162. https://doi.org/10.1002/bbpc.19900940212

Hodge, W. W. (1937). Pollution of Streams by Coal Mine Drainage: Beneficial Effects of Sealing Abandoned Goal Mines. *Industrial and Engineering Chemistry*, *29*(9), 1048–1055. https://doi.org/10.1021/ie50333a019

Hulshof, A. H. M., & Macdonald, A. S. (1998). Dispersion of tailings from the Stirling Zn-Pb-Cu mine site, Cape Breton Island, Nova Scotia. *Atlantic Geology*, *34*(3), 159–170. https://doi.org/10.4138/2047

Jaynes, D. B., Pionke, H. B., & Rogowski, A. S. (1984a). Acid Mine Drainage From Reclaimed Coal Strip Mines 1. Model Descrition. *Water Resources Research*, *20*(2), 243–250. https://doi.org/10.1029/WR020i002p00243

Jaynes, D. B., Pionke, H. B., & Rogowski, A. S. (1984b). Acid Mine Drainage From Reclaimed Coal Strip Mines 2. Simulation Results of Model. *Water Resources Research*, *20*(2), 243–250.

Kaganer, V. M., & Ostrovskii, B. I. (1991). X-ray scattering in smectic liquid crystals: From ideal- to real-structure effects. *The American Physical Society*, *44*(12), 8158–8166.

Ketcham, R. A., & Carlson, W. D. (2001). Acquisition, optimization and interpretation of x-ray computed tomographic imagery: Applications to the geosciences. *Computers and Geosciences*, *27*, 381–400. https://doi.org/10.1016/S0098-3004(00)00116-3

Lahmira, B., Lefebvre, R., Aubertin, R., & Bussière, B. (2007). Modeling the influence of heterogeneity and anisotropy on physical processes in AMD-producing waste rock piles. *Journal of Contaminant Hydrology*, *184*, 1486–1493. Retrieved from http://dx.doi.org/10.1016/j.jconhyd.2015.12.002

Lakshminarasimha, C. S., & Lucas, J. (1977). The ratio of radial diffusion coefficient to mobility for electrons in helium, argon, air, methane and nitric oxide. *Journal of Physics D: Applied Physics*, *10*(3), 313–321. https://doi.org/10.1088/0022-3727/10/3/011

Lefebvre, R., Hockley, D., Smolensky, J., & Lamontagne, A. (2001). Multiphase transfer processes in waste rock piles producing acid mine drainage. 2. Applications of numerical simulation. *Journal of Contaminant Hydrology*, *52*(1–4), 165–186. https://doi.org/10.1016/S0169-7722(01)00157-7

Lentz, D. R., Goodfellow, W. D., & Brooks, E. (1996). Chemostratigraphy and depositional environment of an Ordovician sedimentary section across the Miramichi Group - Tetagouche Group contact, northeastern New Brunswick. *Atlantic Geology*, *32*(2), 101–122. https://doi.org/10.4138/2081

Loomer, D. B., Scott, L., Al, T. A., Mayer, K. U., & Bea, S. (2013). Diffusion-reaction studies in low permeability shale using X-ray radiography with cesium. *Applied Geochemistry*, *39*, 49–58. https://doi.org/10.1016/j.apgeochem.2013.09.019

Lowson, R. T. (1982). Aqueous Oxidation of Pyrite by Molecular Oxygen. *Chemical Reviews*, *82*(5), 461–497. https://doi.org/10.1021/cr00051a001

Lu, L., Wang, R., Chen, F., Xue, J., Zhang, P., & Lu, J. (2005). Element mobility during pyrite weathering: Implications for acid and heavy metal pollution at mining-impacted sites. *Environmental Geology*, *49*(1), 82–89. https://doi.org/10.1007/s00254-005-0061-8

Lutes, G. G., Venugopal, D. V., & St. Peter, C. J. (2005). *Debrock geology of the Canterbury area (NTS 21 G/14). York Country. New Brunswick. New Brunswick Department of Natural Resources. Minerals. Policy and Planning Division.* https://doi.org/10.1016/j.apgeochem.2007.11.003

Mayer, K. U. (1999). *A Numerical Mode1 for Multicomponent Reactive Transport in Variably Saturated Porous Media*.

Mbonimpa, M., Aubertin, M., Aachib, M., & Bussière, B. (2003). Diffusion and consumption of oxygen in unsaturated cover materials. *Canadian Geotechnical Journal*, *40*(5), 916–932. https://doi.org/10.1139/t03-040

McFarlane, G. A., & Franzin, W. G. (1980). An Examination of Cd, Cu, and Hg Concentrations in Livers of Northern Pike, Esox lucius, and White Sucker, Catostomus commersoni, from Five Lakes near a Base Metal Smelter at Flin Flon, Manitoba. *Canadian Journal of Fish and Aquatic Science*, *37*(1), 1573–1578.

Merchant, V. A., Livingston, M. J., & Pashley, D. H. (1977). Dentin Permeation: Comparison of Diffusion with Filtration. *Journal of Dental Research*, *56*(10), 1161–1164. https://doi.org/10.1177/00220345770560100601

Mercier-Langevin, P., Dubé, B., Hannington, M. D., Richer-Laflèche, M., & Gosselin, G. (2007). The LaRonde Penna Au-rich volcanogenic massive sulfide deposit, Abitibi Greenstone Belt, Quebec: Part II. Lithogeochemistry and paleotectonic setting. *Economic Geology*, *102*(4), 611–631. https://doi.org/10.2113/gsecongeo.102.4.611

Miller, S. D., Jefferry, J. J., & Murray, G. S. C. (1990). Identification and Management of Acid Generating Mine Wastes - Procedures and Practices in South-East Asia and the Pacific Regions. *International Journal of Mine Water*, *9*(1), 57–67.

Mohammad, M., Tariq, M., Qadri, M. S., Latif, M., Tahiri, I. A., & Naz, L. (2015). Diffusion coefficient of iodide ions in aqueous medium and in vacuum: An appraisal. *Journal of the Chemical Society of Pakistan*, *37*(3), 440–446.

Morin, K. A., & Hutt, N. M. (1994). An Empirical Technique for Predicting the Chemistry of Water Seeping from Mine-Rock Piles. *Journal American Society of Mining and Reclamation*, *1994*(1), 12–19. https://doi.org/10.21000/jasmr94010012

Nakashima, Y. (2000). The use of X-ray CT to measure diffusion coefficients of heavy ions in water-saturated porous media. *Developments in Geotechnical Engineering*, *84*I, 11–17. https://doi.org/10.1016/s0013-7952(99)00130-1

Nicholson, R. V., Gillham, R. W., Cherry, J. A., & Reardon, E. J. (1989). Reduction of acid generation in mine tailings through the use of moisture-retaining cover layers as oxygen barriers. *Canadian Geotechnical Journal*, *26*(1), 1–8. https://doi.org/10.1139/t89-001

Nordstrom, D. K., & Southam, G. (1997). Geomicrobiology of sulfide mineral oxidation. *Geomicrobiology: Interactions Between Microbes and Minerals*, *35*(Reviews in Mineralogy), 361–390. https://doi.org/10.1515/9781501509247

Nunn, J. (2018). *Investigations of Partial Gas Saturation on Diffusion in Low- permeability Sedimentary Rocks*.

Nunn, J. A., Xiang, Y., & Al, T. A. (2018). Investigation of partial water saturation effects on diffusion in shale. *Applied Geochemistry*, *97*(July), 93–101. https://doi.org/10.1016/j.apgeochem.2018.08.004

Ouandji, F., Potter, E., Chen, W. R., & Liu, H. (2002). <title>Impact of focal spot size on the spatial resolution of a digital x-ray imaging system for small-animal studies</title>. *Biomedical Diagnostic, Guidance, and Surgical-Assist Systems IV*, *4615*, 109–116. https://doi.org/10.1117/12.466639

Palut, J. M., Montarnal, P., Gautschi, A., Tevissen, E., & Mouche, E. (2003). Characterisation of HTO diffusion properties by an in situ tracer experiment in Opalinus clay at Mont Terri. *Journal of Contaminant Hydrology*, *61*(1–4), 203–218. https://doi.org/10.1016/S0169-7722(02)00134-1

Parker, D. L., Couch, J. L., Peschmann, K. R., & Smith, V. (1982). Structured noise in computed tomography: Effects of peropdic error sources. *American Association of Physics in Medicine*, *9*(5), 722–731.

Parkhurst, D. L. (1995). *User's guide to PHREEQC: A computer program for speciation, reaction-path, advective-transport, and inverse geochemical calculations*.

Phelps, M. E., Gado, M. H., & Hoffman, E. J. (1975). Correlation of effective atomic number and electron density with attenuation coefficients measured with polychromatic x rays. *Radiology*, *117*(3), 585–588. Retrieved from https://ac.els-cdn.com/0016703774901458/1-s2.0-0016703774901458-main.pdf?_tid=b35975da-7bec-4114-bab2-ef1ca3163da1&acdnat=1542644091_a41d580f1d3f24f07fa2219e6d73d4b4

Pollio, F., & Kunin, R. (1967). Ion Exchange Processes for the Reclamation of Acid Mine Drainage Waters. *Environmental Science and Technology*, *1*(3), 235–241. https://doi.org/10.1021/es60003a002

Poludniowski, G., Landry, G., Deblois, F., Evans, P. M., & Verhaegen, F. (2009). SpekCalc: A program to calculate photon spectra from tungsten anode x-ray tubes. *Physics in Medicine and Biology*, *54*, N433–438. https://doi.org/10.1088/0031-9155/54/19/N01

Puura, E., & Neretnieks, I. (2000). Atmospheric oxidation of the pyritic waste rock in Maardu, Estonia, 2: An assessment of aluminosilicate buffering potential. *Environmental Geology*, *39*(6), 560–566. https://doi.org/10.1007/s002540050467

Reed, S. J. B. (2001). *ELECTRON MICROPROBE ANALYSIS AND SCANNING ELECTRON MICROSCOPY IN GEOLOGY*. *Encyclopedia of Materials: Science and Technology*. https://doi.org/10.1016/b0-08-043152-6/00464-2

Roche, R. C., Abel, R. A., Johnson, K. G., & Perry, C. T. (2010). Quantification of porosity in Acropora pulchra (Brook 1891) using X-ray micro-computed tomography techniques. *Journal of Experimental Marine Biology and Ecology*, *396*(1), 1–9. https://doi.org/10.1016/j.jembe.2010.10.006

Sardini, P., Delay, F., Hellmuth, K. H., Porel, G., & Oila, E. (2003). Interpretation of out-diffusion experiments on crystalline rocks using random walk modeling. *Journal of Contaminant Hydrology*, *61*(1–4), 339–350. https://doi.org/10.1016/S0169-7722(02)00124-9

Savoye, S., Goutelard, F., Beaucaire, C., Charles, Y., Fayette, A., Herbette, M., … Coelho, D. (2011). Effect of temperature on the containment properties of argillaceous rocks: The case study of Callovo-Oxfordian claystones. *Journal of Contaminant Hydrology*, *125*(1–4), 102–112. https://doi.org/10.1016/j.jconhyd.2011.05.004

Shackelford, C. D. (1991). Laboratory diffusion testing for waste disposal - A review. *Journal of Contaminant Hydrology*, *7*(3), 177–217. https://doi.org/10.1016/0169-7722(91)90028-Y

Šimůnek, J., Jarvis, N. J., Van Genuchten, M. T., & Gärdenäs, A. (2003). Review and comparison of models for describing non-equilibrium and preferential flow and transport in the vadose zone. *Journal of Hydrology*, *272*(1–4), 14–35. https://doi.org/10.1016/S0022-1694(02)00252-4

Smuda, J., Dold, B., Friese, K., Morgenstern, P., & Glaesser, W. (2007). Mineralogical and geochemical study of element mobility at the sulfide-rich Excelsior waste rock dump from the polymetallic Zn-Pb-(Ag-Bi-Cu) deposit, Cerro de Pasco, Peru. *Journal of Geochemical Exploration*, *92*(2–3), 97–110. https://doi.org/10.1016/j.gexplo.2006.08.001

Soret, M., Bacharach, S. L., & Buvat, I. (2007). Partial-volume effect in PET tumor imaging. *Journal of Nuclear Medicine*, *48*(6), 932–945. https://doi.org/10.2967/jnumed.106.035774

Steefel, C. I., & Lasaga, A. C. (1994). A coupled model for transport of multiple chemical species and kinetic precipitation/dissolution reactions with application to reactive flow in single phase hydrothermal systems. *American Journal of Science*. https://doi.org/10.2475/ajs.294.5.529

Subudhi, R. K., Hussein, E. M. A., & Al, T. A. (2010). Measurement of spatial distribution of total and accessible porosity in sedimentary rocks using isotopic radiation transmission: Device design and testing. *Applied Radiation and Isotopes*, *68*(3), 496–504. https://doi.org/10.1016/j.apradiso.2009.07.014

Sullivan, R. W., & van Staal, C. R. (1990). *U-Pb zircon ages of plagiogranite and gabbro from the ophiolitic Deveraux Formation, Fournier Group, northeastern New Brunswick*.

Taboada, T., & García, C. (1999). Pseudomorphic transformation of plagioclases during the weathering of granitic rocks in Galicia (NW Spain). *Catena*, *35*(2–4), 291–302. https://doi.org/10.1016/S0341-8162(98)00108-8

Tidwell, V. C., Meigs, L. C., Christian-frear, T., & Boney, C. M. (2000). Effects of spatially heterogeneous porosity on matrix diffusion as investigated by X-ray absorption imaging. *Journal of Contaminant Hydrology*, *42*, 285–302.

Tits, J., Jakob, A., Wieland, E., & Spieler, P. (2003). Diffusion of tritiated water and 22Na+ through non-degraded hardened cement pastes. *Journal of Contaminant Hydrology*, *61*(1–4), 45–62. https://doi.org/10.1016/S0169-7722(02)00112-2

Ussing, H. H. (1949). The Distinction by Means of Tracers Between Active Transport and Diffusion. *Acta Physiologica Scandinavica*, *19*(1), 43–56. https://doi.org/10.1111/j.1748-1716.1949.tb00633.x

Van Brakel, J., & Heertjees, P. M. (1974). Analysis of diffusion in macroporous media in terms of a porosity, a tortuosity and a constrictivity factor. *International Journal of Heat and Mass Transfer*, *17*(9), 1093–1103. https://doi.org/10.1080/14767058.2017.1403580

Van Der Kamp, G., Van Stempvoort, D. R., & Wassenaar, L. I. (1996). The radial diffusion method. 1. Using intact cores to determine isotopic composition, chemistry, and effective porosities for groundwater in aquitards. *Water Resources Research*, *32*(6), 1815–1822. https://doi.org/10.1029/95WR03719

van Genuchten, M. T., & Wierenga, P. J. (1976). Mass Transfer Studies in Sorbing Porous Media I. Analytical Solutions. *Soil Science Society of America Journal*, *40*(4), 473–480. https://doi.org/10.2136/sssaj1976.03615995004000040011x

Van Loon, L. R., Baeyens, B., & Bradbury, M. H. (2005). Diffusion and retention of sodium and strontium in Opalinus clay: Comparison of sorption data from diffusion and batch sorption measurements, and geochemical calculations. *Applied Geochemistry*, *20*(12), 2351–2363. https://doi.org/10.1016/j.apgeochem.2005.08.008

Van Loon, L. R., Soler, J. M., Jakob, A., & Bradbury, M. H. (2003). Effect of confining pressure on the diffusion of HTO, 36Cl- and 125I- in a layered argillaceous rock (Opalinus Clay): Diffusion perpendicular to the fabric. *Applied Geochemistry*, *18*(10), 1653–1662. https://doi.org/10.1016/S0883-2927(03)00047-7

Van Loon, L. R., Soler, J. M., Müller, W., & Bradbury, M. H. (2004). Anisotropic diffusion in layered argillaceous rocks: A case study with Opalinus Clay. *Environmental Science and Technology*, *38*(21), 5721–5728. https://doi.org/10.1021/es049937g

Wang, J. H., & Kennedy, J. W. (1950). Self-diffusion Coefficients of Sodium Ion and Iodide Ion in Aqueous Sodium Iodide Solutions. *Journal of the American Chemical Society*, *72*(5), 2080–2083. https://doi.org/10.1021/ja01161a056

Wersin, P., Van Loon, L. R., Soler, J. M., Yllera, A., Eikenberg, J., Gimmi, T., … Boisson, J. Y. (2004). Long-term diffusion experiment at Mont Terri: First results from field and laboratory data. *Applied Clay Science*, *26*(1-4 SPEC. ISS.), 123–135. https://doi.org/10.1016/j.clay.2003.09.007

Whalen, J. B., Percival, J. A., McNicoll, V. J., & Longstaffe, F. J. (2004). Geochemical and isotopic (Nd-O) evidence bearing on the origin of late- to post-orogenic high-K granitoid rocks in the Western Superior Province: Implications for late Archean tectonomagmatic processes. *Precambrian Research*, *132*(3), 303–326. https://doi.org/10.1016/j.precamres.2003.11.007

White, W. W., & Jeffers, T. H. (1994). Chemical Predictive Modeling of Acid Mine Drainage from Metallic Sulfide-Bearing Waste Rock. *American Chemical Society*, 608–630. https://doi.org/10.1021/bk-1994-0550.ch037

Wildenschild, D., Hopmans, J. W., Vaz, C. M. P., Rivers, M. L., Rikard, D., & Christensen, B. S. B. (2002). Using X-ray computed tomography in hydrology: systems, resolutions, and limitations. (Special Issue: Non-invasive methods in hydrology). *Journal of Hydrology*, *267*(3–4), 285–297. Retrieved from http://ovidsp.ovid.com/ovidweb.cgi?T=JS&CSC=Y&NEWS=N&PAGE=fulltext&D=caba5&AN=20023163752http://ucelinks.cdlib.org:8888/sfx_local?sid=OVID:cabadb&issn=00221694&isbn=&volume=267&issue=3%2F4&spage=285&date=2002&title=Journal+of+Hyrology+%28Amsterdam%29&at

Wunderly, M. D., Blowes, D. W., Frind, E. O., & Ptacek, C. . . (1996). Sulfide mineral oxidation and subsequent reactive transport of oxidation products in mine tailings impoundments: A numerical model. *WATER RESOURCES RESEARCH*, *32*(10), 3173–3187.

Xiang, Y., Al, T., Scott, L., & Loomer, D. (2013). Diffusive anisotropy in low-permeability Ordovician sedimentary rocks from the Michigan Basin in southwest Ontario. *Journal of Contaminant Hydrology*, *155*, 31–45. https://doi.org/10.1016/j.jconhyd.2013.09.002

Xu, T., Spycher, N., & Sonnenthal, E. (2004). *TOUGHREACT User's Guide: A Simulation*

Program for Non-isothermal Multiphase Reactive Transport in Variably Saturated Geologic Media, version 2.0. *Lawrence Berkeley National Laboratory University of California, Berkeley, CA 94720*. https://doi.org/10.2172/943451

Yanful, K. (1993). Oxygen Diffusion Through Soil Covers on Sulphidic Mine Tailings. *Journal of Geotechnieal Engineering*, *119*(8), 1207–1228.

Appendices

Appendix A Radiography Experiment Background

A1. Diffusive solute transport in porous geologic media

The diffusive flux (J) of molecules dissolved in a medium (minerals, liquids, gases, glasses, etc.) in direction i is proportional to the following concentration gradient. In a steady state medium, conservative solute transport can be defined using Fick's first law (Crank, 1975);

$$J_{Di} = -D\frac{\partial C}{\partial x_i}$$

where D (m^2/s) is a solute specific diffusion coefficient, C (mol/m^3) is the concentration of that solute over distance x (m) in direction i. Under transient conditions, the derivative of Fick's first law (Fick's second law) describes the rate of compositional change over time as being proportional to the rate of change in the concentration gradient;

$$\frac{\partial C}{\partial t} = D\frac{\partial^2 C}{\partial x^2}$$

In geologic media, where diffusive transport is the dominant process in regions of hydraulic conductivity less than 10e-10 m/s such as micro-fractures, matrix pore space and secondary mineral coatings. The path by which the solute travels is affected by tortuosity (τ), constrictivity (δ) (Van Brakel and Heertjees, 1974);

$$D_P = D_0\,{}^{\delta}\!/_{\tau}$$

Where the pore diffusion (D_p) is proportional to the free water diffusion coefficient of the solute, constrictivity; a geometric parameter relating pore-throat to solute size (Boving and Grathwohl, 2001) and tortuosity; a term that accounts for the actual path (le) a solute may travel through the geometry of pore and void space over the pathlength (l) in direction i (Van Brakel and Heertjees, 1974). Constrictivity and tortuosity can be defined together as the tortuosity factor (τ_f). Together, D_p; how a solute will travel through a porous medium and porosity (ϕ_I); the amount of pore (non-solid) space available for a solute to travel through, are proportionate to the effective diffusion coefficient (D_e).

Not all pores are interconnected or available for the solute to access due to pore-throat size and diffuse-double layer effects (Bolt, 1979). Therefore, in tracer experiments, this porosity term can be defined more explicitly by the solute accessible porosity term; (ϕ_s) where s is the symbol of the tracer element. Once the tracer has completely saturated the pore space to maximum capacity (reached steady-state), f_s is determined using radiography techniques described by Cavé et al., 2009.

A2. X-ray Radiography

A2.1. Principles of Radiography

Radiography is an imaging method that uses a source to emit a spectrum of X-ray energies (keV) and intensities (mA). The incident cone beam travels through the material on the stage (the object) and the transmitted beam continues on to the detector where the partially attenuated photon energy is quantized by a detector as a two-dimensional array of counting statistics (Fig. A.1). The amount of X-ray energy that is attenuated is proportional to the physical density, chemical composition and path length through each respective material in the object being imaged as well as the distance from the source to the detector (air) (Deslattes, 1969; Phelps et al., 1975).

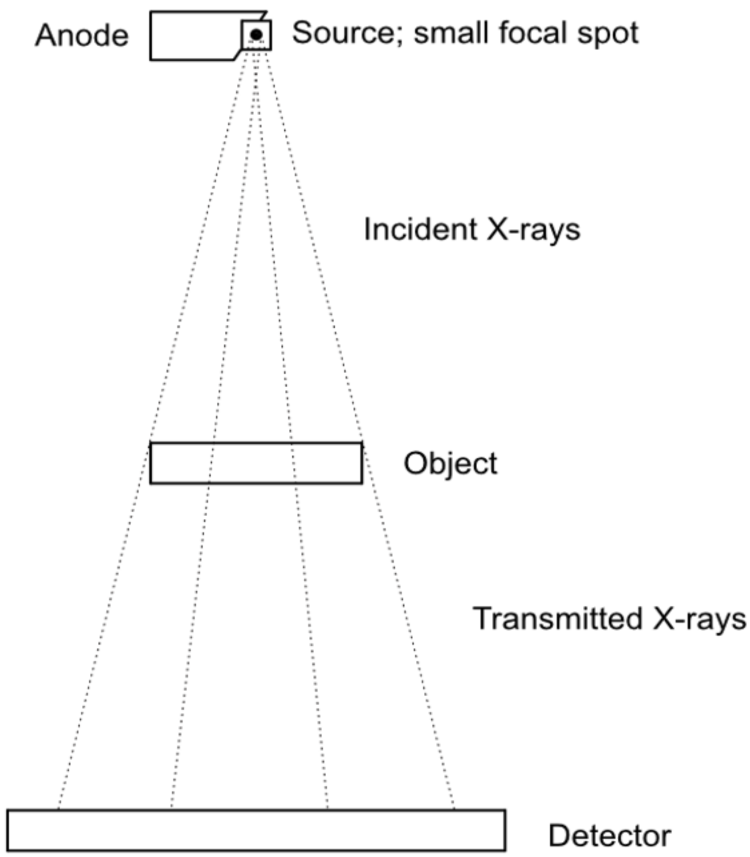

Figure A. 1. *Geometry the internal parts of an x-ray instrument used to generate radiographs. After* (J. Nunn, 2018).

A2.2. The Source

X-ray radiation is produced by applying an AC to a cathode wire where the current heats up the wire causing exited electrons to exit their orbitals and leave the wire (Boone and Seibert, 1997; Desponds et al., 1991). As they leave the wire, they move across the electric potential between the negatively charged cathode and positive anode (Fig. A.2). At the Tungsten anode, the electron will either knock out an electron from an inner orbital releasing what is called characteristic photon energy or it will pass by the tungsten atoms and bend (Nakashima, 2000; Wildenschild et al., 2002).

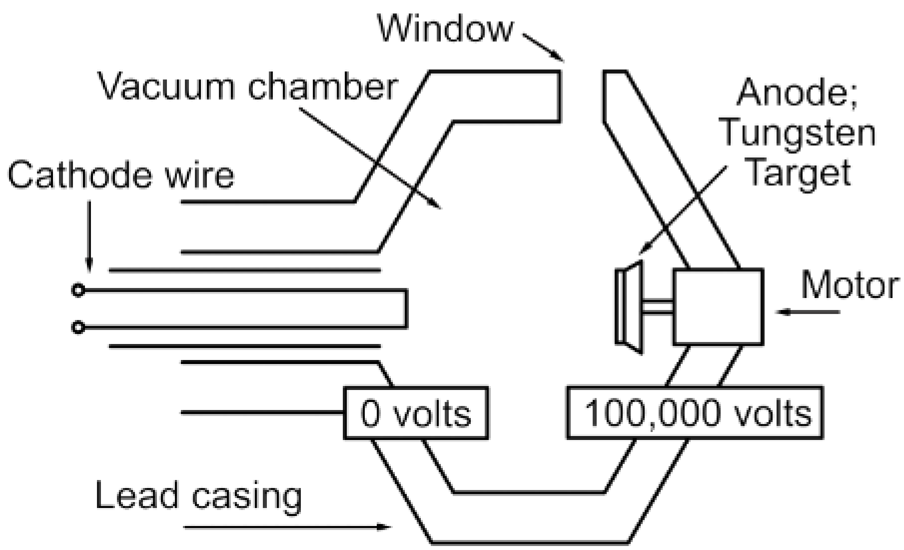

Figure A. 2. *Schematic of an x-ray tube used to generate photons for radiography. Electrons travel from the cathode across the tube to the turning anode where photons are released and exit the chamber through a window where they become the transmitted spectrum.*

If the electron passes close to the atom, it’s path will be bent more than an electron passing at a greater distance. This change in direction causes the electron to first accelerate then slow down at a rate dependent on proximity, the amount an electron is accelerated is proportional to the release of energy upon slowing down ,this is called Bremsstrahlung radiation. This variance in energy release produces the continuum of energies seen in Fig. A.3. As a result, Bremsstrahlung radiation accounts for most of the area under the curve while characteristic x-rays are illustrated by the peak in intensity; number of photons emitted at a specific energy (Reed, 2001). These processes combine to produce a polychromatic X-ray spectrum (PCXS).

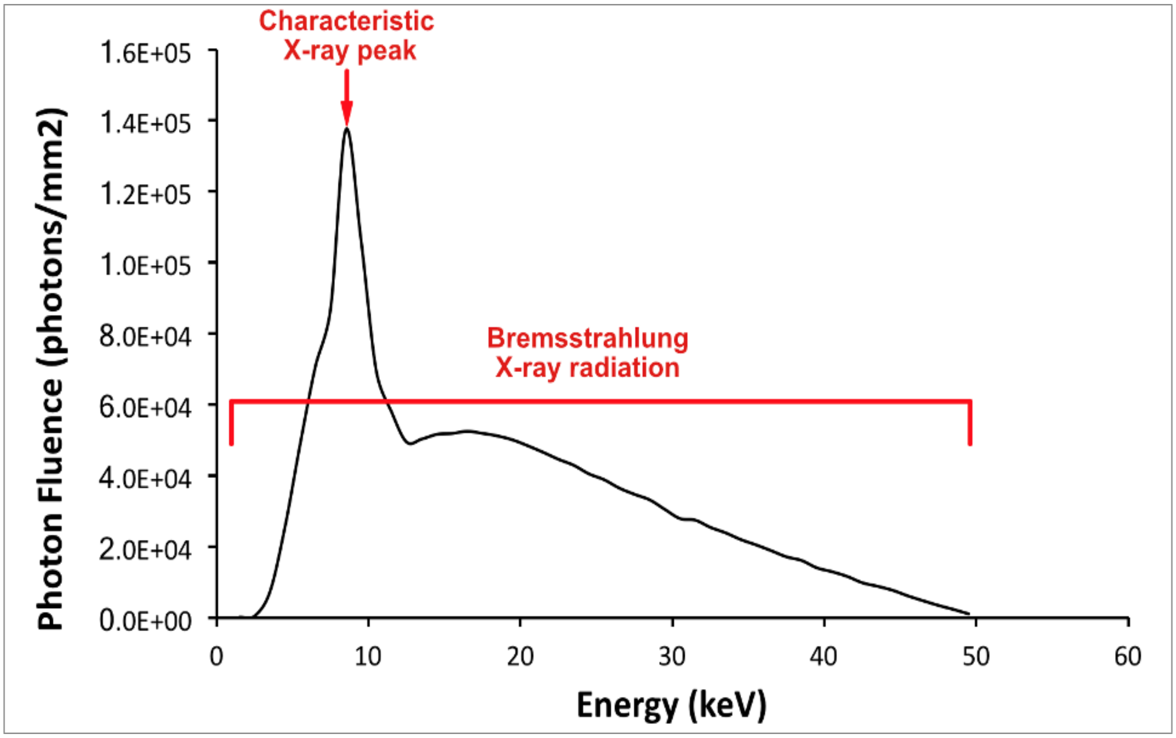

Figure A. 3. *Calculated x-ray emissions spectrum with a peak energy of 50 keV by the tungsten anode spectral model using interpolating cubic splines (TASMICS) (Hernandez and Boone 2014). Calculations were conducted with SpekCalc* (Poludniowski et al., 2009). *After* (J. Nunn, 2018).

As X-rays increase in energy, their wavelength decreases. X-rays of shorter wavelength have more penetrative ability than longer ones. Energies in the lower end of this spectrum (1-10 keV) are considered "soft X-rays" because they are more sensitive to elements with lower atomic numbers and are readily adsorbed by these materials. The higher end of this spectrum known as "hard X-rays" (11-50 keV) is less sensitive to chemical composition due to its greater penetrative ability. Therefore, dense, thick or highly attenuating samples require higher energies to produce a significant number of photons that penetrate the object. Another method for producing more photons in the transmitted spectrum and as a result higher counting statistics, the user can increase the current, which increases the number of photons in the incident spectrum.

A2.3 X-ray attenuation

The difference in number of photons between the incident and transmitted spectrum is controlled by the attenuation properties of the object. Photon attenuation will occur either through absorption or scattering. Depending on the energy of the photon in question, one of the following three process will be responsible for attenuation; the photo electric effect, Compton scattering or pair production.

> 1. Photo electric effect; observed from >1 to 100 keV. An incident photon loses all of its energy to an inner shell electron during an inelastic interaction that ejects the electron from its orbital, for this occur; the binding energy of this electron must be greater than the energy of the incident photon (Hussein, 2007). Additionally, if the energy of the incident

photon is proportional to the binding energy of an elements k shell (innermost) electron, there is an increased likelihood of photoelectric absorption occurrence. The binding energy of the inner-shell electrons for each element is called the k-edge.

2. Compton scattering; observed from 50 to 150 keV, typically the dominant attenuation process between 60 to 100 keV. Occurs when an incident photon ejects an atoms outer shell electron from its orbital and deflects in another direction having lost energy during the interaction (Hussein, 2007).

3. Pair production; is the dominant attenuation process over 100 keV. This is a photon absorption event where the incident photon interacts with a neutron, producing both an electron and positron (Hussein, 2007).

The basic attenuation equation detailing the attenuation a mono-energetic incident photon beam interacting with a homogeneous material is Beer's law;

$$I = I_0 \exp\,(-\mu d)$$

Where I is the transmitted intensity, I_0 is the incident intensity, m is the attenuation coefficient of the specific material and x is the linear path-length through the material.

For objects comprised of multiple materials along the same path-length; the term containing the attenuation coefficient and path-length is updated to sum the attenuation coefficients of all materials over their respective extents of the photon path-length through the object;

$$I = I_0 \exp\,[-\Sigma_i(\mu_i x_i)]$$

For polychromatic X-ray sources, a comprehensive equation is used to estimate the transmitted intensity by quantifying the amount of attenuation for the range of incident energies and intensities along a path-length through a heterogeneous-multicomponent object.
where d is a porosity term.

A2.4. Detector

The detector used for this research is a flat-panel amorphous-silicon based (Varian PaxScan1313DX) 2D-digital image receptor. Images are generated by 1024 by 1024 array of CsI scintillators that produce light energy for every X-ray photon that hits a grid cell on the panel. Within each cell, the light of numerous photons is converted into electrons that are counted and quantized into 16-bit greyscale values by photodiodes (pixel pitch 127 mm^2, limiting resolution; 3.94 1p/mm) and recorded by a thin film transistor (TFT) grid.

A2.5 Image magnification and resolution

The instrument geometry and parameter settings can be manipulated to obtain higher resolution and control the signal to noise ratio (SNR) (Giger et al., 1986). As electrons from the cathode strike the tungsten anode, X-rays are generated from the interaction zone in the anode called the focal spot. If we have a high current, we must have a correspondingly large focal spot to distribute the current over an area that does not result in burning of the tungsten anode. Choosing a high photon flux and larger focal spot will increase SNR. Alternatively, with less current we can reduce the spot size, providing higher spatial resolution which can be explained by the penumbra effect (or "shadow") (Fig. A.4) (Ouandji et al., 2002). For both small and large focal spot sizes, a point source generates divergent photons (a cone beam) that interact with an object and produce blurring along all edges of subjects in the object that are not positioned directly between the center of the source and the detector. Small spot sizes produce a sharp rim and larger focal spots produce a shadow of significant finite width.

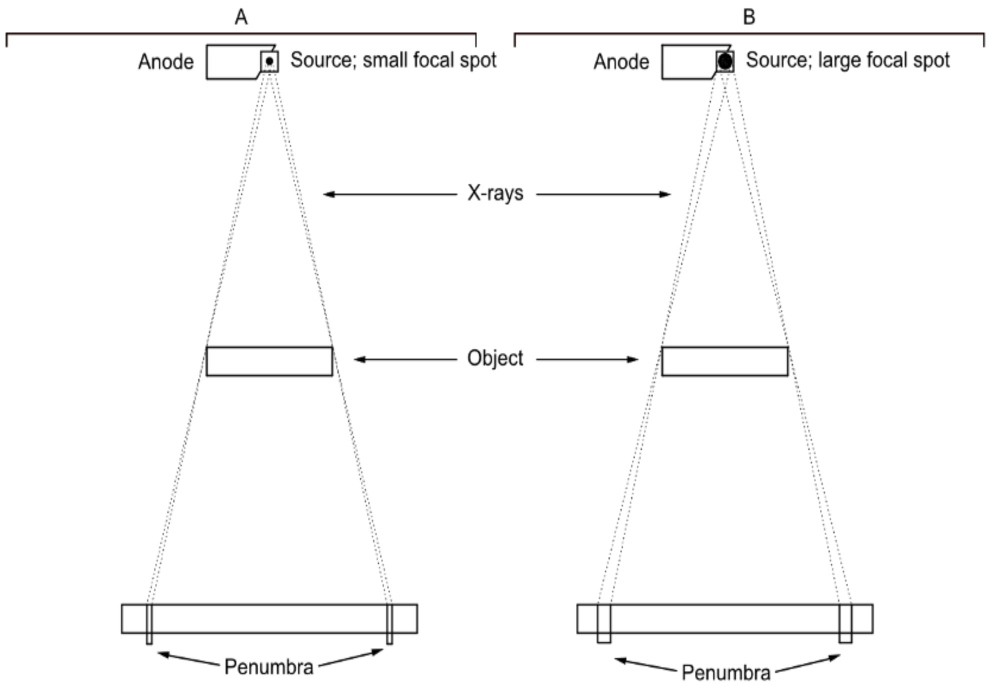

Figure A. 4. *Difference in penumbra magnitude generated by both a small (scenario A) and large focal spot (scenario B). After* (J. Nunn, 2018).

Spatial resolution of the object itself can be heightened by decreasing magnification (increasing SOD and decreasing ODD) (Fig. A.5). Magnification can be adjusted using the following calculation;

$$M = \frac{SDD}{SOD}$$

Where SDD is the source to detector distance and SOD is the source to object distance.

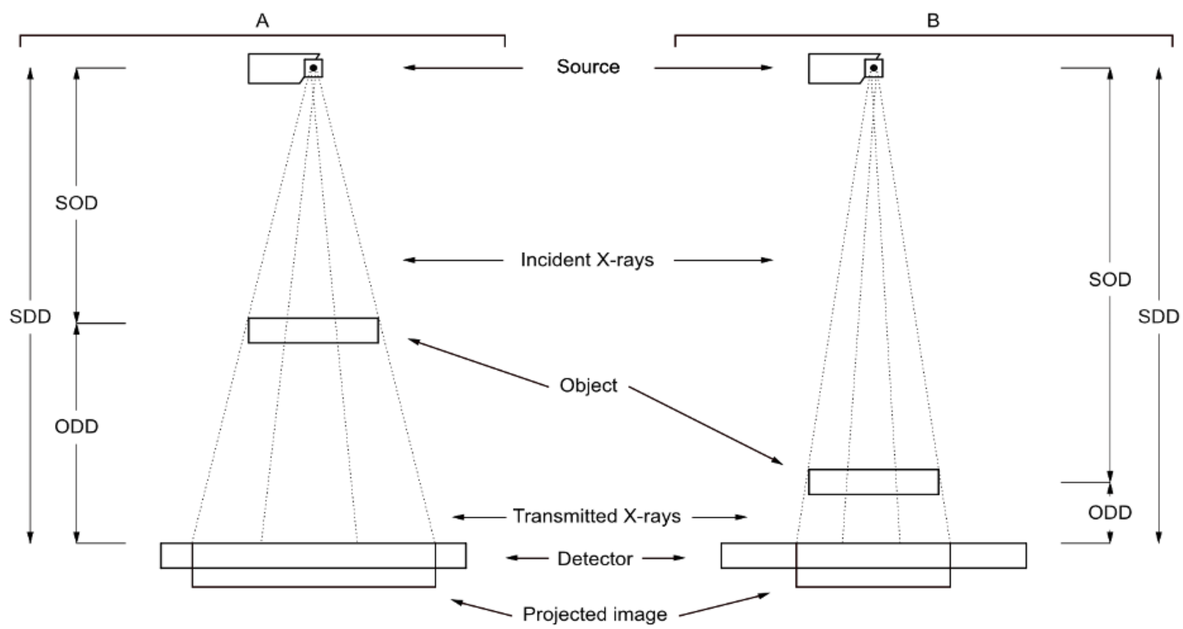

Figure A. 5. Difference in magnification due to adjustments in instrument geometry depicted by scenario A and B. The magnification of an object (projected image) will decrease as SOD increases. *After* (J. Nunn, 2018).

A2.6 Limitations of X-ray radiography using a polychromatic source

For the purposes of this section, limitations can be thought of possible sources of error that if considered, planned for and designed around before starting the experimental process, are able to be reduced. Previous investigations and method development in determining the porosity of geologic media (Agbogun et al., 2013; Cavé et al., 2009; Tidwell et al., 2000; Xiang et al., 2013) and tracer diffusion (Agbogun et al, 2013; Altman et al, 2004; Cavé et al, 2009; Loomer et al, 2013; Xiang et al., 2013) have advanced radiographic approaches and are valuable resources for mitigating error in current experiments. Possible limitations or sources of error may be the result of; poor SNR, beam hardening, instrumental drift, misalignment and partial volume effects.

For conservative-tracer imaging in geologic media, the elemental composition and attenuation properties of the solid porous media are assumed to remain constant though-out the experiment. The signal of interest for this research is the additional attenuation caused by the increase of attenuating-tracer quantity within pore space. Noise can be defined as fluctuations in background attenuation (geologic media) not caused by tracer attenuation (Giger et al., 1986; Ketcham and Carlson, 2001). Examples of noise include a “hot” pixel, random differences in source-detector pairs between radiographs, low current (too few photons to acquire good signal) also known as the quantum mottle effect and high current/energy leading to detector saturation. SNR can be calculated using the following equation;

$$SNR = \frac{\Delta I}{\sigma}$$

Where ΔI is the change in background intensity due to tracer attenuation (Fig. A.6) and σ is the change in overall intensity between multiple-consecutive images of an object without significant difference between radiographs (must be aligned & normalized).

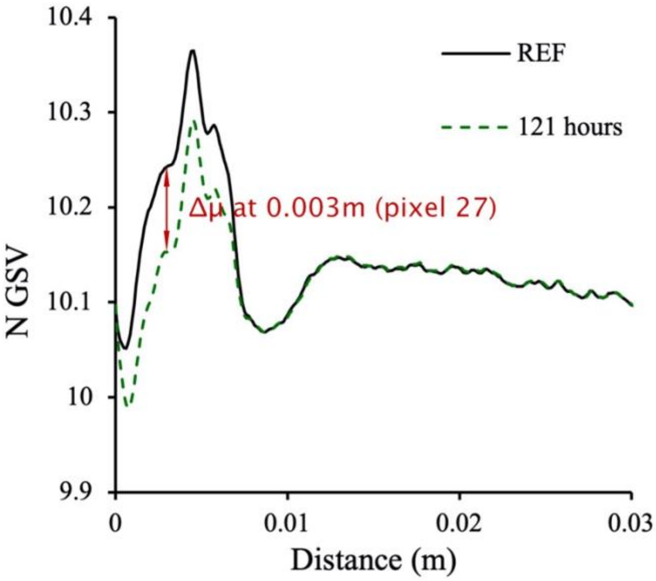

Figure A. 6. *Greyscale value (GSV) profiles from a region of interest (ROI) in sample STB using x-ray radiography and difference imaging* (Cavé et al., 2009) *to display the change in overall intensity due to the ingress of 0.5 M Iodide tracer. After* (J. Nunn, 2018).

Considering that there may always be a small amount of noise, the solution for achieving the best SNR is to set the instrument parameters such that there is both significant penetration without reaching transmitted intensities that harm or saturated the detector and sensitivity to all the features of interest.

Beam hardening (most frequently encountered during X-ray CT scans) is the preferential attenuation of "soft" X-rays when using a polychromatic source (Clausnitzer and Hopmans, 2000; Ketcham and Carlson, 2001; Roche et al., 2010). This artifact may be identified by materials in areas of lower thickness appear to be more attenuating than the same materials in areas of higher object thickness due to the equal removal of lower energy photons across the surface the heterogeneous object. Note, in both areas the effective attenuation coefficient will appear to increase (Ketcham and Carlson, 2001). The artifact may also be observed when the center of spherical or cylindrical objects appear to be more attenuating (darker) than the edges of the object where it is most thin (Ketcham and Carlson, 2001).

Many sample preparation and data processing solutions exist to remedy this artifact. The most effective mitigation techniques are to use smaller sample sizes or to the pre-harden the beam by fixing a copper, brass or aluminum plate over the source (Ketcham and Carlson, 2001). This plate will vary in thickness to remove photons of the user's desired energies. Alternatively, the user could implement a monochromatic beam if available.

Despite the user entering a specific current and amperage between successive radiographs or between time series radiographs of the same sample. Instrumental drift is the artificial variance in transmitted photon counts that may be observed in regions where attenuation properties have not changed between radiographs. There are many causes for drift such as the inherent statistical variability involved with the production of X-ray photons by Bremsstrahlung radiation, heating of the source anode fluctuations in power supply of the energy grid, variance in time in between each radiograph to allow the detector to recover (return to baseline), calibration drift, setting parameters manually and more. One method of mitigation is to include an internal standard in sample preparation and normalize all data to the first (or any) radiograph of that sample (Agbogun et al., 2013; Cavé et al., 2009).

Sample misalignment between time series radiographs and successive radiographs of similar instrument geometry with different samples is a common occurrence. For time series radiographs, misalignment is often caused by slight error in the instrument sensors when parts are digitally repositioning for the homing sequence or to pre-set geometries. This error can be mitigated using alignment guides; have attenuation contrast from other materials, spatially comprise one pixel, more than three are used. With these guides the user can manually change the geometry such that the guides fixed to the sample are in the same position for all radiographs (Cavé et al., 2009).

Partial volume effects are to be expected when conducting attenuating tracer tests on heterogeneous porous geologic media (Ketcham and Carlson, 2001). The use of pre-filtered X-ray beams (between 40 to 60 keV) and high current (between 30 and 50 mA) are commonly used settings to obtain adequate SNR. The use of high energies and intensities require a large focal spot size and thus limited resolution. This effect occurs within the pixels or cells of the TFT detector grid where the transmitted photons from two or more materials proximal in physical space are registered within the same cell. In other words, the output data for cell volumes comprised of more than one materials transmission data are reporting averaged counting statistics defined by the proportional representation of each material property in that cell (Fig. A.7) (Ketcham and Carlson, 2001).

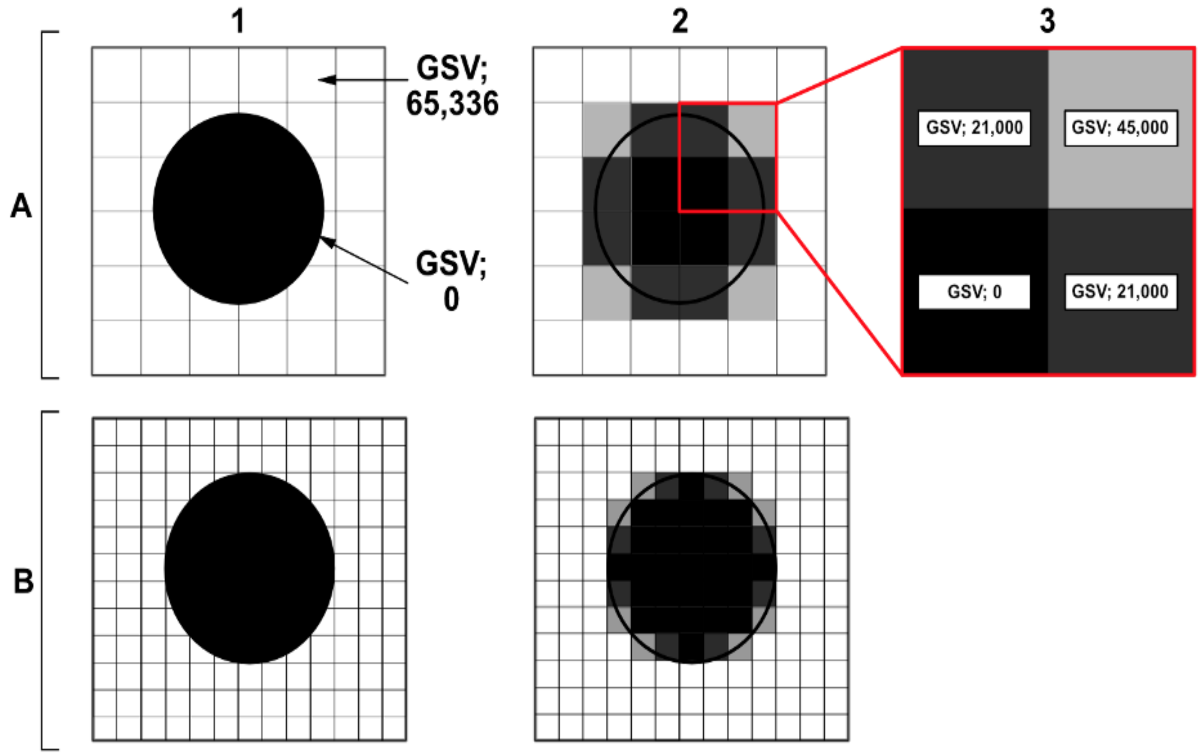

Figure A. 7. *A1) Signal of an object on a detector. A2) Spatial distribution of signal in a lower resolution grid. A3) greyscale value at each pixel showing ratio of attenuating object (0) to un-attenuated source-detectors path values (65,336) B1 & 2) show the same physical properties as in scenario A, with increased resolution (pixel count) resulting in more defined and less blended features in the projected image of the object. Figure modified from* (Soret et al, 2007)*, after* (J. Nunn, 2018).

Appendix B Measuring D_P in one-dimension; LaRonde and Restigouche Mine Samples

B.1 Introduction

In metal mining operations, species concentrations and persistence of hazardous leachate from variably saturated waste rock is estimated using predictive models that have been developed using estimated or no diffusion coefficient input (Banwart and Malmström, 2001; Eriksson and Destouni, 1997; Lahmira et al., 2007; Morin and Hutt, 1994; White and Jeffers, 1994). It is common that sources of error in these models can be attributed to reaction and transport rates controlling solute mobility and discharge quality. Additionally, conceptual models neglect how diffusive transport rates may evolve as a result of sulfide mineral oxidation leading to changes in porosity, tortuosity, and secondary mineral precipitation. The objective of this research is to;

1) quantify the change in diffusive properties between the unaltered core and oxidized rim of common acid generating rock types, and
2) quantify the difference between the diffusive properties of these rocks when solutes are travelling parallel and normal to the dominant foliation plane by measuring their respective D_P in one-dimension.

B.2 Methods

B.2.1 Sample descriptions

B.2.1.1 Laronde Mine; quartz-sericite schist

A foliated and minimally oxidized waste rock from the metamorphosed basaltic to rhyolitic sequences of the upper member Bousquet Formation in the Blake River Group was chosen for this study based on its acid generating potential and anisotropic solute transport properties. The dominant mineralogical assemblage is quartz (45%), sericite (30%), and sulfides (15%). The waste rock fragment has a general plated structure and is split along foliation planes into thin sub-millimeter layers and sulfide minerals occurring primarily along foliation planes.

B.2.1.2 Restigouche Mine; quartz-biotite schist, quartz-muscovite schist, and meta-volcanic rock.

Waste rock fragments at the Restigouche Mine come from the Mount Brittain Formation of the California Lake Group. This group represents a felsic volcanic succession composed dominantly of feldspar-quartz porphyritic dacitic to rhyolitic volcanic rocks. The quartz-biotite schist was chosen because of its sulfide content and mineralogical heterogeneity characterized by a distinct oxidized rim (>1.5cm thick) surrounding the unaltered core. The quartz-muscovite schist in addition to a thin oxidized rim (<6mm) displayed foliation and an unaltered mineral assemblage inclined to display significant changes in diffusive properties post-sulfide mineral oxidation due to the presence of a primary carbonate mineral phase. The meta-volcanic rock was also chosen based on its heterogeneous mineralogical properties between the unaltered core and intermediate oxidized rim (approximately 1cm thick). The dominant mineralogy of these lithologies and their respective sub-types can be found in Table 1.

B.2.2 Measuring porosity and D_P in 1-D

B.2.2.1 Sample preparation and acquisition parameters

Samples prepared for one-dimensional analysis were drilled using a diamond coring bit 20 mm in diameter. Drilled cores range from 11 to 20mm in length, using water to cool the bit. Oxygen held within the pore space was flushed out and replaced with water soluble CO_2. The sample is then placed in a beaker within a vacuum chamber to become saturated with a 0.5 M $NaNO_3$ synthetic pore-water (SPW). One-fourth of the samples height of SPW is added to the beaker daily until the core is submerged and left undisturbed for two weeks allowing the SPW to access all available porosity. Preparing the core to be mounted on the diffusion cell (Fig. 2.2) requires the peripheral surface of the core is patted dry with Kim-wipes® and a thin layer of 100% silicone rubber sealant is applied to the dried surface once removed from the vacuum chamber. A felt pad 1.9cm in diameter is placed on the top and bottom diffusive surfaces with an aluminum standard set above the top felt pad. Heat-shrink tubing is used to secure this assemblage, which is then fixed on the diffusion cell using West System epoxy (105 resin and 205 fast hardener). To ensure a tight seal between to peripheral surface of the sample and the inner surface of the heat-shrink tube, a heat-shrink clamp (13/16" to 15/16" in diameter) is placed from bottom of the core to the bottom of the aluminum standard. Finally, a lead ball is fixed to the aluminum standard for registration.

Porosity and T-SPW measurements are conducted using the radiography techniques of Cavé et al., (2009). Experimental measurements were conducted on an x-ray CT system (Pinnacle, X-ray Systems, Atlanta, Georgia) equipped with a Varian® NDI-160/22 source that used a Gulmay® CPL series (CP2-1402) 3000W generator to emit a spectrum of energies and intensities, quantified by an amorphous-silicon flat-panel detector (Varian PaxScan® 1313DX). All images were taken as triplicate 16-bit or duplicate 32-bit tiff files, the acquisition parameters used for radiography can be found in Table (2.2).

B.2.2.2 Radiography

The experiment begins when SPW in the reservoir is replaced with a 0.5M NaI T-SPW. The reservoir (Fig. 2.2) is positioned below the sample to eliminate the risk of the higher density T-SPW mixing with the SPW within the pore space of the sample. Reference images (t = 0) are taken as soon as possible after the introduction of the tracer. All radiographs of a sample are acquired using the same sample positioning and operating conditions. Additionally, radiographs collected after the reference image are converted into one-dimensional profiles that quantify changes in x-ray attenuation along the height of the core using the method described by Cavé et al., (2009). Subsequent radiographs are acquired at 4, 10, 24, 35 and 48 hours, and then daily. T-SPW in the diffusion cell reservoir is replaced after each radiograph to remove depleted tracer solution and maintain a constant tracer concentration at the influx boundary to rock fragment pore space. When tracer breakthrough is observed at the top of the sample, T-SPW is introduced at both the top and bottom of the sample to achieve complete saturation indicated by no change in attenuation ($\Delta\mu$) between radiographs. At which point, final tracer-saturated images are acquired and Iodide accessible porosity (ϕ_I) and relative concentration (C/C_0) profiles can be quantified based on methods described by Xiang et al. (2013) and Cavé et al. (2009) respectively.

B.3 Results

B.3.1 Porosity

Intro explaining how many samples there were and why only a certain amount of samples were used for porosity 2D representations.

B.3.1.1 Quartz-sericite schist

Processed x-ray radiography images indicate significant fluctuations in porosity (Fig. A.B.1) along the one-dimensional profiles. The average ϕ_I values along the 1-D profiles are 0.088, 0.111, 0.096 and 0.146 (Table 3.7), indicating that ϕ_I ranges from 37 to 61% of the ϕ_w values measured. The fluctuation in porosity is greater when represented in two-dimensions and can be attributed to the heterogeneity of geologic material within the core sample (Fig. A.B.2). This increase in fluctuation is best represented in sample LR11b where porosity ranges from 0.09 to 0.13 along the 1-D profile of averaged ϕ_I values, contrast to the range of 0.02 to 0.24 observed in the 2-D porosity distribution along the same diffusion profile. Coordinate locations of high and low porosity intersect with regions of high and low gsv, respectively. Mineral phases found in this rock type associated with high and low gsv are quartz or sericite, and sulfides veins, respectively. A porosity distribution of this sample (Fig. A.B.3) displays a multimodal curve indicating a heterogeneous material with multiple mineral phases controlling porosity. Samples LR11a and LR13 are strongly bimodal to weekly multimodal.

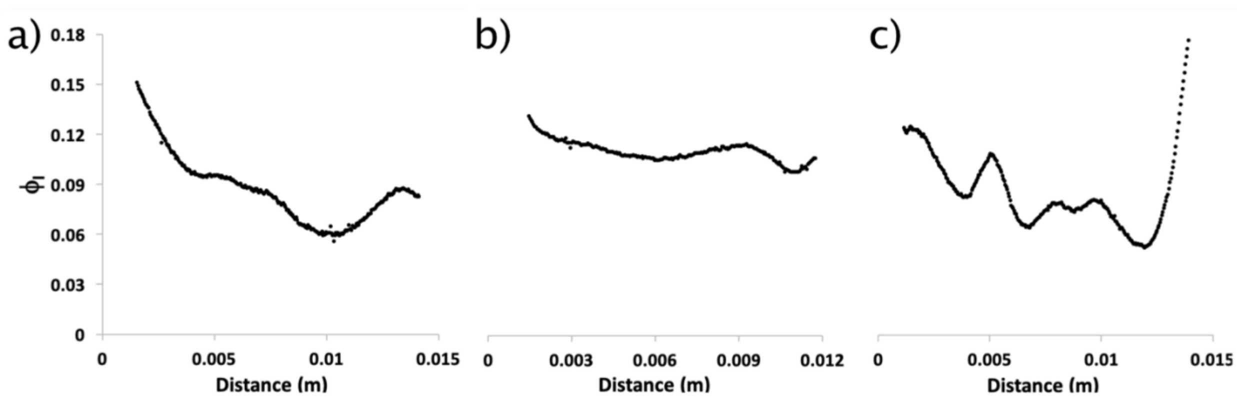

Figure B. 1. *Spatial distribution of ϕ_I values along the 1-D profile of cores drilled parallel (a and b) and normal (c) to the dominant foliation plane of a quartz-sericite schist waste rock fragment from Laronde Mine.*

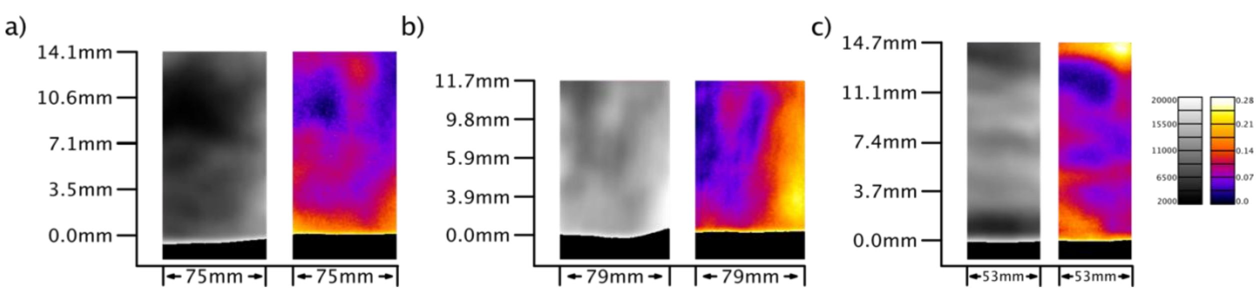

Figure B. 2. *2-D distribution of ϕ_I values, reconstructed using the 1-D profiles of the quartz-sericite schist waste rock fragment from Laronde Mine.*

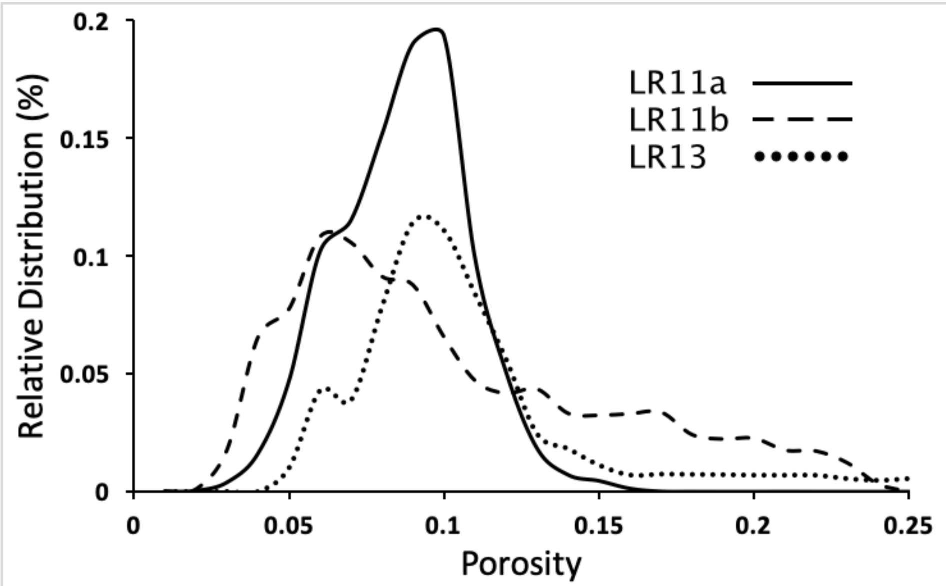

Figure B. 3. *Relative porosity distribution within sub-samples of the quartz-sericite schist waste rock fragment from Laronde Mine.*

B.3.1.2 Quartz-biotite schist

Processed x-ray radiograph images of the partially oxidized core (RM33) (Fig. A.B.4a) display minor fluctuations in porosity and larger fluctuations along the one-dimensional profile the unaltered core (RM32a) (Fig. A.B.4b). The average φ_I values along the 1-D profile of the oxidized and unaltered cores are 0.74 and 0.084, respectively, and are approximately equal to the measured values of ϕ_w (Table 3.7). 2-D regions of high and low porosity in the unaltered core intersect with areas of high, and both high and low gsv, respectively (Fig. A.B.5a). The partially-oxidized core has a less extreme porosity distribution (Fig. A.B.5b), high and low porosity regions both intersect with areas of high and low gsv. Mineral phases found in this rock type associated with high and low gsv are quartz, or biotite, and sulfides grains, ferrihydrite, or arsenic-rich iron-oxide, respectively. The 2-D porosity reconstruction of the unaltered 1-D profile (Fig. A.B.6) displays a wide unimodal distribution compared to oxidized unimodal porosity distribution. The singular peak of the unaltered distribution may be caused a homogenous distribution of the quartz-biotite matrix surrounding sulfide grains across the length of the core. Relative to the unaltered core, the peak of the oxidized distribution has increased in frequency, shifted to a lower mean porosity, and the distribution of high porosity values (12-20%) has remained equivalent. The shift may have been caused by iron-oxide or ferrihydrite precipitating in matrix pore space after the dissolution of sulfide grains, contributing to the maintenance of the high-porosity relative distribution.

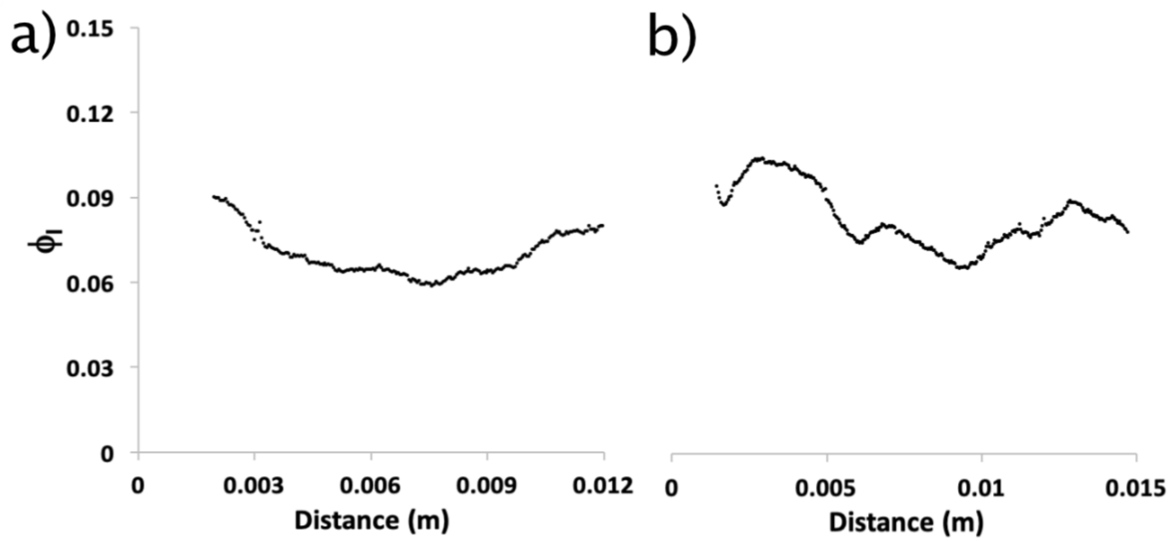

Figure B. 4. *Spatial distribution of ϕ_I values along the 1-D profile of cores drilled parallel to the dominant foliation plane in the a) oxidized and b) unaltered domain of a quartz-biotite schist waste rock fragment from Restigouche Mine.*

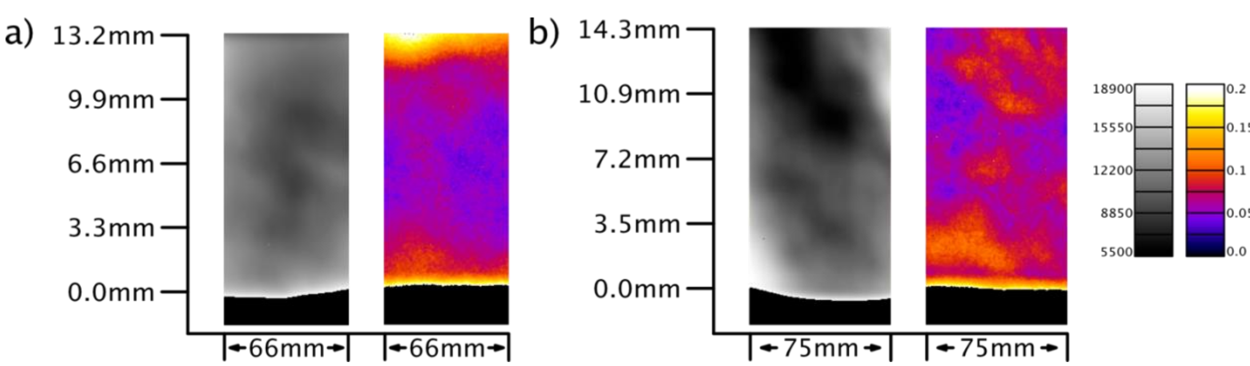

Figure B. 5. *2-D distribution of ϕ_I values, reconstructed using the 1-D profiles of the quartz-biotite schist waste rock fragment from Restigouche Mine.*

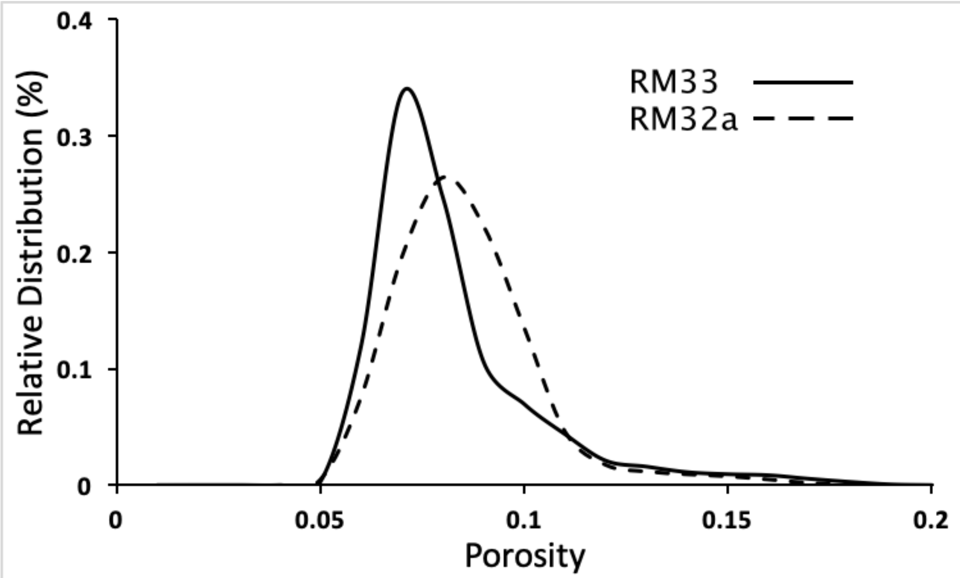

Figure B. 6. *Relative porosity distribution within sub-samples of the quartz-biotite schist waste rock fragment from Restigouche Mine.*

B.3.1.3 Meta-volcanic rock

Processed x-ray radiography images indicate minor fluctuations in porosity (Fig. A.B.7) along the one-dimensional profiles of cores RM41 and RM44a. The oxidized core (RM41) displays two segments of increased porosity along the declining profile that align with the location of two large oxidized pyrite grains. The declining profile may be caused by the greater degree of oxidation and weathering the outer-most region waste rock fragment received, the mechanical disruption caused by drilling, and/or the potential lack of complete Iodide tracer saturation. The unaltered core (RM44a) has an initial declining trend that stabilizes after 0.004m. The average ϕ_I values along the 1-D profile of the oxidized and unaltered cores are 0.06 and 0.095, respectively, and are approximately equal to the ϕ_I values measured (Table 3.7). The porosity increase in the oxidized core over the region of the two large oxidized sulfide grains is confirmed by the two-dimensional representation (Fig. A.B.8a). A similar observation is quantified in the 2-D porosity distribution of the unaltered core (Fig. A.B.8b) where porosity is higher where sulfide grains are located. Mineral phases found in this rock type associated with high and low gsv are quartz, or muscovite, and sulfides grains, ferrihydrite, or arsenic-rich iron-oxide, respectively. The 2-D porosity reconstruction of the unaltered 1-D profile (Fig. A.B.9) displays a narrow distribution compared to oxidized porosity distribution that is multimodal. The singular narrow peak of the unaltered distribution may be caused by the overlapping of similar diffusion properties of two or more geologic materials, or a homogenous distribution of the quartz-muscovite matrix across the length of the core. The multimodal distribution of the oxidized core suggests the dissolution of the material accounting for 10% porosity and the precipitation of minerals phases that have dominantly reduced and in-part increased porosity.

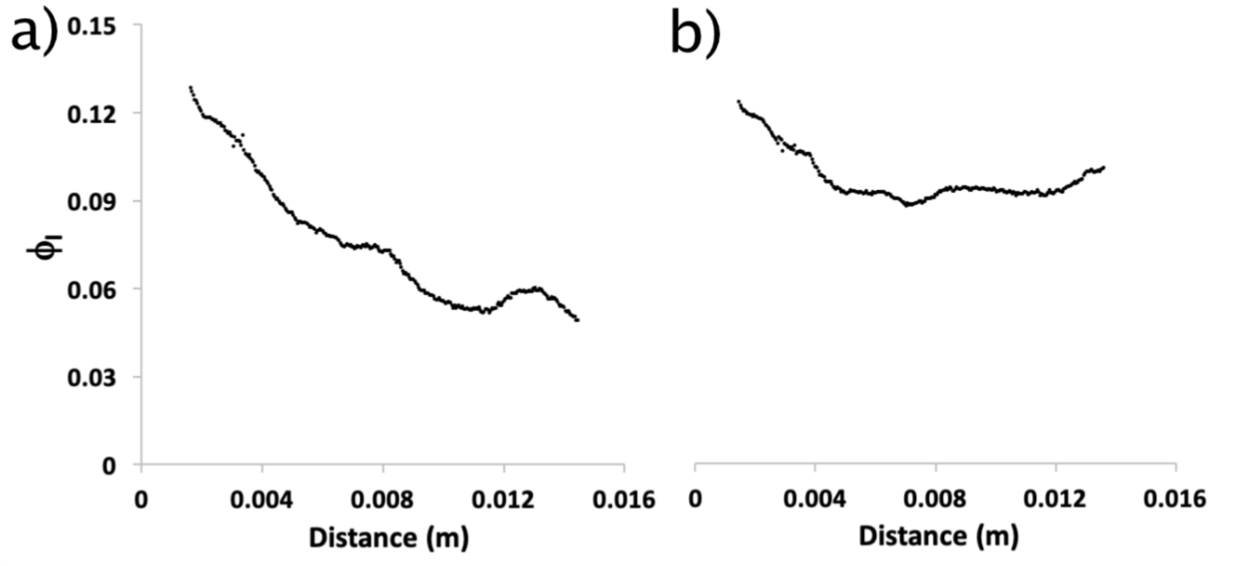

Figure B. 7. *Spatial distribution of ϕ_I values along the 1-D profile of cores drilled in the oxidized (a) and unaltered domain (b) of a meta-volcanic waste rock fragment from Restigouche Mine. No dominant foliation plane.*

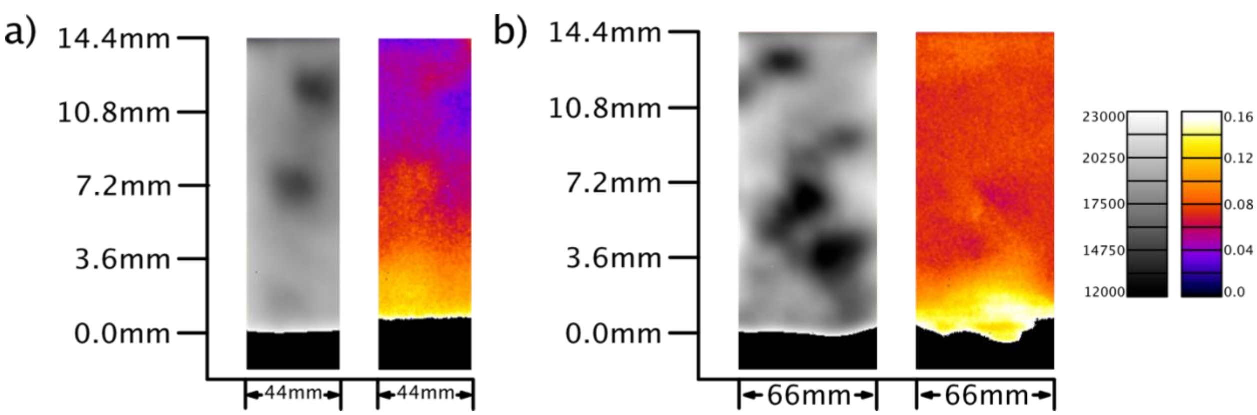

Figure B. 8. *2-D distribution of ϕ_I values, reconstructed using the 1-D profiles of the meta-volcanic waste rock fragment from Restigouche Mine.*

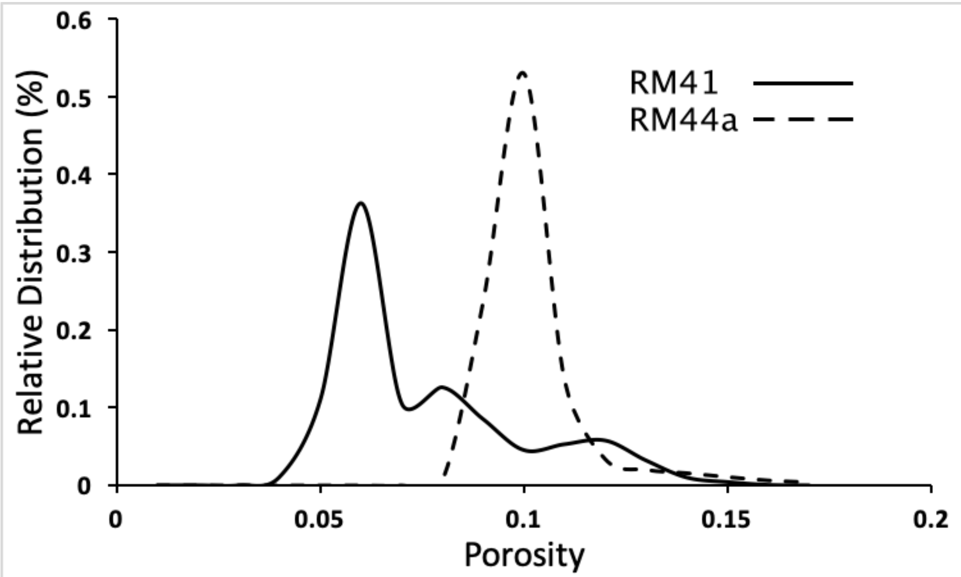

Figure B. 9. *Relative porosity distribution within sub-samples of the meta-volcanic waste rock fragment from Restigouche Mine.*

B.3.1.4 Quartz-muscovite schist

Processed x-ray radiography images indicate minor fluctuations in porosity (Fig. A.B.10) along the one-dimensional profiles of cores RM91 and RM91a, both cored parallel to foliation. However, sharp increases are observed at the bottom and top of the profile. In core RM94a -cut normal to foliation- major fluctuations in porosity are observed. The average ϕ_I values along the 1-D profiles are 0.048, 0.051, and 0.042 (Table 3.7), which are approximately equal to the ϕ_w values measured. The fluctuation in porosity is greater when represented in two-dimensions and can be attributed to the heterogeneity of geologic material within the core sample (Fig. A.B.11). This increase in fluctuation is best represented in sample RM91a where porosity is nearly uniform -0.049 to 0.055- from 0.003 to 0.013m along the 1-D profile of averaged ϕ_I values, contrast to the range of 0.03 to 0.07 observed in the 2-D porosity distribution along the same diffusion profile. Both samples cored parallel to foliation have dampened porosity contrast because the general foliation plane was not aligned for radiography, this contrast can be observed in sample RM94a. Coordinate locations of high and low porosity intersect with regions of high and low gsv, respectively. Mineral phases found in this rock type associated with high and low gsv are quartz, calcite, or muscovite, and sulfides veins, respectively. The 2-D porosity reconstruction of the 1-D profiles for all three samples (Fig. A.B.12) display narrow distributions. This is often indicative of a homogenous material or a heterogeneous material with similar pore-space accessibility. Unaltered samples, RM91 and RM94a, have a lower regions and average porosity than the slightly more oxidized sample, RM91a.

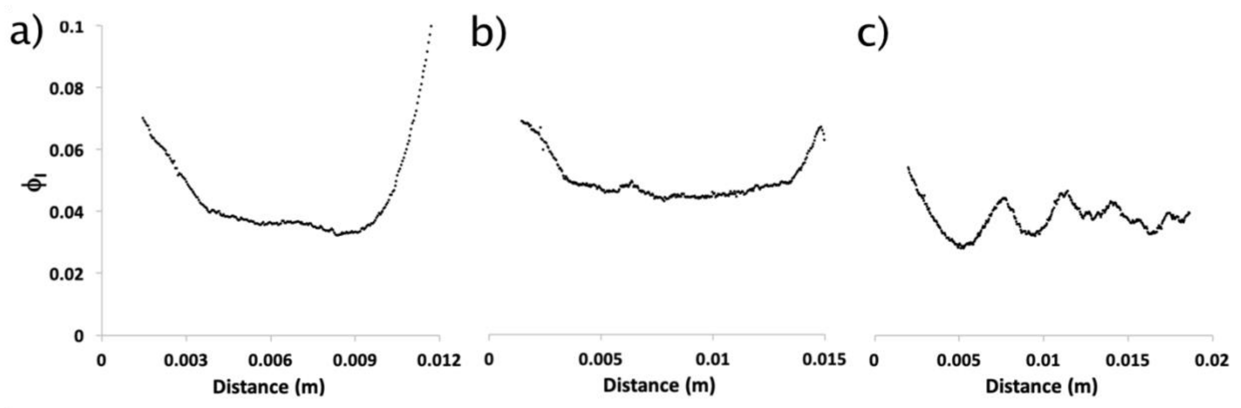

Figure B. 10. *Spatial distribution of ϕ_I values along the 1-D profile of cores drilled parallel (a and b) and normal (c) to the dominant foliation plane of a quartz-muscovite schist waste rock fragment from Restigouche Mine. Profiles b and c are derived from slightly more oxidized cores than profile c.*

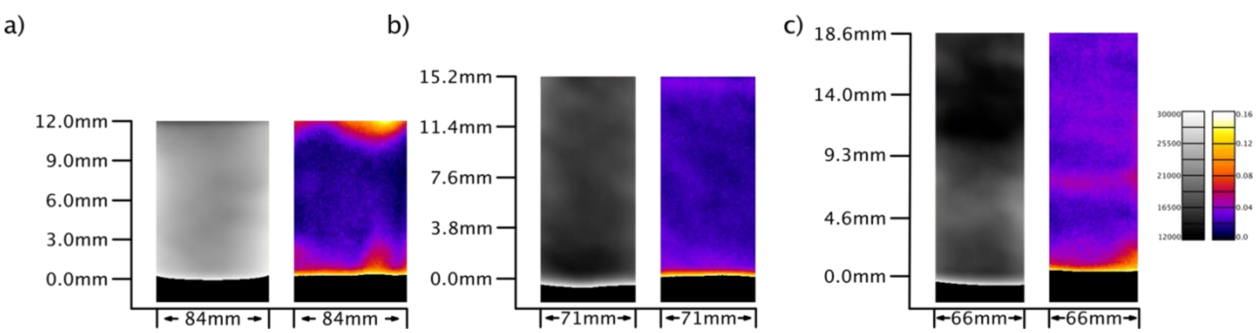

Figure B. 11. *2-D distribution of ϕ_I values, reconstructed using the 1-D profiles of the quartz-muscovite schist waste rock fragment from Restigouche Mine.*

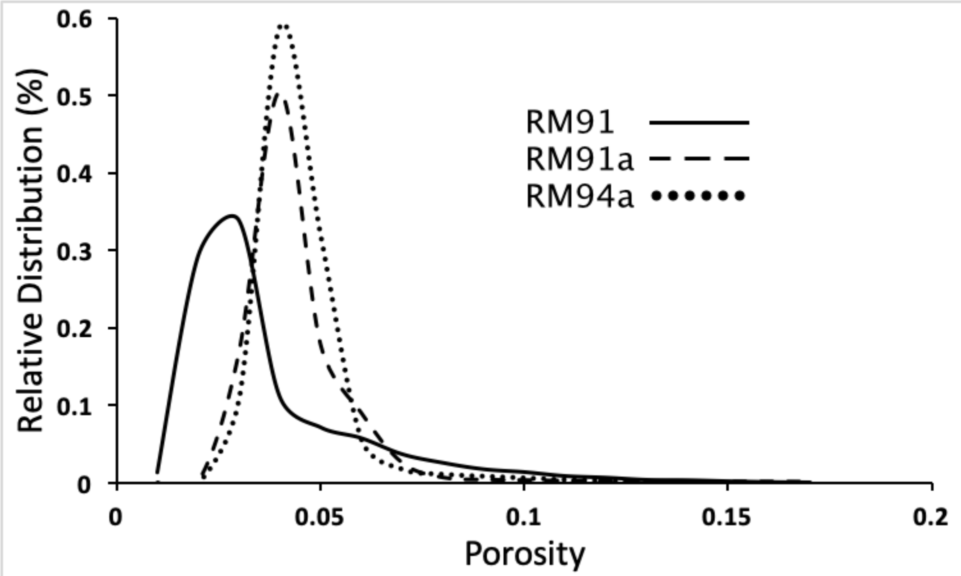

Figure B. 12. *Relative porosity distribution within sub-samples of the quartz-muscovite schist waste rock fragment from Restigouche Mine.*

B.3.2 Diffusion

B.3.2.1 Quartz-Sericite Schist

The 1-D time-series profiles of C/C_0 within the unaltered domain of a quartz-sericite schist are shown in figures A.B.13, 15, 17, and, 19. In cores where diffusion was measured parallel to the dominant foliation plane, average D_P values derived by fitting the experimental data to the analytical solution are 2.8 x 10^{-10} m^2/s and 3.0 x 10^{-10} m^2/s, with a relative standard deviation of 2.5 x 10^{-11} m^2/s and 6.5 x 10^{-11} m^2/s (Fig. A.B.13 and 15). In cores where diffusion was measured normal to foliation, the average D_P values are 7.6 x 10^{-11} m^2/s and 6.0 x 10^{-11} m^2/s, with a relative standard deviation of 5.2 x 10^{-12} m^2/s and 3.5 x 10^{-12} m^2/s (Fig. A.B.17 and 19).

Samples LR11a and LR11b (Fig. A.B.13 and 15) show very few signs of alteration, weathering or oxidation. Figures A.B.14 and 16 show the 2-D distribution of $\Delta\mu$ in both samples, indicating that areas of high gsv show greater $\Delta\mu$ than areas of low gsv in both the early-time data series' and final saturated images. However, in the slightly oxidized core drilled normal to foliation (LR13), $\Delta\mu$ is first observed in regions of low gsv (Fig. A.B.18) and in the fully saturated image. This trend may be observed because the pore space between mineral grains is difficult to access, or iodide is oxidizing to iodate and sorbing to sulfide mineral surfaces.

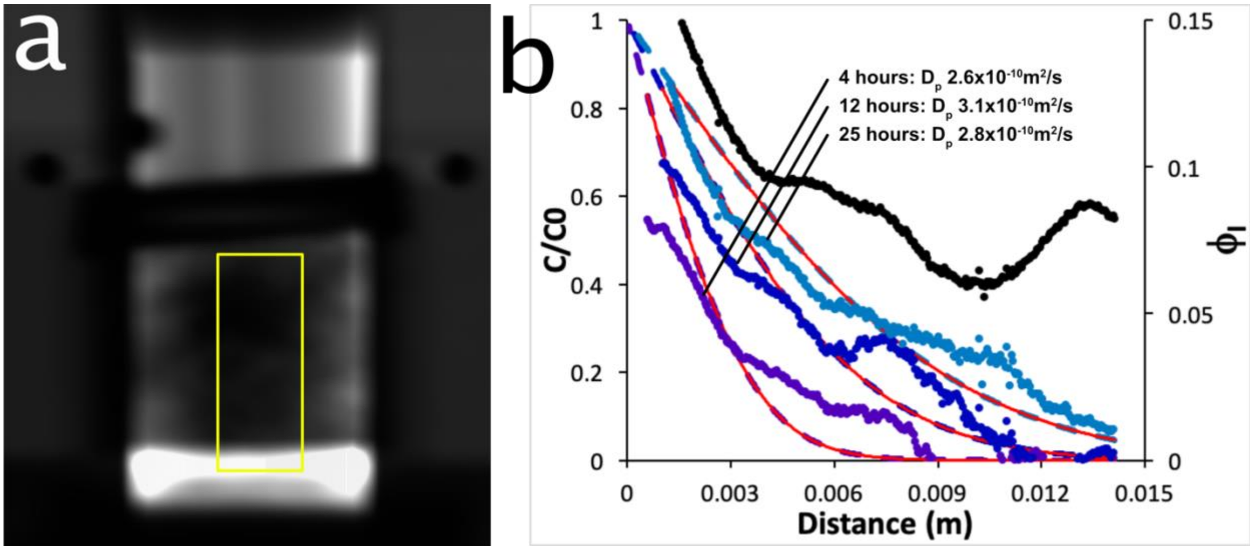

Figure B. 13. *1-D One dimensional profiles of relative tracer concentration (C/C_0; blue-shade profiles) and ϕ_I (black profiles). a) Greyscale Radiograph and ROI (yellow) of rock core sample LR11a b) C/C_0 data were collected at discrete times during the 1-D diffusion experiments. The dashed profiles are modelled lines that were fit to the section of the sample indicated by the red lines.*

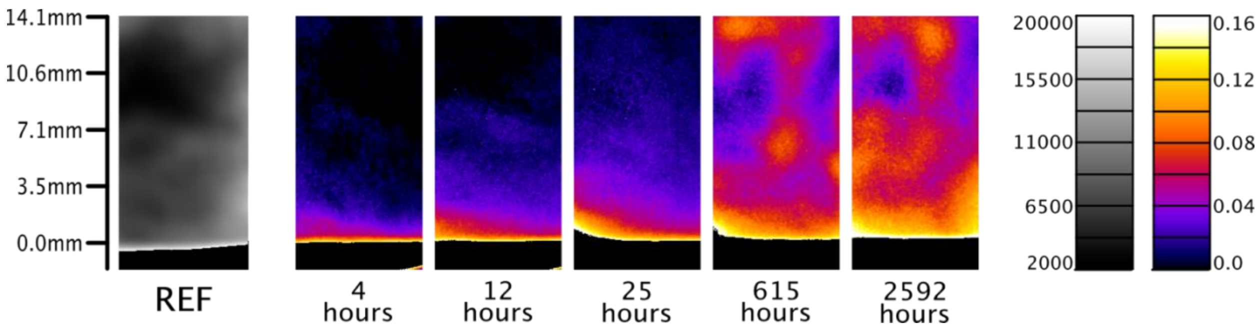

Figure B. 14. *LR11a drill core from the oxidized portion of sample, 2-D reference radiograph (REF), ϕ_I distribution within the ROI, and five time-series $\Delta\mu$ images, along with legends for the grey-scale values (gsv) and $\Delta\mu$.*

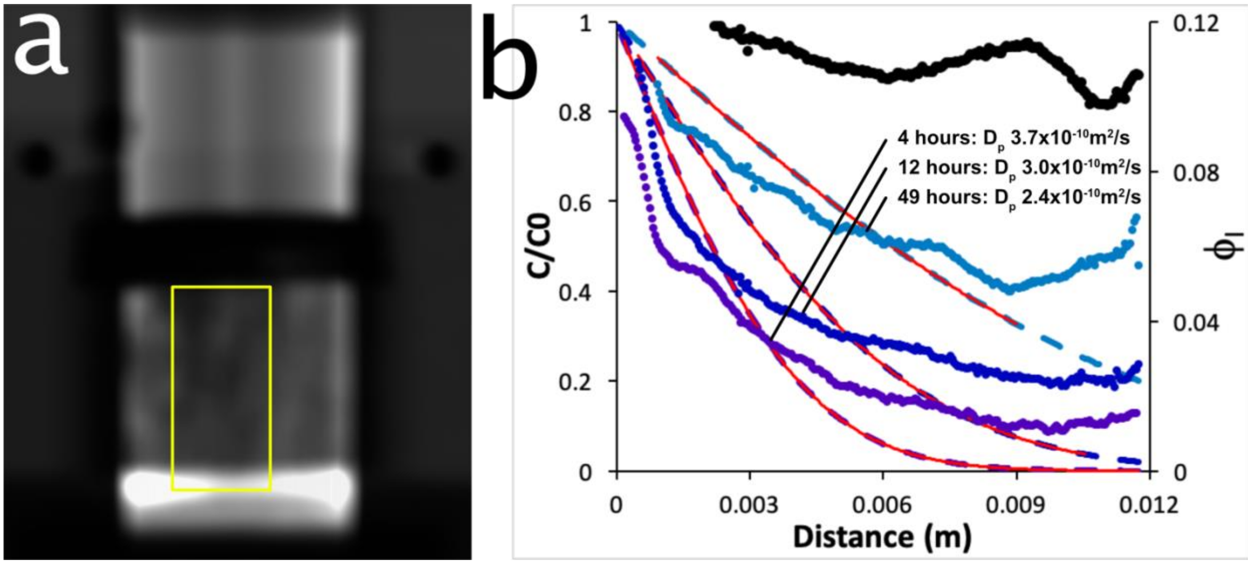

Figure B. 15. *1-D One dimensional profiles of relative tracer concentration (C/C_0; blue-shade profiles) and ϕ_I (black profiles). a) Greyscale Radiograph and ROI (yellow) of rock core sample LR11b b) C/C_0 data were collected at discrete times during the 1-D diffusion experiments. The dashed profiles are modelled lines that were fit to the section of the sample indicated by the red lines.*

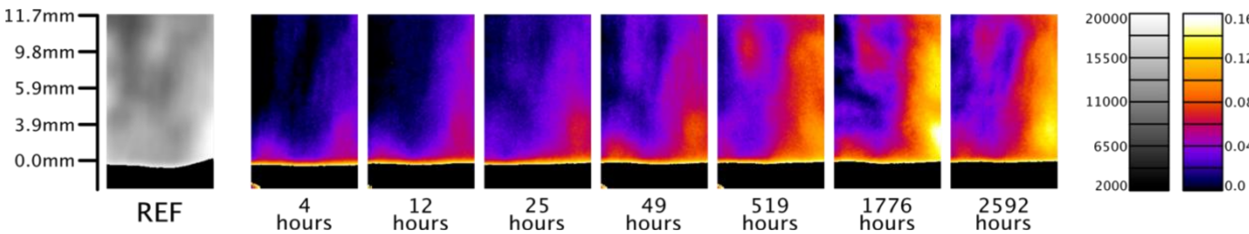

Figure B. 16. *LR11b drill core from the oxidized portion of sample, 2-D reference radiograph (REF), ϕ_I distribution within the ROI, and five time-series $\Delta\mu$ images, along with legends for the grey-scale values (gsv) and $\Delta\mu$.*

Sample LR14 (Fig. A.B.19) also shows very few signs of alteration, weathering or oxidation. However, sample LR13 (Fig. A.B.17) shows yellow-orange stained sericite regions, indicating minor oxidation. Figure A.B.18 illustrates the 2-D Δμ distribution in the slightly core drilled normal to foliation. Contrary to the less oxidized samples, Δμ is first observed in regions of low gsv in the time-series images and in the fully saturated image. This may be observed because oxidation has created preferential solute transport pathways along sulfide veins and has not precipitated an amount of secondary iron-oxides that would retard solute mobility between sericite foliation planes, or iodide is oxidizing to iodate and sorbing to sulfide mineral surfaces.

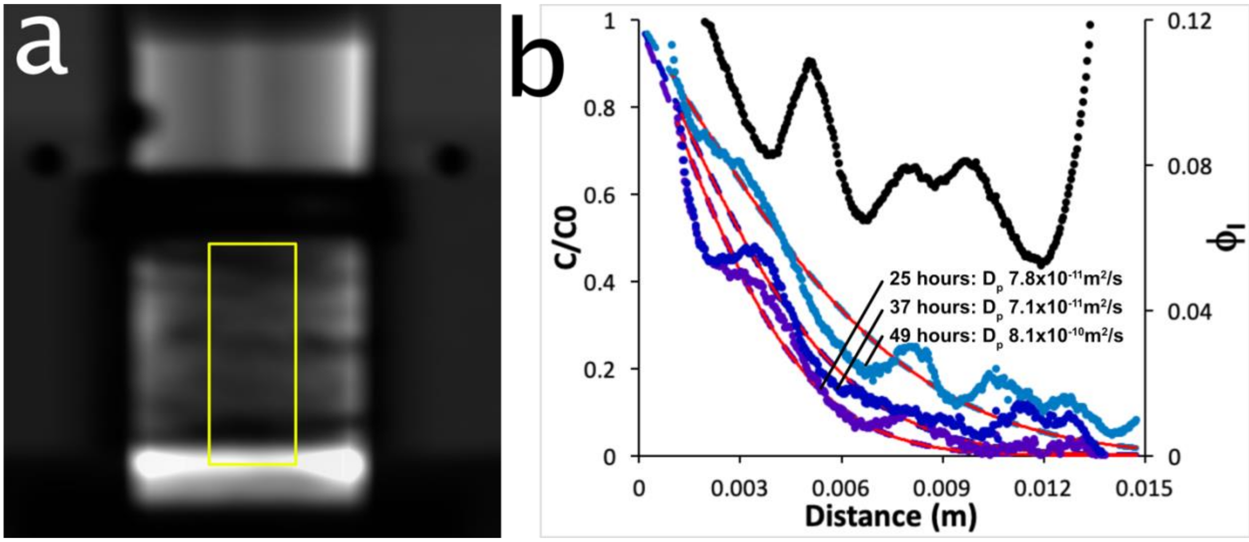

Figure B. 17. *1-D One dimensional profiles of relative tracer concentration (C/C_0; blue-shade profiles) and ϕ_I (black profiles). a) Greyscale Radiograph and ROI (yellow) of rock core sample LR13 b) C/C_0 data were collected at discrete times during the 1-D diffusion experiments. The dashed profiles are modelled lines that were fit to the section of the sample indicated by the red lines.*

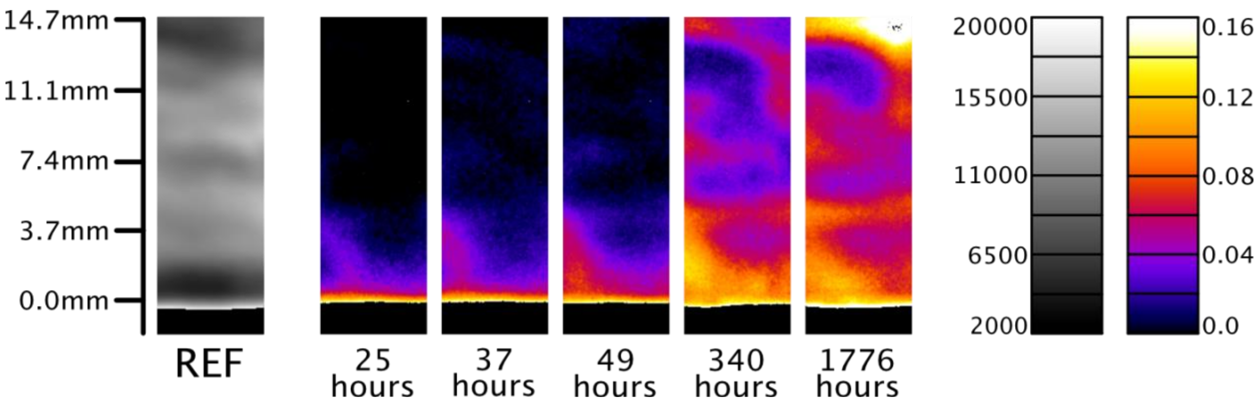

Figure B. 18. *LR13 drill core from the oxidized portion of sample, 2-D reference radiograph (REF), ϕ_I distribution within the ROI, and five time-series $\Delta\mu$ images, along with legends for the grey-scale values (gsv) and $\Delta\mu$.*

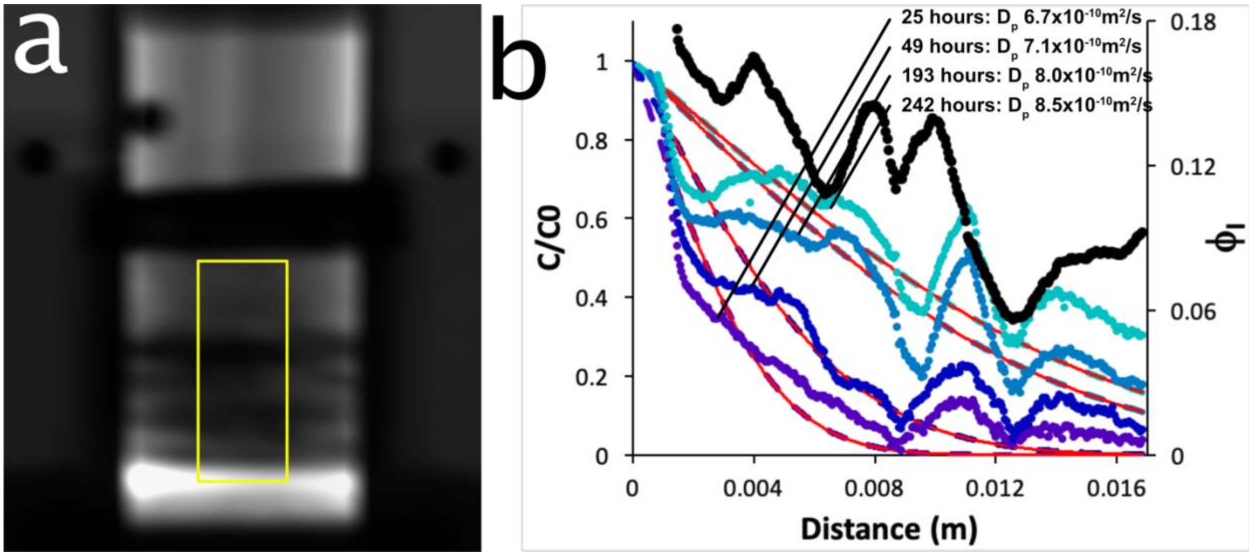

Figure B. 19. *1D One dimensional profiles of relative tracer concentration (C/C_0; blue-shade profiles) and ϕ_I (black profiles). a) Greyscale Radiograph and ROI (yellow) of rock core sample LR14 b) C/C_0 data were collected at discrete times during the 1-D diffusion experiments. The dashed profiles are modelled lines that were fit to the section of the sample indicated by the red lines.*

B.3.2.2 Meta-Volcanic Rock

The 1-D time-series profiles of C/C_0 capturing diffusion a meta-volcanic waste rock are shown in figures A.B.20, 22, 23, 24 and 26. In cores where diffusion was measured in the oxidized domain, the average D_P values derived by fitting the experimental data to the analytical solution are 2.4 x 10^{-11} m^2/s, 2.8 x 10^{-11} m^2/s and 4.7 x 10^{-10} m^2/s, with a relative standard deviation of 5.8 x 10^{-13} m^2/s, 9.6 x 10^{-12} m^2/s and 1.2 x 10^{-11} m^2/s. In cores where diffusion was measured in the unaltered domain, the average D_P values are 2.2 x 10^{-11} m^2/s and 2.6 x 10^{-11} m^2/s, with a relative standard deviation of 3.6 x 10^{-12} m^2/s and 2.5 x 10^{-12} m^2/s.

In the oxidized core, sample RM41 (Fig. A.B.21), the diffusion rate greatly accelerates near regions of low gsv, located at 0.006 to 0.009 and 0.011 and 0.013m from the cores influx boundary. In the fully iodide-saturated images, these areas also have greater ϕ_I and $\Delta\mu$ values, compared to the geologic material of the surrounding regions. The opposite trend is observed in another oxidized core, RM41a, where the region of low gsv and largest final-saturated ϕ_I values align with a retarded diffusion rate (Fig. A.B.25). This suggests that there may be both a retardation and an increase in diffusion rate associated with oxidized pyrite grains/clusters.

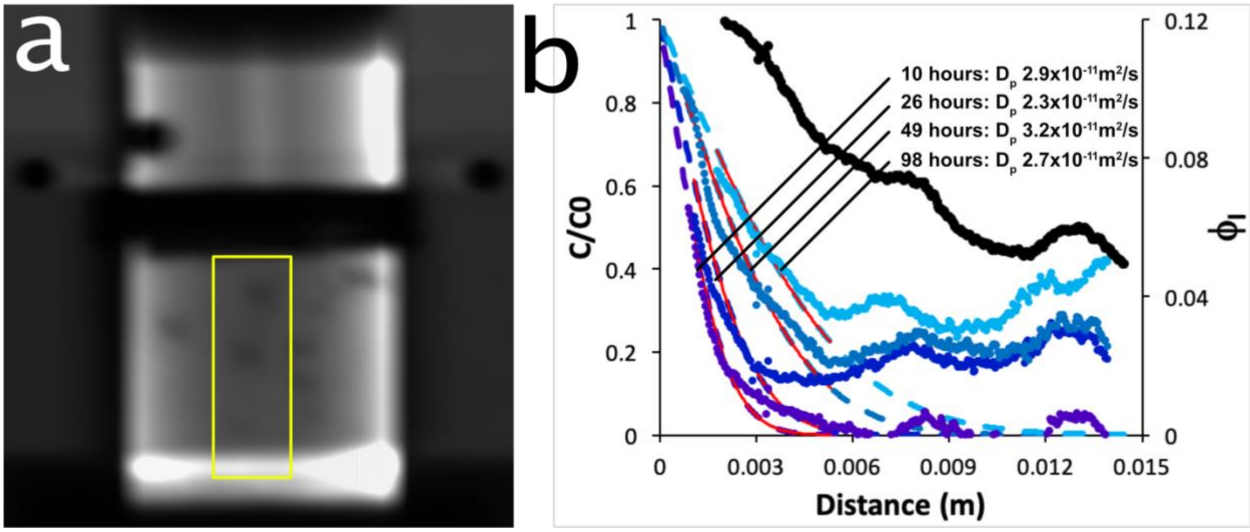

Figure B. 20. *1-D One dimensional profiles of relative tracer concentration (C/C_0; blue-shade profiles) and ϕ_I (black profiles). a) Greyscale Radiograph and ROI (yellow) of rock core sample RM41 b) C/C_0 data were collected at discrete times during the 1-D diffusion experiments. The dashed profiles are modelled lines that were fit to the section of the sample indicated by the red lines.*

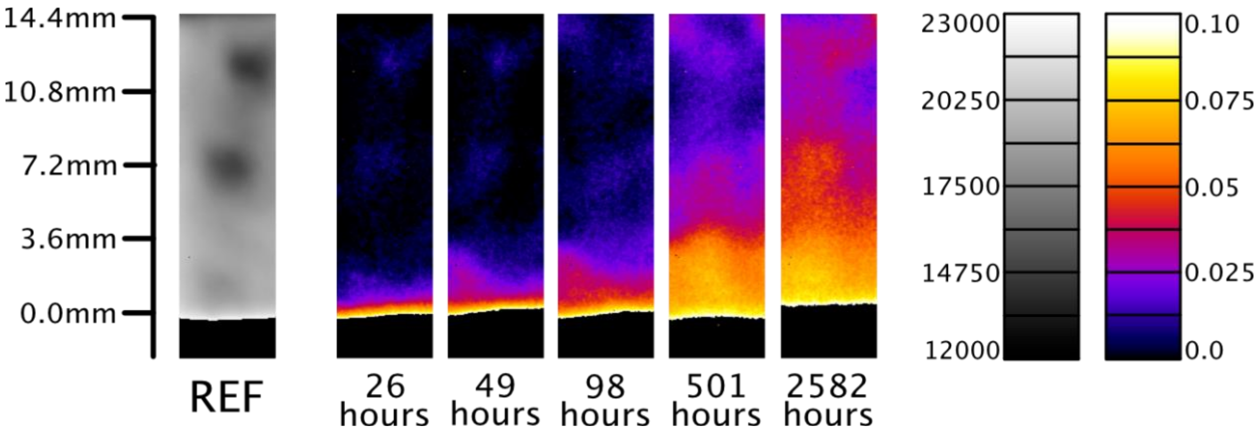

Figure B. 21. *RM41 drill core from the oxidized portion of sample, 2-D reference radiograph (REF), ϕ_I distribution within the ROI, and five time-series $\Delta\mu$ images, along with legends for the grey-scale values (gsv) and $\Delta\mu$.*

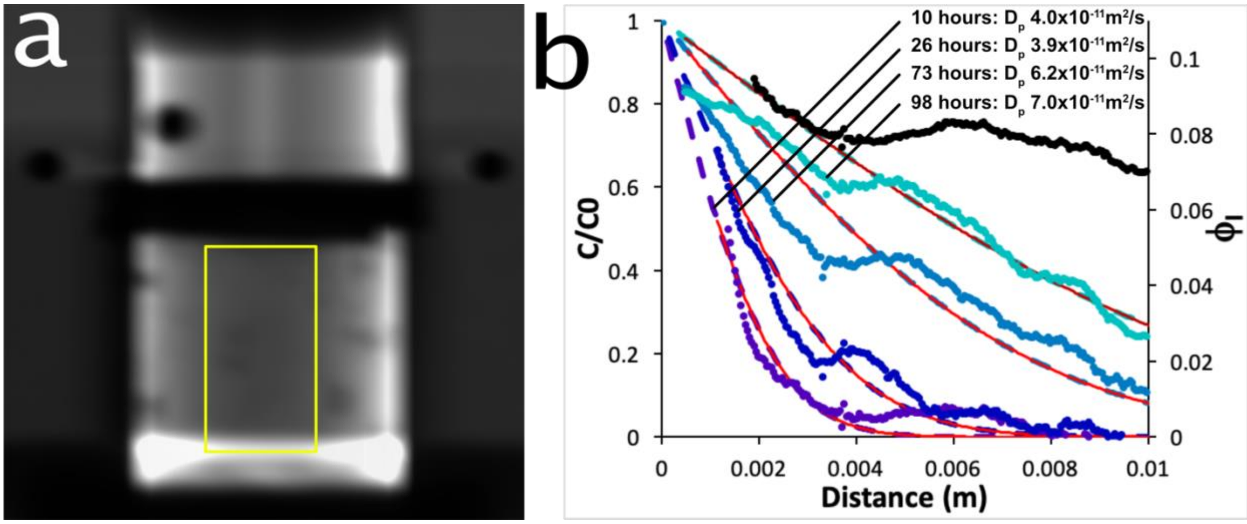

Figure B. 22. *1-D One dimensional profiles of relative tracer concentration (C/C_0; blue-shade profiles) and ϕ_I (black profiles). a) Greyscale Radiograph and ROI (yellow) of rock core sample RM42 b) C/C_0 data were collected at discrete times during the 1-D diffusion experiments. The dashed profiles are modelled lines that were fit to the section of the sample indicated by the red lines.*

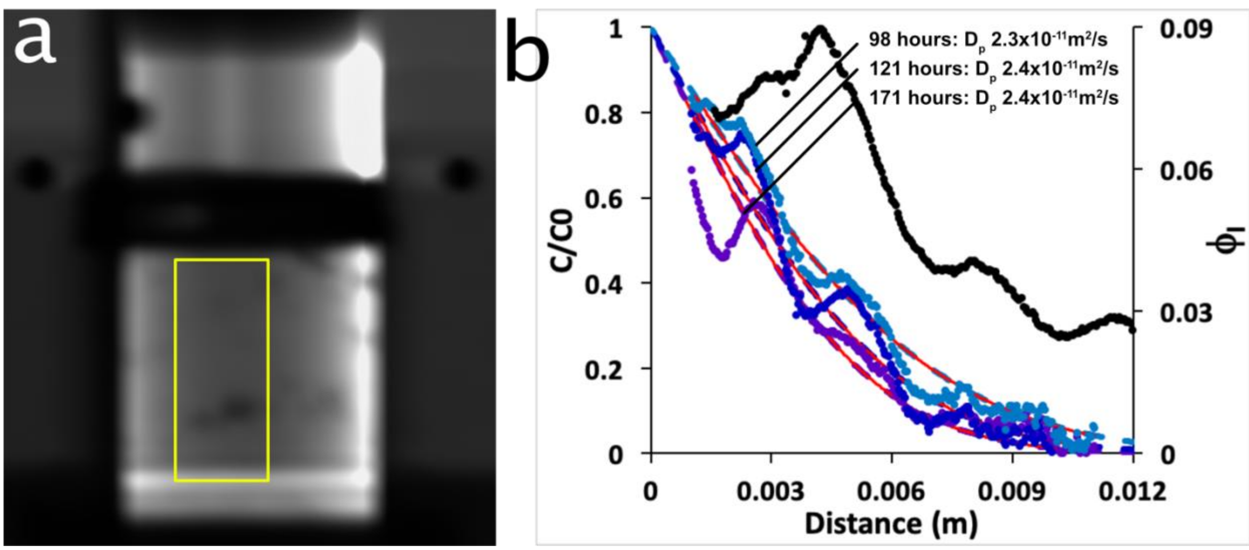

Figure B. 23. *1-D One dimensional profiles of relative tracer concentration (C/C_0; blue-shade profiles) and ϕ_I (black profiles). a) Greyscale Radiograph and ROI (yellow) of rock core sample RM44 b) C/C_0 data were collected at discrete times during the 1-D diffusion experiments. The dashed profiles are modelled lines that were fit to the section of the sample indicated by the red lines.*

In both unaltered cores, RM1a and 4a, the 2-D movement of the iodide-tracer favors solute-transport pathways in regions of low gsv (Fig. A. 26 and 28). In addition, the fully iodide-saturated images indicate that these areas also have greater φ_I and $\Delta\mu$ values than the geologic material of high gsv.

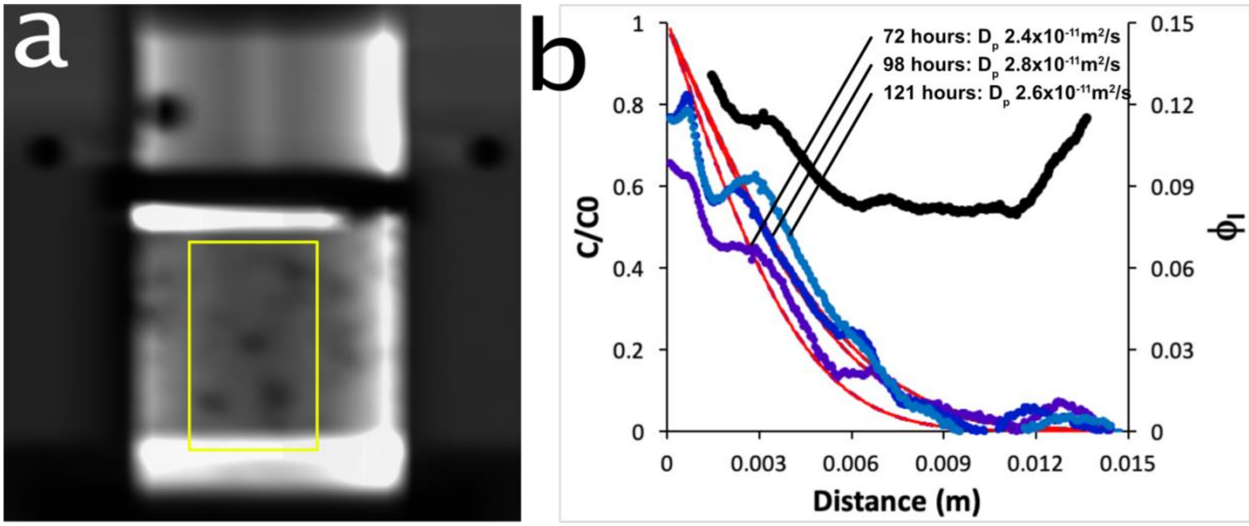

Figure B. 24. *1-D One dimensional profiles of relative tracer concentration (C/C_0; blue-shade profiles) and ϕ_I (black profiles). a) Greyscale Radiograph and ROI (yellow) of rock core sample RM41a b) C/C_0 data were collected at discrete times during the 1-D diffusion experiments. The dashed profiles are modelled lines that were fit to the section of the sample indicated by the red lines.*

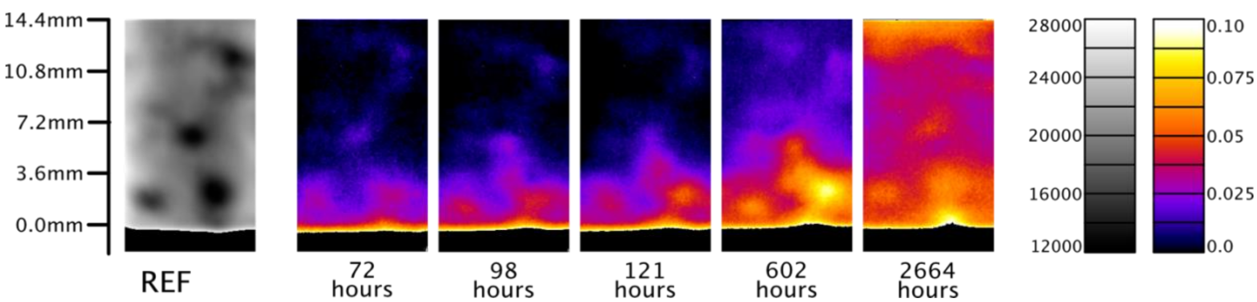

Figure B. 25. *RM41a drill core from the oxidized portion of sample, 2-D reference radiograph (REF), ϕ_I distribution within the ROI, and five time-series $\Delta\mu$ images, along with legends for the grey-scale values (gsv) and $\Delta\mu$.*

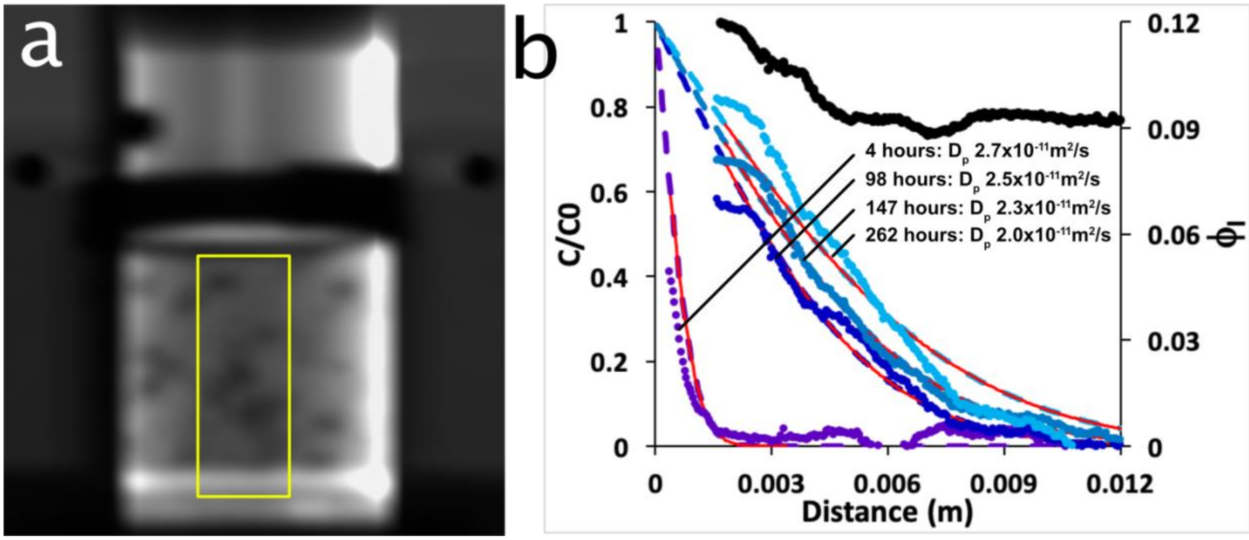

Figure B. 26. *1-D One dimensional profiles of relative tracer concentration (C/C_0; blue-shade profiles) and ϕ_I (black profiles). a) Greyscale Radiograph and ROI (yellow) of rock core sample RM44a b) C/C_0 data were collected at discrete times during the 1-D diffusion experiments. The dashed profiles are modelled lines that were fit to the section of the sample indicated by the red lines.*

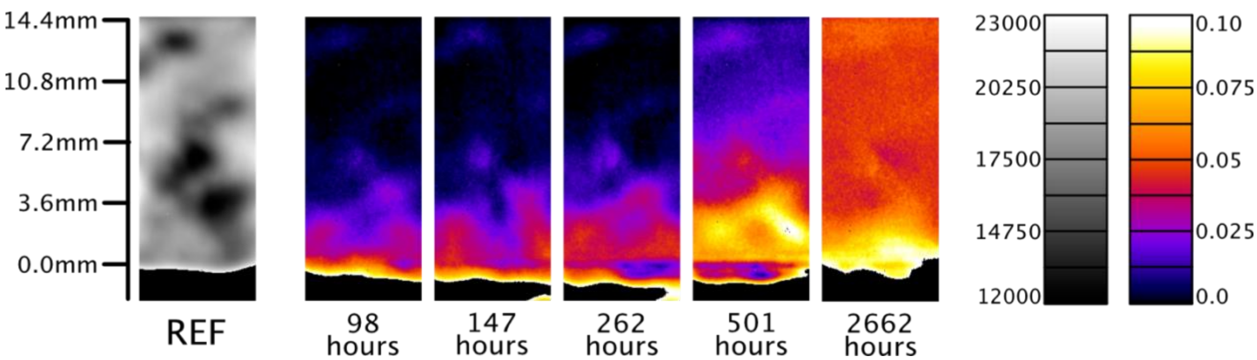

Figure B. 27. *RM44a drill core from the oxidized portion of sample, 2-D reference radiograph (REF), ϕ_I distribution within the ROI, and five time-series $\Delta\mu$ images, along with legends for the grey-scale values (gsv) and $\Delta\mu$.*

B.3.2.3 Quartz-Biotite Schist

The 1-D time series profiles of C/C_0 capturing diffusion in a quartz-biotite schist waste rock fragment are shown in figures A. 29, 30, 32 and 34. In cores where diffusion was measured in the oxidized domain, the average D_P values derived by fitting the experimental data to the analytical solution are 1.2 x 10^{-10} m^2/s and 3.2 x 10^{-10} m^2/s, with a relative standard deviation of 9.6 x 10^{-12} m^2/s and 2.6 x 10^{-10} m^2/s. In cores where diffusion was measured in the unaltered domain, the average D_P values are 2.1 x 10^{-10} m^2/s and 2.5 x 10^{-10} m^2/s, with a relative standard deviation of 1.0 x 10^{-11} m^2/s and 5.3 x 10^{-11} m^2/s.

Samples RM31 and RM33 are oxidized up to 9mm and 11mm from the influx boundary, respectively, and diffusion rate is calculated using values from this domain (Fig. A. 28b and 29b). Although average Δμ is lower in oxidized pore space, diffusion rate is greater within the oxidized domain and decreases near the transition zone to the unaltered domain. Early-time data indicates the tracer movement is most rapid in areas of high gsv (Fig. A. 30).

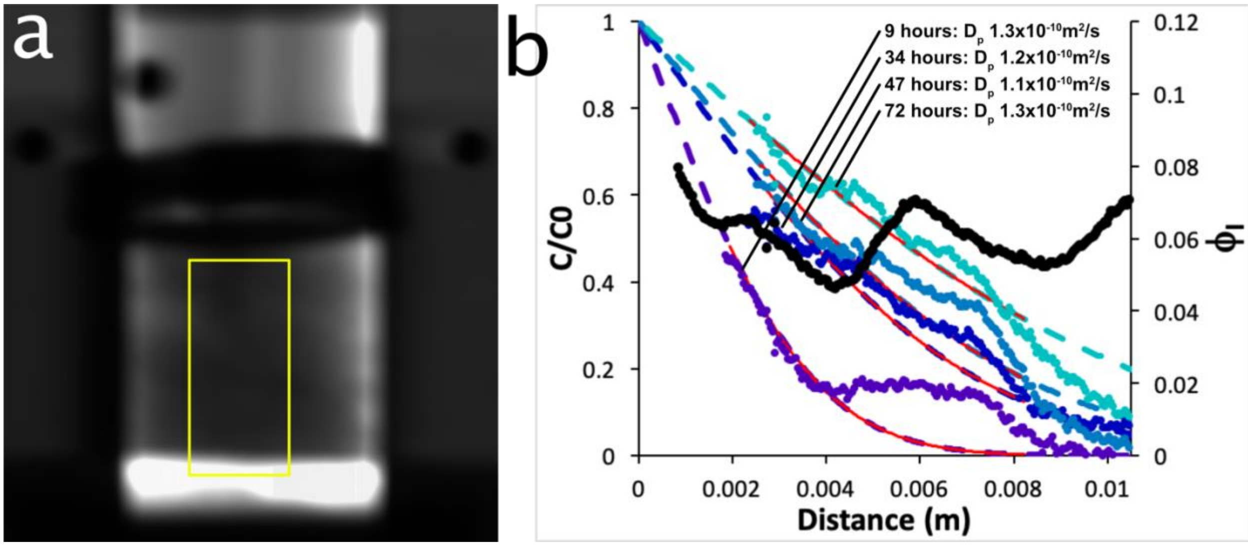

Figure B. 28. *1-D One dimensional profiles of relative tracer concentration (C/C₀; blue-shade profiles) and ϕI (black profiles). a) Greyscale Radiograph and ROI (yellow) of rock core sample RM31 b) C/C₀ data were collected at discrete times during the 1-D diffusion experiments. The dashed profiles are modelled lines that were fit to the section of the sample indicated by the red lines.*

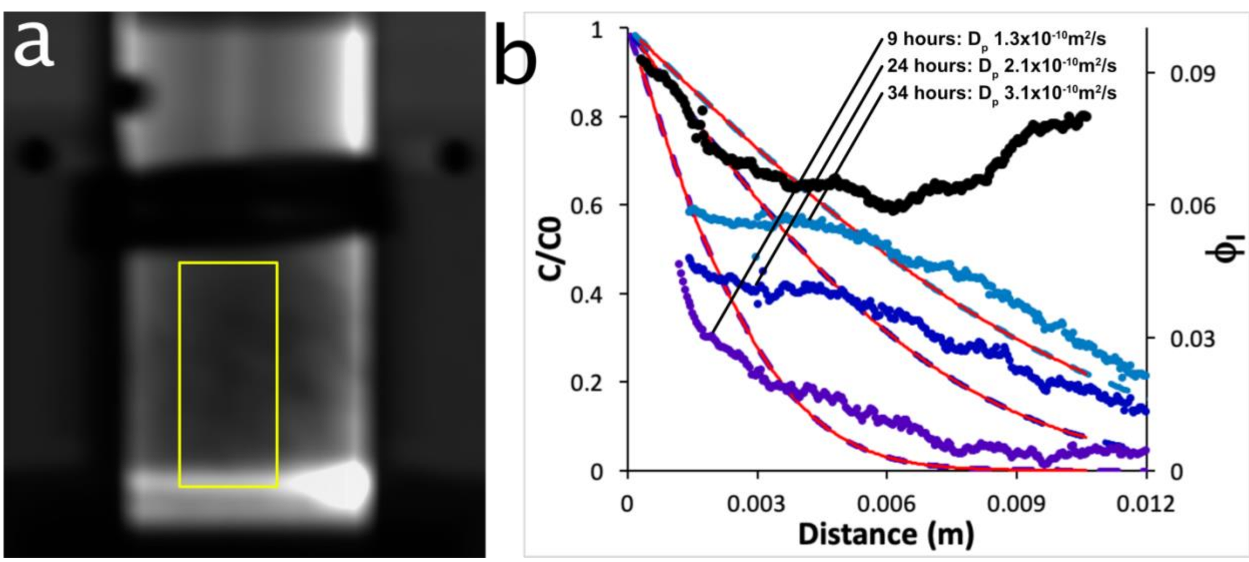

Figure B. 29. *1-D One dimensional profiles of relative tracer concentration (C/C₀; blue-shade profiles) and ϕI (black profiles). a) Greyscale Radiograph and ROI (yellow) of rock core sample RM33 b) C/C₀ data were collected at discrete times during the 1-D diffusion experiments. The* *dashed profiles are modelled lines that were fit to the section of the sample indicated by the red lines.*

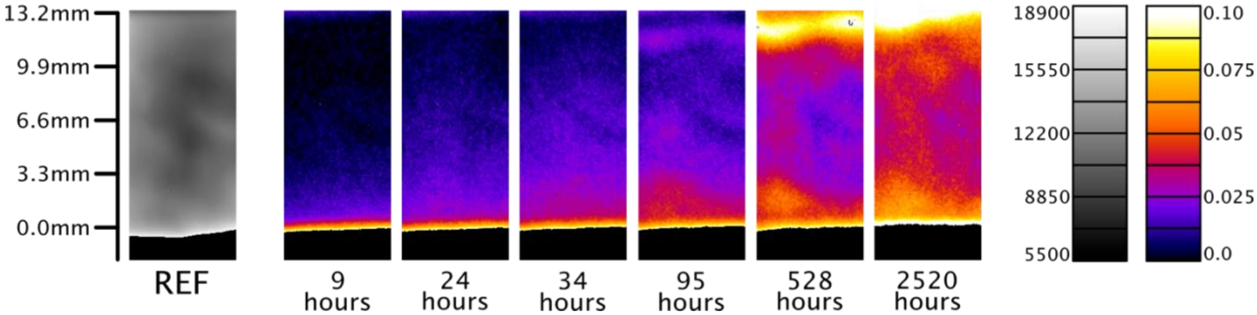

Figure B. 30. *RM33 drill core from the oxidized portion of sample, 2-D reference radiograph (REF), ϕ_I distribution within the ROI, and five time-series $\Delta\mu$ images, along with legends for the grey-scale values (gsv) and $\Delta\mu$.*

In unaltered core, sample RM32a and RM33a, solute transport is most rapid in areas of high gsv (Fig. A. 32). In addition, the fully iodide-saturated images indicate that these areas have greater Δμ values than the geologic material of low gsv.

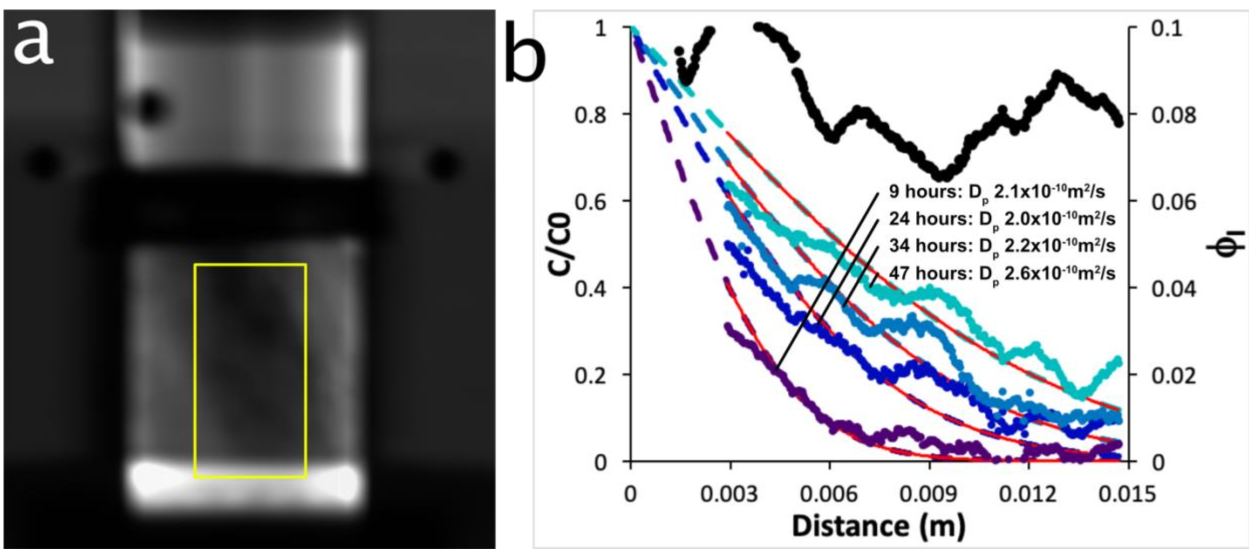

Figure B. 31. *1-D One dimensional profiles of relative tracer concentration (C/C_0; blue-shade profiles) and ϕ_I (black profiles). a) Greyscale Radiograph and ROI (yellow) of rock core sample RM32a b) C/C_0 data were collected at discrete times during the 1-D diffusion experiments. The dashed profiles are modelled lines that were fit to the section of the sample indicated by the red lines.*

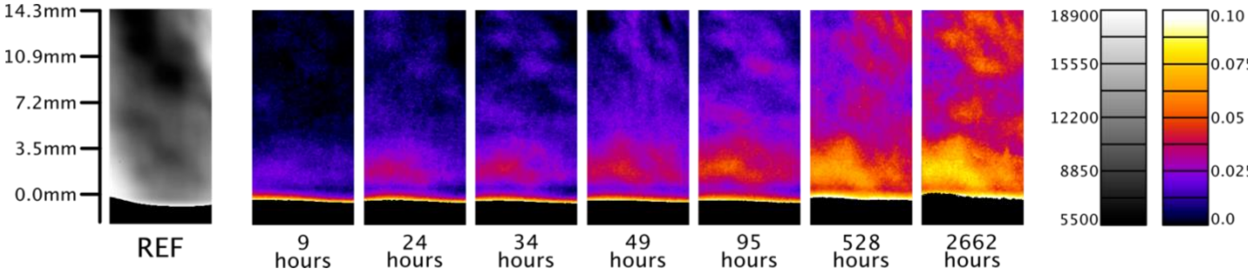

Figure B. 32. *RM32a drill core from the oxidized portion of sample, 2-D reference radiograph (REF), ϕ_I distribution within the ROI, and five time-series $\Delta\mu$ images, along with legends for the grey-scale values (gsv) and $\Delta\mu$.*

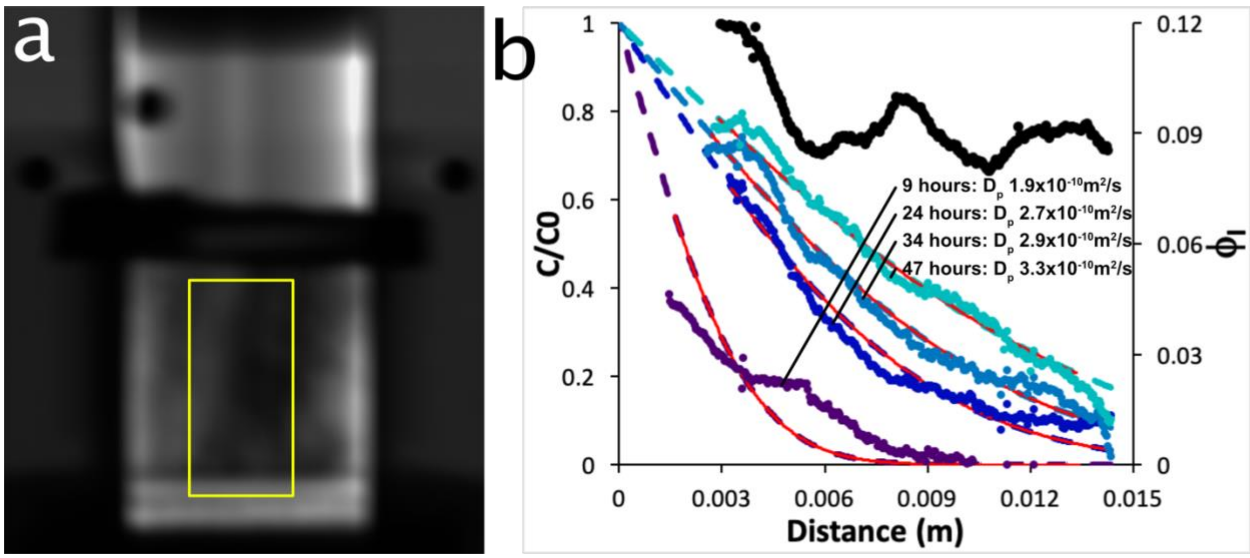

Figure B. 33. *1D One dimensional profiles of relative tracer concentration (C/C_0; blue-shade profiles) and ϕ_I (black profiles). a) Greyscale Radiograph and ROI (yellow) of rock core sample RM33a b) C/C_0 data were collected at discrete times during the 1-D diffusion experiments. The dashed profiles are modelled lines that were fit to the section of the sample indicated by the red lines.*

B.3.2.4 Quartz-Muscovite Schist

The time-series profiles for C/C_0 within the unaltered domain of a quartz-muscovite schist, are shown in figures A.B.34, 36, and 38. In cores where diffusion was measured parallel to the foliation plane, the average D_P values derived by fitting the experimental data to the analytical solution are 4.2 x 10^{-11} m^2/s and 5.6 x 10^{-11} m^2/s, with a relative standard deviation of 9.6 x 10^{-12} m^2/s and 2.6 x 10^{-10} m^2/s. In the core where diffusion was measured normal to the foliation plane, the average D_P value is 2.8 x 10^{-11} m^2/s, with a relative standard deviation of 1.5 x 10^{-12} m^2/s.

Samples RM91 and RM91a (Figures. A. 34 and 36) are partially oxidized, indicated by the weathering of sulfides and yellow-orange discoloration on muscovite grains and foliation planes. Sample RM91a has more prominent visible weathering features and has a more rapid diffusion rate. However, this 1-D model does not account for heterogeneity and as a result, we have a muted increase in quantified diffusion coefficient (Table 3.2). Figures. A. 35 and 37 indicate that areas of high gsv show greater Δμ than areas of low gsv in both the early-time data series' and final saturated images.

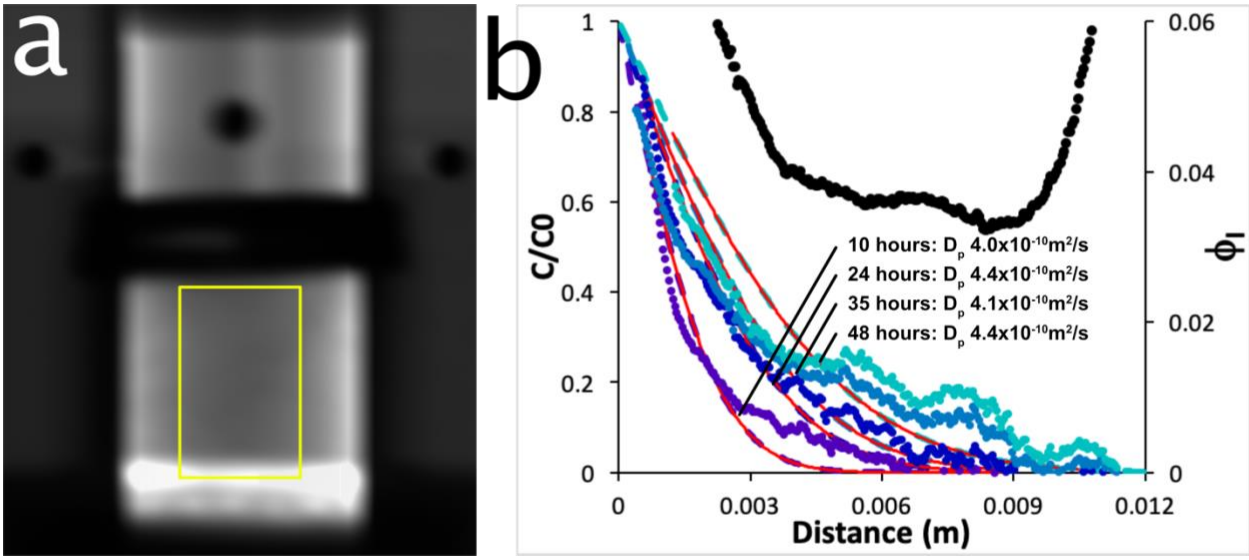

Figure B. 34. *1-D One dimensional profiles of relative tracer concentration (C/C_0; blue-shade profiles) and ϕ_I (black profiles). a) Greyscale Radiograph and ROI (yellow) of rock core sample RM91 b) C/C_0 data were collected at discrete times during the 1-D diffusion experiments. The dashed profiles are modelled lines that were fit to the section of the sample indicated by the red lines.*

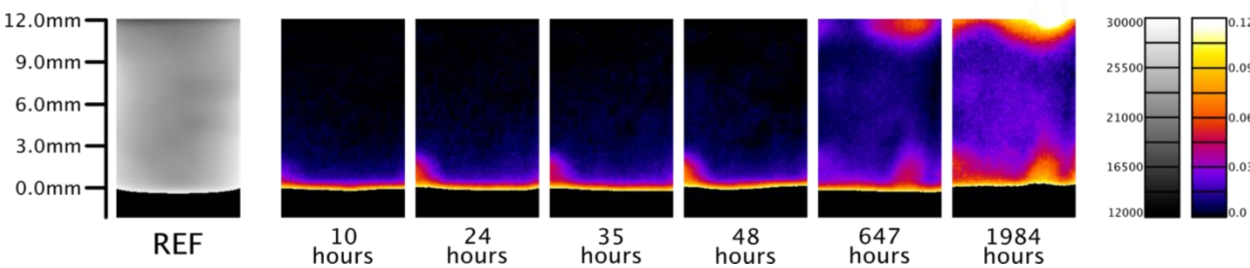

Figure B. 35. *RM91 drill core from the oxidized portion of sample, 2-D reference radiograph (REF), ϕ_I distribution within the ROI, and five time-series $\Delta\mu$ images, along with legends for the grey-scale values (gsv) and $\Delta\mu$.*

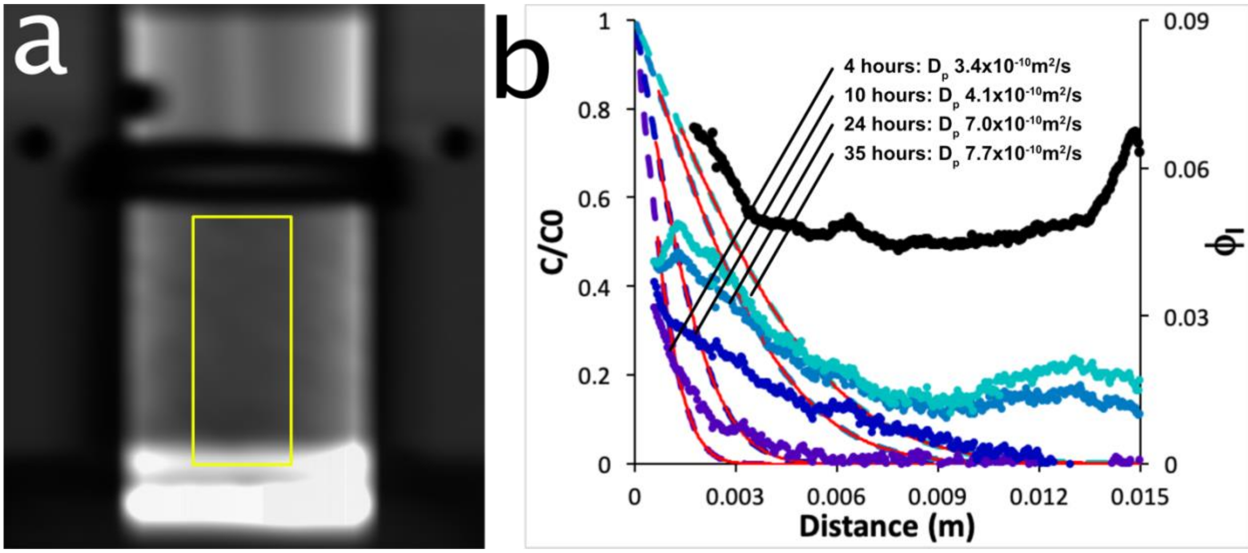

Figure B. 36. *1-D One dimensional profiles of relative tracer concentration (C/C_0; blue-shade profiles) and ϕ_I (black profiles). a) Greyscale Radiograph and ROI (yellow) of rock core sample RM91a b) C/C_0 data were collected at discrete times during the 1-D diffusion experiments. The dashed profiles are modelled lines that were fit to the section of the sample indicated by the red lines.*

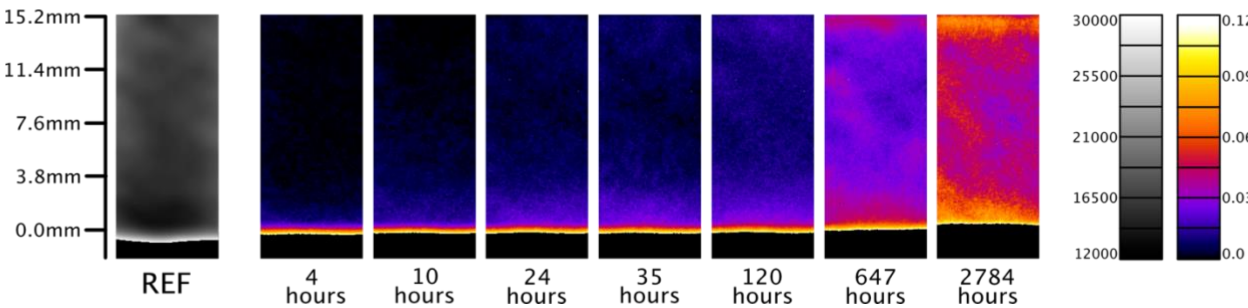

Figure B. 37. *RM91a drill core from the oxidized portion of sample, 2-D reference radiograph (REF), ϕ_I distribution within the ROI, and five time-series $\Delta\mu$ images, along with legends for the grey-scale values (gsv) and $\Delta\mu$.*

Core RM94a is oxidized to a similar degree of core RM91a. In Figure. A.B. 39, Δμ first appears in regions of high gsv. Opposite to this trend, the final saturated image indicates that areas of greatest Δμ correspond to areas of low gsv. This may be observed because the pore space between mineral grains is difficult to initially access, or iodide is oxidizing to iodate and sorbing to sulfide mineral surfaces.

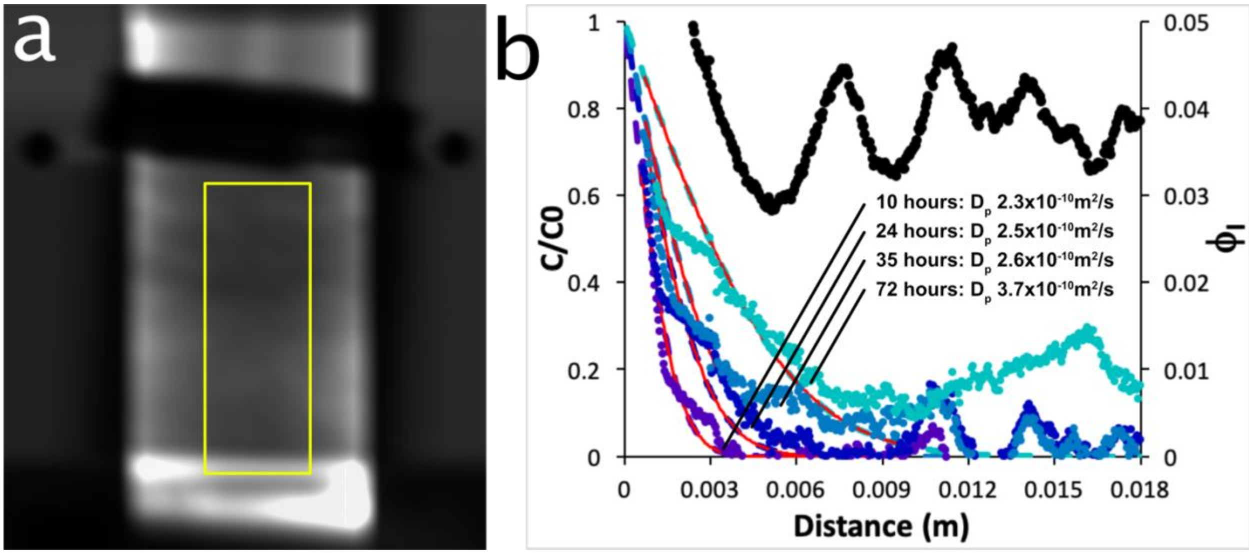

Figure B. 38. *1-D One dimensional profiles of relative tracer concentration (C/C_0; blue-shade profiles) and ϕ_I (black profiles). a) Greyscale Radiograph and ROI (yellow) of rock core sample RM94a b) C/C_0 data were collected at discrete times during the 1-D diffusion experiments. The dashed profiles are modelled lines that were fit to the section of the sample indicated by the red lines.*

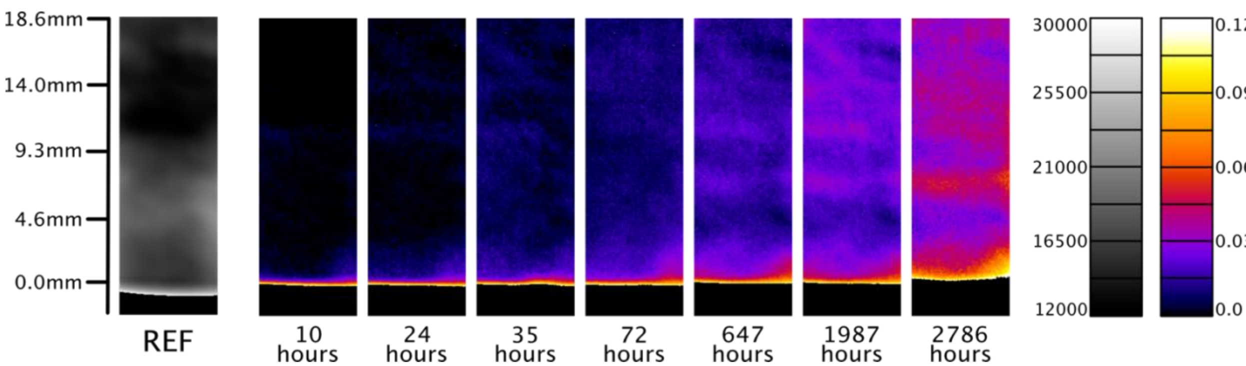

Figure B. 39. *RM94a drill core from the oxidized portion of sample, 2-D reference radiograph (REF), ϕ_I distribution within the ROI, and five time-series $\Delta\mu$ images, along with legends for the grey-scale values (gsv) and $\Delta\mu$.*

Appendix C Measuring D_P in two-dimensions; Rock Cut Near Meductic Sample; MIN3P

MIN3P is run with the parameter estimation code PEST to achieve the least sum of squared residuals between simulated and measured tracer distributions by making iterative changes in D_e

values. D_e values are estimated by adjusting the tortuosity factor as the pore diffusion coefficient and iodide accessible porosity are measured values.

Creating the .dat file & reasons for decisions

Data Block 1 Global Control parameters

The global control parameters under flow simlution are set to steady state and fully saturated. These settings ensure the magnitude and direction of flow are constant throughout the domain and all model pore space is saturated with solution, no gas, no solids. No additional keywords are added to invoke additional capabilities.

Data Block 2 Geochemical System

No Geochemical reactions occurs in this simulation. The geochemical system has 1 component, i-(iodide). Reaction temperature is 25 degrees Celsius. The database in the directory is used to select the one component and inputs are defined as mol/l.

Data Block 3 Spatial Discretization

A 2-D numerical grid was developed in MIN3P where the number and size of each voxel in the x and y dimensions correspond to the 161×161 area of pixels in the radiographs. The dimensions of this simulation are specified in 2-D (rectangle), the geometry of the domain is defined in Cartesian coordinates. The model grid is assigned 163 subblocks in the x and z dimensions to represent radiographs binned to images of 161x161 pixels. 2 additions rows and columns are added to assign domain boundary conditions. The Length and width of the model domain is 0.115639 m. Spatial discretization of the model rock slab is achieved by importing experimentally determined porosity values.

Data Block 4 Time Step Control

The model took a lot of processing power as it was run through PEST. Time unit is in seconds hours, start time is 0 hours (mandatory). The final solution time is matched to the time series radiograph taken at 22 hours of tracer exposure. Iodide concentration values of iodide distribution within sample pore space will be output at this time. The time minimum time step to start the simulation is 1.66667d-20 hours, the maximum time step is 20 hours.

Data Block 5 Control Parameters-Local Chemistry

Default used.

Data Block 6 Control Parameters – Variably Saturated Flow;

Default used. Input units for boundary and initial conditions is hydraulic head.

Data Block 7 Control Parameters Reactive Transport;

The 'update tortuosity' was included to set a blanket of Tortuosity factor values for PEST to used as adjustable parameters and observations. The data input file was created using the process detailed in Appendix E.

Data Block 8 Output Control

This section was specified to output at time 0 and at the end of the simulation, 22hours.

Data Block 9 Physical Parameters: Porous Medium;

One property zone is used, the extent of the zone is identical to the spatial discretization of the model grid; 0.115639m x 0.115639m in the x and z dimensions. The physical extent of the model rock slab within the model domain is defined with a specific porosity and tortuosity values read from a .por and .tor file.

Data Block 10 Physical Parameters-Variably Saturated Flow;

One zone is specified in data block 9, hydraulic conductivity is specified by an external .hyc file. The conditions are not "variably-saturated" so hydraulic function parameters do not need to be specified.

Data Block 11 Physical Parameters Reactive Transport

One zone is specified in data block 9, hydraulic conductivity is specified by an external .hyc file. The conditions are not "variably-saturated" so hydraulic function parameters do not need to be specified. The diffusion coefficient specified is 1.9d-9. More than one control volume is specified in the x-direction, longitudinal dispersity is specified at 0.1 and the transverse vertical dispersity is specified at 0.01 because there is more than one control volume in the x and y directions.

Data Block 12 Initial Condition – Variably Saturated Flow

The initial condition is defined for fully saturated flow. The distribution of the hydraulic head (1.5m) parameter is discretized the extend of the model domain 0.115639m x 0.115639m. No initial condition for pressure head (variably saturated flow) and gas saturation.

Data Block 13 Boundary Conditions – Variably Saturated Flow

Three boundary conditions are specified in the solution domain. Two inflow boundaries are Dirichlet type with a specified head of 2.0m. One outflow boundary is Dirichlet type with a specified head of 1.0m. This gradient was verified by analysing simulation start and end time output. Iodide values in model space representing the diffusion cells reservoir reported maximum tracer concentrations, no build up and minimal depletion. The inflow boundaries are positioned above and below the region of the model grid representing the rock fragment. The zone extent for both boundaries is >0.015m, both located at the beginning of the model's x dimension. The outflow boundary is positioned at the end of the model's x dimension. The zone extent is >0.024m. No energy balance, heat transport is not being simulated.

Data Block 14 Batch Reactions

No reactions, no input. The purpose of this simulation is to model a conservative tracer.

Data Block 15 Initial Condition – Reactive Transport Data

The initial condition for the reactive transport problem is read from an external aqueous component concentration file (.aqt) and pH is set to 7.0. The zone extent is distributed over the entire model model domain 0.115639m x 0.115639m.

Data Block 16 Initial Condition – Reactive Transport Data

The two inflow boundaries are Dirichlet type with a specified concentration of Iodide fixed at 0.5 mol/l and pH 7.0. The outflow boundary is Neumann type with a specified pH of 7.0.

MIN3P.dat file – 120 hours

```
!
! Data Block 1: global control parameters
! -------------------------------------------------
!
'global control parameters'
'Diffusion - No Advection'
.true.          ;varsat_flow
.true.          ;steady_flow
.true.          ;fully_saturated
.true.          ;reactive_transport

'done'

!
! Data Block 2: geochemical system
! -------------------------------------------------
!
'geochemical system'

'use new database format'




'database directory'
'../database'

'define input units'
'mol/l'

'components'
1           ;number of components
'i-1'

'done'

!
! Data Block 3: spatial discretization
! -------------------------------------------------
!
```

```
'spatial discretization'
1               ;number of discretization intervals in x
163             ;number of control volumes in x
0 0.115639              ;xmin,xmax
1               ;number of discretization intervals in y
1               ;number of control volumes in y
0 1             ;ymin,ymax
1               ;number of discretization intervals in z
163             ;number of control volumes in z
0 0.115639              ;zmin,zmax

'done'

!
! Data Block 4: time step control - global system
! -------------------------------------------------
!
'time step control - global system'
'hours'             ;time unit
0.0             ;time at start of solution
120.0               ;final solution time
20.0            ;maximum time step
1.66667d-20             ;minimum time step

'done'

!
! Data Block 5: control parameters - local geochemistry
! -------------------------------------------------
!
'control parameters - local geochemistry'

'newton iteration settings'
0.0001              ;factor for numerical differentiation
1.d-6               ;convergence tolerance

'maximum ionic strength'
2.0             ;maximum ionic strength

'minimum activity for h2o'
0.5             ;minimum activity for h2o

'output time unit'
'days'

'activity update settings'
```

```
'time_lagged'            ;type of activity update

'done'

!
! Data Block 6: control parameters - variably saturated flow
! ---------------------------------------------------
!
'control parameters - variably saturated flow'

'mass balance'

'input units for boundary and initial conditions'
'hydraulic head'            ;input unit

'compute underrelaxation factor'
10.0            ;max allowed update

'solver settings'
0            ;level_vs, incomplete factorization level
1000            ;msolvit_vs, maximum number of solver iterations
0            ;idetail_s, solver information level
1.d-7            ;restol_vs, solver residual tolerance
1.d-7            ;deltol_vs, solver update tolerance

'newton iteration settings'
0.0001            ;increment for numerical differentiation
15            ;max. number of newton iterations
1.d-6            ;convergence tolerance
0.1            ;sw_star

'done'

!
! Data Block 7: control parameters - reactive transport
! ---------------------------------------------------
!
'control parameters - reactive transport'

'mass balance'

'spatial weighting'
'upstream'            ;spatial weighting

'activity update settings'
'time_lagged'            ;type of activity update
```

```
'tortuosity correction'
!no correction
'assigned tau'                ;tortuosity is specified in another file with porosity

'update tortuosity'

'user-specified underrelaxation factor'
1.0

'solver settings'
0               ;level_vs, incomplete factorization level
100              ;msolvit_vs, maximum number of solver iterations
1               ;idetail_s, solver information level
1.d-7                ;restol_vs, solver residual tolerance
1.d-7                ;deltol_vs, solver update tolerance

'newton iteration settings'
0.0001                ;increment h for numerical differentiation
12                ;anticipated number of Newton iterations
15                ;max. number of Newton iterations
0.5                ;anticipated update in log cycles
1.0                ;maximum update in log cycles
1.d-6                ;convergence tolerance (global system)

'done'

!
! Data Block 8: output control
! -------------------------------------------------
!
'output control'

'output of spatial data'
2               ;number of output times
0.0 120.0

'done'

!
! Data Block 9: physical parameters - porous medium
! -------------------------------------------------
!
'physical parameters - porous medium'
1               ;number of property zones
! -------------------------------------------------
```

```
'read porosity field from file'
'read tortuosity field from file'
! ------------------------------------------------
'number and name of zone'
1
'All parameters'
1.0             ;porosity
0.002           ;tortuosity

'extent of zone'
0.0 0.115639 0.0 1.0 0.0 0.115639

'end of zone'
! ------------------------------------------------

'done'

!
! Data Block 10: physical parameters - variably saturated flow
! ------------------------------------------------
!
'physical parameters - variably saturated flow'

! ------------------------------------------------
'read hydraulic conductivity field from file'
! ------------------------------------------------
'All parameters'            ;name of zone

'hydraulic conductivity in x-direction'
1.0d-12

'hydraulic conductivity in y-direction'
0.0

'hydraulic conductivity in z-direction'
1.0d-12

'specific storage coefficient'
0.0

'soil hydraulic function parameters'
0.0             ;residual saturation
0.0             ;van genuchten - alpha
0.0             ;van genuchten - n
0.0             ;expn
0.0             ;air entry pressure
```

```
0.0             ;max bubble entrapment

'end of zone'
! -------------------------------------------------

'done'

!
! Data Block 11: physical parameters - reactive transport
! -------------------------------------------------
!
'physical parameters - reactive transport'

'diffusion coefficients'
1.9d-9          ;aqueous phase
0.0             ;gaseous phase

!
! -------------------------------------------------
'All parameters'          ;name of zone

'longitudinal dispersivity'
0.1
'transverse horizontal dispersivity'
0.01
'transverse vertical dispersivity'
0.01
'end of zone'
! -------------------------------------------------

'done'

!
! Data Block 12: initial condition - variably saturated flow
! -------------------------------------------------
!
'initial condition - variably saturated flow'
1               ;number of initial condition zones

! -------------------------------------------------
'number and name of zone'
1
'All Parameters'

'initial condition'
1.2
```

```
'initial gas saturation'
0.0

'extent of zone'
0.0 0.115639 0.0 1.0 0.0 0.115639

'end of zone'
! -------------------------------------------------

'done'

!
! Data Block 13: boundary conditions - variably saturated flow
! -------------------------------------------------
!
'boundary conditions - variably saturated flow'
3              ;number of zones

! -------------------------------------------------
'number and name of zone'
1
'inflow boundary 1'

'boundary type'
'first' 1.4           ;hydraulic head

'extent of zone'
0.0 0.0 0.0 1.0 0.0 0.005

'end of zone'
! -------------------------------------------------
'number and name of zone'
2
'inflow boundary 2'

'boundary type'
'first' 1.4           ;hydraulic head

'extent of zone'
0.0 0.0 0.0 1.0 0.110827 0.115639

'end of zone'
! -------------------------------------------------
'number and name of zone'
3
```

```
'outflow boundary'

'boundary type'
'first' 1.0                ;hydraulic head

'extent of zone'
0.115639 0.115639 0.0 1.0 0.05 0.06

'end of zone'
! --------------------------------------------------

'done'


!
! Data Block 15: initial condition - reactive transport
! --------------------------------------------------
!
'initial condition - reactive transport'
1                ;number of initial condition zones
! --------------------------------------------------
'read initial aqueous component concentrations from file'
! --------------------------------------------------
'number and name of zone'
1
'All Parameters'

'concentration input'              ;All Parameters
1.d-10 'free' ; i-1

'guess for ph'
7.0

'extent of zone'
0.0 0.115639 0.0 1.0 0.0 0.115639

'end of zone'
! --------------------------------------------------

'done'

!
! Data Block 16: boundary conditions - reactive transport
! --------------------------------------------------
!
'boundary conditions - reactive transport'
```

```
3               ;number of initial condition zones

! -------------------------------------------------
'number and name of zone'
1
'inflow bounadry 1'

'boundary type'
'first'

'concentration input'           ;inflow bounadry 1
0.5 'free' ; i-1

'guess for ph'
7.0
'extent of zone'
0.0 0.0 0.0 1.0 0.0 0.005

'end of zone'
! -------------------------------------------------
'number and name of zone'
2
'inflow boundary 2'

'boundary type'
'first'

'concentration input'           ;inflow boundary 2
0.5 'free' ; i-1

'guess for ph'
7.0
'extent of zone'
0.0 0.0 0.0 1.0 0.110827 0.115639

'end of zone'
! -------------------------------------------------
'number and name of zone'
3
'outflow boundary '

'boundary type'
'second'

'guess for ph'
7.0
```

'extent of zone'
0.115639 0.115639 0.0 1.0 0.05 0.06

'end of zone'
! ---

'done'

MIN3P Input.por, .tor, .hyc, and .aqt files – 120 hours

These files are too large, found elsewhere.

Appendix D Measuring D_P in two-dimensions; Rock Cut Near Meductic Sample; Parameter Estimation Software (PEST)

P.E.S.T. requires 3 files to run;
1) Template file; One for each model input file
2) Instruction file; One for each model output file in which model generated observations exist
3) A control file, giving pest; template, instruction, model input and model output file names as well as control parameters, problem size, initial values, etc.

Pest Template File - notes

The template file is a replica of the input file except in the location of the parameter you wish P.E.S.T. to optimize. In these locations the parameter is replaced with a series of charaters. At top of the file, must input "pft" "space" then the parameter delimiter (EX: pft %). The delimited must not be present anywhere else in the input file. The name of the parameter "Tau" must be placed between the two delimiters (EX: %Tau %).

To endow the parameter with the ideal amount of precision, specify the number of spaces between the final character and the delimiter to that which the model uses to calculate parameters from the input file. MIN3P's free field to uses 7 numbers of precision, therefore, 7 spaces are placed between the u and last delimiter "%"; %Tau   %.

P.E.S.T. has a max precision of 13 characters. As a rule of thumb, give P.E.S.T. a little more precision, it helps it run better as it is able to distinguish parameter values (model values) Vs. incrementally varied parameter values (P.E.S.T. values).

PRECIS is a control that must be specified as either "single" or "double". If "Single" is chosen any amount of characters more than which you have specified are reduced to the given amount. Good idea maybe to select "double". If you do chose "single", specify 13 characters.

DPOINT is a control variable that squeezes the max amount of precision into a variable, to have this command executed, specify the string "no point", if you do not want character squeezing, specify "point".

Each observation much have a unique name (EX: p1 = Tau_1…. P2 = Tau_2)

Once the template file has been written TEMPCHEK is run to verify the file does not have any syntax errors.

Pest Template File (.tpl)

This file is too large, found elsewhere.

Pest Instruction File - notes

This file iteratively runs model simulations until the coupled PEST & Model output data outputs the minimum sum of squared weighted residuals between laboratory generated (measured) data and model output (modelled) data. This file is given the extension ".ins".

For PEST to read model output, output files must be saved as .txt documents. For binary output, write a program that converts the output into ACSII, a format PEST can read.

This file provides PEST with a list of instructions on how to find observations. PEST reads model output files in from top to bottom and left to right. Instructions must occur in this order, PEST cannot back track to complete instructions.

The first line of this file must read “pif” (pest instruction file) followed by one space, followed by the marker delimiter “$” (pif $). The role of these delimiters are used only to define the character range of the marker (EX: !con1!). These delimiters are placed immediately before and after the first and last character of the marker. The delimiter must not appear anywhere else in the file.

Each observation name (unlike parameter names) must have a unique name (EX: con1, con2, etc). These observation names must be provided in the control file where measurement values and weights are provided. Dummy observations “dum” tell PEST that the dummy observation in the model output file does not need to match the measurement defined by the laboratory data.

The line advance function “ln” (where l initiates the function, and n defines the line number) is used to scan for the values PEST will solve for (EX: “l889” will bring you to line 889 of the text file).

Once the instruction file has been written INSCHEK is run to verify the file does not have any syntax errors.

Not used in this study, helpful notes:

On the line in question that your observation is on, you may use the white space command to have pest move its cursor to the number on that line you are interested in (EX: “L654 w w w w !obs1!” will move the cursor to line 654 of the text file and to the 4^{th} number on that line).

The tab function “tn” is used to bring the cursor to a specified column within the already specified line, where n = characters to the right of the line, starting at 1 (EX: l4 t60 %=% !a3!).

The %=% brings the cursor to the next = sign and from there PEST can read the last number on the line as a non-fixed observation.

Fixed observations are effective in for tabular output files (EX: l543 [obvs1] 21:31 [obvs2] 37:47 [obvs3] 49:59).

Semi fixed observations are effective when changing precision (character numbers) in observations between simulations (EX: l543 (obvs1) 21:31 (obvs2) 37:47 (obvs3) 49:59).

Non Fixed observations allows you to find the number as specified by any amount of characters that begin and end with a blank space (EX: !Obvs1!). This can be mixed with white spaces if they are far into a line.

Pest Instruction File (.ins)

This file is too large, found elsewhere.

Pest Control File - notes

The PEST control file must have the extension ".pst".

The first line of this file must read "pcf".

Each section of the control file must begin with a "*" character, followed by a space, then the header (EX: * control data); refer to figure a1.1 in user manual.

Mandatory sections of the control file in order:

1) Control data: problem dimensions, mode of PEST operation, termination criteria, change limits and other control data;
2) Parameter groups; variables which govern the way in which finite-difference derivatives are calculated;
3) Parameter data; initial parameter values, define data and the transformation status, bounds, groups, scales and offsets;
4) Observation groups; list of observation groups and includes names of files holding observation covariance matrices.
5) Observation data; provides measured values of observation, weights and groups to which observations belong.
6) Model command line; provides one or a number of command lines used by PEST to run the model; and
7) Model input/output; lists template and corresponding model input files as well as instruction and corresponding model input files.

CONTROL DATA

```
* control data
RSTFLE PESTMODE
NPAR NOBS NPARGP NPRIOR NOBSGP [MAXCOMPDIM] [DERZEROLIM]
NTPLFLE NINSFLE PRECIS DPOINT [NUMCOM JACFILE MESSFILE] [OBSREREF]
RLAMBDA1 RLAMFAC PHIRATSUF PHIREDLAM NUMLAM [JACUPDATE] [LAMFORGIVE] [DERFORGIVE]
RELPARMAX FACPARMAX FACORIG [IBOUNDSTICK UPVECBEND] [ABSPARMAX]
PHIREDSWH [NOPTSWITCH] [SPLITSWH] [DOAUI] [DOSENREUSE] [BOUNDSCALE]
NOPTMAX PHIREDSTP NPHISTP NPHINORED RELPARSTP NRELPAR [PHISTOPTHRESH] [LASTRUN] [PHIABANDON]
ICOV ICOR IEIG [IRES] [JCOSAVE] [VERBOSEREC] [JCOSAVEITN] [REISAVEITN] [PARSAVEITN] [PARSAVERUN]
```

Figure D. 1. *PEST control data format. After* (Doherty, 2018b).

LINE 1:
* control data

LINE 2:
RSTFLE; enter ether "restart" or "norestart". Norestart is chosen, if the simulation is terminated for any reason, it will not recommence where it left off.

PESTMODE; enter either "estimation", "regularisation", "prediction" or "pareto".

LINE 3:
NPAR; total number of parameters in the current case (integer); 1946
NOBS; number of observations in the current case (integer (not including dummys)); 324
NPARGP; number of parameter groups (integer); 1
NPRIOR; number of prior information files in the parameter estimation process (integer); 0
NOBSGP; Number of observation groups in the pest control file (integer); 1

LINE 4:
NTPLFLE; number of template files (integer); 1
NINSFLE; number of instruction files (integer); 1
PRECIS; enter either "single" or "double"; single will have parameter generation of values less than 13 characters, if you need more, use double (26 characters).
DPOINT; enter either "point" or "nopoint"; no point removes the decimal point (used if they are redundant or if extra precision is needed.
[NUMCOM JACFILE MASSFILE]; for normal operation (how pest obtains derivatives from the model) use the following configuration; 1 0 0

LINE 5:
LAMBDA1; initial value of Marquadt Lambda; suggested at 10.0, Tom has his set to 5.0…probably to increase simulation speed.
RLAMFAC; factor the lambda variable is adjusted by; suggestions; 2.0
PHIRATSUF; phi ratio sufficient; suggested 0.3. This term is the goal of the iteration, once achieved, pest will move to the next.
PHIREDLAM; backup criterion used if PHIRATSUF cannot be achieved; suggested 0.01-0.05, (to large; may not try enough lambda/criterion to easy. To small; may try too many lambas); 0.01 to optimize!
NUMLAM; upper limit of lambdas tested during one iteration; suggested 5-10 (higher); 10.

LINE 6:
RELPARMAX; maximum relative charge that a parameter undergoes in an optimization iteration; ideally set to 10, but lower if the problem is highly non-linear; 5.0 (cannot be less than 1).
FACPARMAX; maximum factor of change of that parameter; ideally set to 10, but lower if the problem is highly non-linear; 3.0 or 5.0 as it is very non-linear (can be less than 1as long as no upper or lower bounds are of opposite sign (-ve/+ve).
ABSPARMAX; maximum absolute change parameters assigned to group (N) undergo (this variable is actually an array); suggested is 0.001. This study applied 0.05.

LINE 7:
PHIREDSWH; variable coupled with the FORCEN switch code. Suggested value is 0.1 and is applied (may switch to higher order derivatives before needed, too low, may take extra runs to fill the Jacobian matrix).

LINE 8:
NOPTMAX; number of possible iterations in an estimation run; suggested 50; 30.
PHIREDSTP; optimization iterations parameter; suggested 0.005; 0.005

NPHISTP; optimization iterations parameter, CAREFEUL, if set too low and the number is near its lower bound, the number may be over shot; suggested 4; 4.
NPHINORED; an overwrite parameter to terminate run if PEST has failed to lower the objective function over X iterations (integer); suggested 3 or 4; 3
RELPARSTP; if the maximum relative parameter change between iterations is greater than X, simulation will be terminated; suggested 0.005; 0.01
NRELPAR; if the maximum relative parameter change between iterations is greater than X, simulation will be terminated; suggested 3 or 4; 3

LINE 9:
ICOV-ICOR-IEIG; in the case that ISQR nor decomposition are employed in the solution of the inverse problem, the user may set all values either to 0 or 1. 0; no values are recorded/1;all values are recorded; 0 0 0, set all to 0 to know if this is occurring as all values will be output regardless.

Parameter Groups

```
* parameter groups
PARGPNME INCTYP DERINC DERINCLB FORCEN DERINCMUL DERMTHD [S
(one such line for each of NPARGP parameter groups)
```

Figure D. 2. *PEST parameter groups format. After* (Doherty, 2018b).

LINE 1:
PARGPNME; parameter group name; suggested max 6 character; tau
INCTYP; suggested for “relative” or “rel_to_max”
DERINC; for the above “relative” choice, manual suggests 0.01 to 0.02; 0.015
DERINCLB: this is an absolute lower bound placed on al parameter groups for the purposes of reliable derivatives to be calculated; 0.0 (to not place a lower bound).
FORCEN; forward central variable options; “always_2”, “always_3”, “always_5”, “switch” or “switch_5”. always_x values, fill Jacobian matrix through the columns, will require amount of runs for each parameter in the parameter group. Switches switch the forward function to x-point derivatives and this the suggested method; switch; speed takes precedence early, allows precision to take over to increase accuracy and later again speed when precision has been obtained.
DERINCMUL; derivative calculation increment in association with the above term; suggested 1.0 to 2.0
DERMTHD; this informs pest which derivative method to use; option are “parabolic”, “best_fit” or “outside_pts”. Suggestion when FORCEN is switch is for this parameter to be “parabolic, but we want the best fit to our laboratory measurements.

Parameter Data

```
* parameter data
PARNME PARTRANS PARCHGLIM PARVAL1 PARLBND PARUBND PARGP SCALE OFFSET DERCOM
(one such line for each of NPAR parameters)
PARNME PARTIED
(one such line for each tied parameter)
```

Figure D. 3. *PEST parameter data format. After* (Doherty, 2018b).

LINE 1:
PARNME; parameter name; Taux, here x is an integer.
PARTANS; may be "none", "log", "fixed" or "tied". At least one log-transfromed value can increase the success rate of the inversion process and thus the run.
PARCHGLIM; this variable designates whether parameters are factor, absolute or relative limited. Because parameters are log-transformed we may not use absolute limits; "factor"
PARVAL1; is the parameters starting/preferred value to be improved with each iteration, if relative, must be a non-zero value; 8.04e-2
PARLBND; parameter lower bound; 1.0e-06
PARUBND; parameter upper bound; 1.0e-0
PARGP; parameter's group name; tau
SCALE; Allows you to redefine the domain of a parameter. Set to 1.0, we wish to leave the parameter unaffected.
OFFSET; allows you to redefine the domain of a parameter. Set to 0.0, we wish to leave the parameter unaffected.
DERCOM; we are not using PEST's external derivatives; 1.
/ part 2

This section is omitted because there are no tied parameters.

Observation Groups

```
* observation groups
OBGNME [GTARG] [COVFLE]
(one such line for each of NOBSGP observation group)
```

Figure D. 4. *PEST observation groups format. After* (Doherty, 2018b).

LINE 1:
OBGNME; obvsgp

Observation Data

```
* observation data
OBSNME OBSVAL WEIGHT OBGNME
(one such line for each of NOBS observations)
```

Figure D. 5. *PEST observation data format. After* (Doherty, 2018b).

LINE 1:
OBSNME; observation name; unique less than 20 characters; conx, here x is an integer.
OBSVAL; a real variable corresponding to laboratory measurements. Pest reduces the difference between this number and the simulation number counterpart. X, this data is entered using experimental timeseries radiograph measurements.
WEIGHT; weight attached to each residual in the objective function. Higher weights may be assignment to observations with less structural and measurements noise. We want all cells weighted equally, so we are choosing 1.0 for each observation.
OBGNME; observation group name; obvsgp

Model Command Line

It may be the name of an executable file, batch or script file" MIN3P_THCm_win32d.exe < STB22.inp
You may include the path name (location where file is situated) in the model command line.

Model input/Output

This section relates PEST template files to model input files and PEST instruction files to model output files. Seen Below;

```
* model input/output
TEMPFLE INFLE
(one such line for each of NTPLFLE template files)
INSFLE OUTFLE
(one such line for each of NINSLFE instruction files)
```

Figure D. 6. *PEST model input/output format. After* (Doherty, 2018b).

LINE 1:
TEMPFLE; PEST template file; STB22.tpl
INFLE; model input file; STB22.tor

LINE 2:
INSFLE; PEST instruction file; STB22.ins
OUTFLE; model output file; STB22_2.gst

Once the control file has been written PESTCHEK is run to verify the file does not have any syntax errors.

Pest Control File (.pst)

This file is too large, found elsewhere.

Appendix E Measuring D_P in two-dimensions; Rock Cut Near Meductic Sample; Fortran Code

Method of calculating modelled D_P values using Fortran script and Geany

1) Create an array of initial hydraulic conductivity values and initial iodide concentrations (aqueous totals) for the model domain. A grid of pixels from one radiograph .tiff file are converted to a .txt file "stbspw" as an arrangement of formatted values. Geany is used to build and compile Fortran script that writes a unique .hyc and .aqt file in a format MIN3P can read, draw from, and assign to corresponding cells in the model grid at time zero of the simulation.

2) Create an array of initial ϕ_I and τf values for the model domain. A grid of pixels from processed radiograph .tiff gsv and porosity files are converted to .txt files "stbspw" and "stbporosity2732" as an arrangement of formatted values. Geany is used to build and compile Fortran script that writes a unique .por and .tor file in a format MIN3P can read, draw from, and assign to corresponding cells in the model grid at time zero of the simulation.

3) Create an array of C/C_0 values for each of the 5 ROIs in the model domain. A grid of pixels from processed radiograph C/C_0 value and gsv .tiff files are converted to .txt files "c.co120a" and "stbspw" as an arrangement of formatted values. Geany is used to build and compile Fortran script that write a C/C_0 value file in the format a MIN3P output files are written. At the end of the MIN3P run, PEST will calculate the sum of squared weighted residuals between modelled and measured data. Pest will iteratively run simulations changing model τf values each run until the least sum of squared weighted residuals is found between modelled and measured C/C_0 values.

4) Create a PEST template file (.tpl) to identify the location of observations throughout the model grid, two Fortran scripts are written. First, the same process used to create the .tor file is replicated to create the .tpl file except "ptf $" is written on the first line of the file and the file type. Second, the .tpl file values in the tortuosity column are stored as floats by Geany. Each cell within the ROIs are assigned a unique code (ex: $tau1 $). PEST will use these cells to determine the least sum of squared weighted residuals between modelled and measured C/C_0 values. Measured data at these locations are called observations.

5) Create a PEST instruction file (.ins) for PEST to locate the observations throughout the model grid. Geany draws from and reads through the .tpl file writing line advance function and dummy directives to locate observations in the .tpl file.

6) Create a PEST control file (.pst) for PEST to locate the adjustable parameters and observations throughout the model grid. Adjustable parameters (ex:tau1) and observations (ex:con1) are entered into the .pst file using the .tpl file and the txt file "c.co120aa" created in step 3, called the parameter data and observation data, respectively. PEST is also used to enter the control data problem dimensions, mode of PEST operation, termination criteria, change limits, control data, parameter groups, observation groups, model command line, and the model input/output (Appendix D). This

file is used to iteratively run MIN3P simulations adjusting the parameters identified in the .tpl file each run to achieve the parameter (τf) distribution resulting in the least sum of squared weighted residuals.

7) Create a .tiff file of D_P distributions at each time snap shot (22h, 120h, and 333 h) for analyses using Image J. The MIN3P output .tor file at simulation end time is processed in Geany to convert all non-parameter and non-observation cells to 0 value, effectively removing them. All cells with a non-zero value are multiplied by the free-water diffusion coefficient of iodide to create a MIN3P formatted array of modelled D_P values. The file is then formatted into an arrangement of rows and columns which can be converted into a .tiff file for image J analyses.

8) A similar approach (step 7) is used to convert the MIN3P formatted distribution of C/C_0 values into a an arrangement of rows and columns for analyses in image J.

Detailed PEST file walkthrough; creating the .tpl file

The first script calls upon three files.

First, Geany calls for the image J processed time series radiograph of measured C/C_0 values, binned to a 161x161 cell grid. Then asks for the dimensions (numbers and pixels, length and width) of the radiograph to process the information entering and rewrite a .txt file in a format MIN3P can read. The grid is allocated an addition row and column of half-cells at the top, bottom, left, and right to assign boundary conditions in min3p. Another row of cells is allocated for reading each number in a given row.

Every cell in the matrix is populated with C/C_0 values of 0.000 to start, and will be the default value on the borders. The script then iterates over the vertical dimension of the C/C_0 value array, which is 2 greater than pixel number due to the half cell borders – note, a 0.000 value has been added to the beginning and end, which are skipped over as the scan will only consider the assigned <nhpr> number of reads. A single row of digits (& <.>) characters are parsed into a vector of floats, at intervals of 10 (reading from format: 0.0000.000, etc.) resulting in unique C/C_0 value corresponding to which pixel index they appear at in each row. These values are stored and will be assigned throughout the array later in the script.

Second, Geany calls for the image J processed "spw" radiograph binned to a 161x161 cell grid. The "spw" radiograph captures the fully tracer saturated rock slab after 4000h of diffusion with the reservoir filled in synthetic pore water instead of tracer solution. This image allows the the rock slab and the reservoir to be distinguished by the unique ranges of gsvs using Geany. The image is allocated an addition row and column of half-cells at the top, bottom, left, and right to assign boundary conditions in min3p. Another row of cells is allocated for reading each number in a given row.

Every cell in the matrix is populated with gsv of 65536 to start, and will be the default value on the borders. The script then iterates over the vertical dimension of the gsv array, which is 2 greater than pixel number due to the half cell borders – note, a 65536 gsv has been added to the beginning and end, which are skipped over as the scan will only consider the assigned <nhpr>

number of reads. A single row of digits (& <.>) characters are parsed into a vector of floats, at intervals of 10 (reading from format: 0.0000.000, etc.) resulting in unique a gsv corresponding to which pixel index they appear at in each row. These values are stored and will be assigned throughout the array later in the script.

Third, Geany calls for the image J processed "STBporosity2732" radiograph of measured ϕ_I values, binned to a 161x161 cell grid. The "STBporosity2732" file is the difference of the fully saturated radiograph and the reference radiograph. This image allowes the oxidized and unaltered zones of the rock slab to be distinguished by the unique physical properties using Geany. The image is allocated an addition row and column of half-cells at the top, bottom, left, and right to assign boundary conditions in min3p. Another row of cells is allocated for reading each number in a given row.

Every cell in the matrix is populated with porosity value of 1.000 to start, and will be the default value on the borders. The script then iterates over the vertical dimension of the gsv array, which is 2 greater than pixel number due to the half cell borders – note, a porosity value of 1.000 has been added to the beginning and end, which are skipped over as the scan will only consider the assigned <nhpr> number of reads. A single row of digits (& <.>) characters are parsed into a vector of floats, at intervals of 10 (reading from format: 0.0000.000, etc.) resulting in unique a prosody value corresponding to which pixel index they appear at in each row. These values are stored and will be assigned throughout the array later in the script.

Geany writes the first 4 lines of text in the appropriate MIN3P format. The first 3 columns are written, discretizing the model domain in 163x163 cells in the x and z dimensions (length and width). The C/C_0, gsv, and ϕ_I floats are replaced with real values to write the 4^{th} column of the .txt file. At any discrete point, if the gsv is higher than 40000, the cell is allocated a tortuosity value of 1.0000000E+00 to represent the cell reservoir in the model domain. Within a specified range discrete points, if the porosity value is greater than 0.06, the cell is allocated a tortuosity value of 3.0499999E-04 to represent the rock slab's unaltered core in the model domain. At the remaining discrete points, if the C/C_0 value is greater than 0.1, the cell is allocated a tortuosity value of 8.0499999E-02 to represent the rock slab's unaltered core in the model domain. Once Geany has generated the file, enter "6.5336000E+04" into the last cell of the 4^{th} column.

A second Geany script replaces the value entered in the 4^{th} column of the .tpl file with parameter identifiers (ex: $tau1 $) in the 5 regions of interest. The PEST output file only generates the 1 column of values and identifiers, this columns must be copied and pasted into the .tpl created by the first Geany file.

Pest Template File – Incomplete: STB120.tpl

```
program PESTtemplate_file_generator !use file1; STBspw !Use file2: STBporosity2732
implicit none
integer nhpr !number of horizontal pixels radiograph (columns)
integer nvpr !number of vertical pixels radiograph (rows)
integer file
character junk !character data type,
character*72 :: filename !character string data type, character holds a string of n characters
character*1610 :: currentRowString !this character number be x (x is number of characters in each digit) times the number of horizontal pixels (find a way to allocate memory? Put in a subroutine?)
character*1610 :: currentRowString2 !this character number be x (x is number of characters in each digit) times the number of horizontal pixels (find a way to allocate memory? Put in a subroutine?)
character*1610 :: currentRowString3 !this character number be x (x is number of characters in each digit) times the number of horizontal pixels (find a way to allocate memory? Put in a subroutine?)
real, allocatable :: currentRowRealVector(:) !temporaraly storing floats in here between currentRowString and greyscale matrix
real, allocatable :: currentRowRealVector2(:) !temporaraly storing floats in here between currentRowString and greyscale matrix
real, allocatable :: currentRowRealVector3(:) !temporaraly storing floats in here between currentRowString and greyscale matrix
real, allocatable :: greyscale(:,:)!real;approximation of a real number
real, allocatable :: txtc_co(:,:)!real;approximation of a real number
real, allocatable :: txtporval(:,:)!real;approximation of a real number
integer l_filename
integer m_filename
integer n_filename
real plr !pixel length radiography
real hlr !length of x dimension in radiograph
real vlr !length of y dimension in radiograph
real mxl !model x-dimension length
```

```
real mzl !model z-dimension length
integer nxcvm !number of control volumes in x dimension
integer nzcvm !number of control volumes in y dimension
real z, y, x, gsv, restor, oxtor, untor, maxtxtcco, tau, mintxtcco, txtcco, por
character*4 :: tauFormatString, postTauFormatString
character*12 :: tauOutputString
character*6 :: tplfilename
character*1 :: tauDigits, deltaTauDigits
integer :: i, j, k, xValue,yValue, n, m
restor = 1.0000000E+00
oxtor = 8.0499999E-02
untor = 3.0499999E-04
mintxtcco = 0.2500000E+00 !maximum porosity (other files will have max gsv)
maxtxtcco = 1.1000000E+00 !maximum porosity (other files will have max gsv)
tau = 0.0
tplfilename = 'STB120'

write (*,'(a)') 'Welcome to ARRMCo'
write (*,'(a)') 'The AAMGP Radiography to MIN3P Converter'

write (*,'(a)') 'Input the name of the file with relative concentration values. (radiograh to txt, processed in excel back to txt)' !*passed to a subprogram. a is an array of characters
read (*,*) filename !this will be the .txt file with values processed from radiograph in visual studio & excel

l_filename=index(filename,' ')-1 !!!Enter; c.co120a

open (1,file = trim(filename(:l_filename))//'.txt',status='old',form='formatted',access='sequential')!open file stated above
write (*,*) 'opening ', filename(:l_filename), ' for processing'

write (*,*) 'What is the overall horizontal length of your radiograph in meters?' !ex:0.114925
read (*,*) hlr
write (*,*) 'Input the number of horizontal pixels in your radiograph;' !ex:161
read (*,*) nhpr

write (*,*) 'What is the overall vertical length of your radiograph in meters?' !ex:0.114925
read (*,*) vlr
write (*,*) 'Input the number of vertical pixels in your radiograph;' !ex:161
```

```
read (*,*) nvpr

write (*,*) 'What is the overall pixel length of your radiograph pixels in meters?' !ex:0.00071382
read (*,*) plr

write (*,*) nhpr,' columns!'
write (*,*) nvpr,' rows!'

!allocate an extra pixel at the top, bottom, left, and right for min3p boundary half cells.
allocate (txtc_co(nhpr+2,nvpr+2))

!this is for reading each number in a given row so we don't allocate extra space... border does not exist on image.
allocate (currentRowRealVector(nhpr))

!populate the entire matrix with c.co of 0.000 to start, that will be the default value on the borders.
do i=1,nhpr+2
   do j=1,nvpr+2
      txtc_co(i,j) = 0.000 !this value is the default c.co value for borders/margin (must be changed for every file)
   end do
end do

!we're iterating over the vertical dimension of c.co array, which is 2 greater than pixel number (half cell borders)
!but we're adding a 0.000 value to the beginning and end so we skip those. we can only do <nhpr> number of reads!
do i=nvpr+1,2,-1
   read (1,*) currentRowString
   IF ((i < 24).OR.(i > 140)) THEN
      cycle
   END IF

   !parse single row of digits (& <.>) characters into a vector of floats, at intervals of 10 (reading from format:
0.0000.000, etc)
   do k=10,(10*nvpr),10
      read(currentRowString(k-9:k),*) currentRowRealVector(k/10)
   end do

   !now we have our c.co values, corresponding to which pixel index they appear at in each row, so now we store.
   !Would be faster but less semantic to do away with this loop and cram storing logic into the one above, but I won't.
```

```
   do j=2,nhpr+1
      txtc_co(i,j) = currentRowRealVector(j-1)!c/co value read from .txt file (other files will read greyscale)
      end do
end do

write (*,'(a)') 'Input the name of the file used to generate .hyc and .aqt files. (radiograh to txt, processed in excel back to txt)' !*passed to a subprogram. a is an array of characters
read (*,*) filename !this will be the .txt file with values processed from radiograph in visual studio

n_filename=index(filename,' ')-1 !!!Enter; STBspw


open (2,file = trim(filename(:n_filename))//'.txt',status='old',form='formatted',access='sequential')!open file stated above
write (*,*) 'opening ', filename(:n_filename), ' for processing'

!allocate an extra pixel at the top, bottom, left, and right for the min3p boundary
allocate (greyscale(nhpr+2,nvpr+2))

!this is for reading each number in a given row so we don't allocate extra space... border does not exist on image.
allocate (currentRowRealVector2(nhpr))

!populate the entire matrix with gsv of 65536 to start, that will be the default value on the borders.
do i=1,nhpr+2
   do j=1,nvpr+2
      greyscale(i,j) = 65536 !this value is the default greyscale value for borders/margin (must be changed for every file)
   end do
end do

!we're iterating over the vertical dimension of greyscale array, which is 2 greater than pixel number (half cell borders)
!but we're adding a 65536 value to the beginning and end so we skip those. we can only do <nhpr> number of reads!
do i=nvpr+1,2,-1
   read (2,*) currentRowString2
   IF ((i < 24).OR.(i > 140)) THEN
      cycle
   END IF
```

```
   !parse single row of digit (& <.>) characters into a vector of floats, at intervals of 10 (reading from format:
0.0000.000, etc)
   do n=10,(10*nvpr),10
      read(currentRowString2(n-9:n),*) currentRowRealVector2(n/10)
   end do

   !now we have our gsvs, corresponding to which pixel index they appear at in each row, so now we store.
   !Would be faster but less semantic to do away with this loop and cram storing logic into the one above, but we
won't.
   do j=2,nhpr+1
      greyscale(i,j) = currentRowRealVector2(j-1)!gsvs read from .txt file
   end do

end do

write (*,'(a)') 'Input the image J porosity file name' !*passed to a subprogram. a is an array of characters
read (*,*) filename !this will be the .txt file with values processed from radiograph in visual studio

m_filename=index(filename,' ')-1 !!!Enter; STBporosity2732

open (3,file = trim(filename(:m_filename))//'.txt',status='old',form='formatted',access='sequential')!open file stated
above
write (*,*) 'opening ', filename(:m_filename), ' for processing'

!allocate an extra pixel at the top, bottom, left, and right for the min3p half cell boundary
allocate (txtporval(nhpr+2,nvpr+2))

!this is for reading each number in a given row so we don't allocate extra space... border does not exist on image.
allocate (currentRowRealVector3(nhpr))

!populate the entire matrix with pororsity values of 1.000 to start, that will be the default value on the borders.
do i=1,nhpr+2
   do j=1,nvpr+2
      txtporval(i,j) = 1.000 !this value is the default porosity value for borders/margin (must be changed for every file)
   end do
end do
```

```
!we're iterating over the vertical dimension of greyscale array, which is 2 greater than pixel number (half cell borders)
!but we're adding a 1000 value to the beginning and end so we skip those. we can only do <nhpr> number of reads!
do i=nvpr+1,2,-1
   read (3,*) currentRowString3
   IF ((i < 24).OR.(i > 140)) THEN
      cycle
   END IF

   !parse single row of digits (& <.>) characters into a vector of floats, at intervals of 10 (reading from format:
0.0000.000, etc)
   do m=10,(10*nvpr),10
      read(currentRowString3(m-9:m),*) currentRowRealVector3(m/10)
   end do

   !now we have our porosity values, corresponding to which pixel index they appear at in each row, so now we store.
   !Would be faster but less semantic to do away with this loop and cram storing logic into the one above, but we
won't.
   do j=2,nhpr+1
      txtporval(i,j) = currentRowRealVector3(j-1)!porosity value read from .txt file (other files will read greyscale)
   end do
end do

!now we write to a new or existing .tpl file of the same name
open(11,file=(tplfilename)//'.tpl',status='unknown',form='formatted')

write(11,'(a)') 'ptf $'
write(11,'(a)') 'title = stb120'
write(11,'(150a)') 'variables = "x", "y", "z", "tortuosity"'
write(11,'(a)') 'zone t= "T-j, initial", i = 163, j = 163, k = 1, f=point'

nxcvm = nhpr+2 !number of model control volumes x-dimension is equal to radiography number of horizontal pixels
plus 2 half cells
nzcvm = nvpr+2 !number of model control volumes z-dimension is equal to radiography number of vertical pixels plus
2 half cells

mxl = hlr+plr!total length in x dimension (m) !!!plus one hpl to add a half cell on both sides of model grid
```

```
mzl = vlr+plr!total length in z dimension (m) !!!plus one vpl to add a half cell on top and bottom of model grid

do i=1,nzcvm
   z = (i-1)*plr !this (i-1) term indicates where the reading starts and increases; from 0
   y=0
   do j=1,nxcvm
      txtcco = txtc_co(i,j) ! floats are replaced with real values
      gsv = greyscale(i,j) ! floats are replaced with real values
      txtpor = txtporval(i,j) !!this replaces greyscale floats with real numbers
      x = (j-1)*plr !this (i-1) term indicates where the reading starts and increases from (0)
      write (11,"(ES13.7)", advance='no') x
      write (11, "(a3)", advance='no') "
      write (11,"(ES13.7)", advance='no') y
      write (11, "(a3)", advance='no') "
      write (11,"(ES13.7)", advance='no') z
      write (11, "(a3)", advance='no') "
!tau values
      IF (gsv >= 40000) THEN
         write (11,"(ES13.7)") restor
      ELSE IF (((i <= 123).AND.(i >= 36).AND.(j <= 95)).AND.(txtpor <= 0.06))  THEN
         write (11,"(ES13.7)") untor
      ELSE IF (txtcco >= 0.1) THEN
         ! OK, this is a doozy! This is the best to support more than 9 tau values.
         ! It outputs something like '$tau<n>     $' where n increments each time.
         tau = tau + 1
         write(tauDigits, "(I1)") int(log10(tau))+1
         write(deltaTauDigits, "(I1)") 7 - int(log10(tau))
         write (tauOutputString, "(I"//tauDigits//")") int(tau)
         tauFormatString = "(a"//tauDigits//")"
         postTauFormatstring = "(a"//deltaTauDigits//")"
         write (11, "(a4)", advance='no') '$tau'
         write (11, tauFormatString, advance='no') tauOutputString
         write (11, postTauFormatString, advance='no') "
         write (11, "(a1)") '$'
      ELSE IF (cco /= 65336) THEN
         write (11,"(ES13.7)") oxtor
      ELSE
```

```
      END IF
   end do
end do

write (*,*)
write (*,*) 'Your "STBhour" template file is now ready - Good luck!'
write (*,*) 'write 6.5336000E+04 as the 4th column value on the last row of your processed .tpl file'
write (*,*) 'now use the second .tpl file geneator to locate the obsevations in the .tpl file'

write (*,'(a)') 'Processing complete!'
write (*,'(a)') 'Goodbye!'

end program PESTtemplate_file_generator
```

PEST Template File – 4th column: STB120f.tpl

```
program PESTtemplate_file_generator !use file1; STB120.tpl
implicit none
integer file
character junk !character data type,
character*72 :: filename !character string data type, character holds a string of n characters
integer l_filename
character*4 :: tauFormatString, postTauFormatString
character*12 :: tauOutputString
character*7 :: tplfilename
character*1 :: tauDigits, deltaTauDigits
integer :: i, j, k, xValue,yValue, n, m, eof
real x, y, z, x1, x1a, z1, z1a, x2, x2a, z2, z2a, x3, x3a, z3, z3a, x4, x4a, z4, z4a, x5, x5a, z5, z5a, x6, x6a, z6, z6a
character*13 :: tplval!value from 4th column in .tpl file
real restor, oxtor, untor, tau
restor = 1.0000000E+00
oxtor = 8.0499999E-02
untor = 3.0499999E-04
tau = 0.0
tplfilename = 'STB120f'

x1 = 1.5704039E-02
x1a = 1.7131679E-02
```

```
z1 = 8.6372219E-02
z1a = 9.5651880E-02
x2 = 7.9234019E-02
x2a = 8.0661662E-02
z2 = 6.4243801E-02
z2a = 8.2803115E-02
x3 = 8.6372219E-02
x3a = 1.0921445E-01
z3 = 5.0681219E-02
z3a = 5.2108858E-02
x4 = 6.9954358E-02
x4a = 7.1382001E-02
z4 = 2.1414600E-02
z4a = 3.8546279E-02
x5 = 2.2128420E-02
x5a = 2.3556059E-02
z5 = 1.9273140E-02
z5a = 2.4983700E-02

write (*,'(a)') 'Welcome to ARRMCo'
write (*,'(a)') 'The AAMGP Radiography to MIN3P Converter'

write (*,'(a)') 'Input the pest template filename for this timeseries' !*passed to a subprogram. a is an array of
characters
read (*,*) filename !this will be the .txt file with values processed from radiograph in visual studio & excel

l_filename=index(filename,' ')-1 !!!Enter; STB120.tpl

open (1,file = trim(filename(:l_filename))//'.tpl',status='old',form='formatted',access='sequential')!open file stated above
write (*,*) 'opening ', filename(:l_filename), ' for processing'

!now we write to a new or existing f.tpl file of the same name
open(11,file=(tplfilename)//'.tpl',status='unknown',form='formatted')

write(11,'(a)') 'ptf $'
write(11,'(a)') 'title = stb120'
write(11,'(150a)') 'variables = "x", "y", "z", "tortuosity"'
```

```
write(11,'(a)') 'zone t= "T-j, initial", i = 163, j = 163, k = 1, f=point'

!read ptf (pest template file (.tpl)) file to 5th line where values reside
read (1,*)
read (1,*)
read (1,*)
read (1,*)

10 read (1, '(ES13.7,3x,ES13.7,3x,ES13.7,3x,a13)', iostat=eof) x, y, z, tplval
    IF (tplval(1:4) == '$tau') THEN
            tau = tau + 1
            write(tauDigits, "(I1)") int(log10(tau))+1
            write(deltaTauDigits, "(I1)") 7 - int(log10(tau))
            write (tauOutputString, "(I"//tauDigits//")") int(tau)
            tauFormatString = "(a"//tauDigits//")"
            postTauFormatstring = "(a"//deltaTauDigits//")"
            write (11, "(a4)", advance='no') '$tau'
            write (11, tauFormatString, advance='no') tauOutputString
            write (11, postTauFormatString, advance='no') ''
            write (11, "(a1)") '$'
            go to 10
! section of interest 1
    ELSE IF ((x >= x1).AND.(x <= x1a).AND.(z >= z1).AND.(z <= z1a)) THEN
       tau = tau + 1
            write(tauDigits, "(I1)") int(log10(tau))+1
            write(deltaTauDigits, "(I1)") 7 - int(log10(tau))
            write (tauOutputString, "(I"//tauDigits//")") int(tau)
            tauFormatString = "(a"//tauDigits//")"
            postTauFormatstring = "(a"//deltaTauDigits//")"
            write (11, "(a4)", advance='no') '$tau'
            write (11, tauFormatString, advance='no') tauOutputString
            write (11, postTauFormatString, advance='no') ''
            write (11, "(a1)") '$'
            go to 10
! section of interest 2
    ELSE IF ((x >= x2).AND.(x <= x2a).AND.(z >= z2).AND.(z <= z2a)) THEN
       tau = tau + 1
```

```
         write(tauDigits, "(I1)") int(log10(tau))+1
         write(deltaTauDigits, "(I1)") 7 - int(log10(tau))
         write (tauOutputString, "(I"//tauDigits//")") int(tau)
         tauFormatString = "(a"//tauDigits//")"
         postTauFormatstring = "(a"//deltaTauDigits//")"
         write (11, "(a4)", advance='no') '$tau'
         write (11, tauFormatString, advance='no') tauOutputString
         write (11, postTauFormatString, advance='no') ''
         write (11, "(a1)") '$'
         go to 10
! section of interest 3
   ELSE IF ((x >= x3).AND.(x <= x3a).AND.(z >= z3).AND.(z <= z3a)) THEN
      tau = tau + 1
         write(tauDigits, "(I1)") int(log10(tau))+1
         write(deltaTauDigits, "(I1)") 7 - int(log10(tau))
         write (tauOutputString, "(I"//tauDigits//")") int(tau)
         tauFormatString = "(a"//tauDigits//")"
         postTauFormatstring = "(a"//deltaTauDigits//")"
         write (11, "(a4)", advance='no') '$tau'
         write (11, tauFormatString, advance='no') tauOutputString
         write (11, postTauFormatString, advance='no') ''
         write (11, "(a1)") '$'
         go to 10
! section of interest 4
   ELSE IF ((x >= x4).AND.(x <= x4a).AND.(z >= z4).AND.(z <= z4a)) THEN
      tau = tau + 1
         write(tauDigits, "(I1)") int(log10(tau))+1
         write(deltaTauDigits, "(I1)") 7 - int(log10(tau))
         write (tauOutputString, "(I"//tauDigits//")") int(tau)
         tauFormatString = "(a"//tauDigits//")"
         postTauFormatstring = "(a"//deltaTauDigits//")"
         write (11, "(a4)", advance='no') '$tau'
         write (11, tauFormatString, advance='no') tauOutputString
         write (11, postTauFormatString, advance='no') ''
         write (11, "(a1)") '$'
         go to 10
! section of interest 5
```

```
   ELSE IF ((x >= x5).AND.(x <= x5a).AND.(z >= z5).AND.(z <= z5a)) THEN
     tau = tau + 1
        write(tauDigits, "(I1)") int(log10(tau))+1
        write(deltaTauDigits, "(I1)") 7 - int(log10(tau))
        write (tauOutputString, "(I"//tauDigits//")") int(tau)
        tauFormatString = "(a"//tauDigits//")"
        postTauFormatstring = "(a"//deltaTauDigits//")"
        write (11, "(a4)", advance='no') '$tau'
        write (11, tauFormatString, advance='no') tauOutputString
        write (11, postTauFormatString, advance='no') ''
        write (11, "(a1)") '$'
        go to 10
   ELSE IF (tplval == '1.0000000E+00') THEN
        write (11,"(ES13.7)") restor
        go to 10
   ELSE IF (tplval == '8.0499999E-02') THEN
        write (11,"(ES13.7)") oxtor
        go to 10
   ELSE IF (tplval == '3.0499999E-04') THEN
        write (11,"(ES13.7)") untor
        go to 10
   ELSE IF (tplval == '6.5336000E+04') THEN
      go to 20
20    END IF

write (*,*)
write (*,*) 'Your "STBhourf" template file is now ready - Good luck!'
write (*,*) 'write 6.5336000E+04 as the 4th column value on the last row of your processed .tpl file'
write (*,*) 'now replace the tortuosity column generated by the "STBhourtpl" script with the coumn generated by this
script.'

write (*,'(a)') 'Processing complete!'
write (*,'(a)') 'Goodbye!'

end program PESTtemplate_file_generator
```

All other Fortran scripts used in Geany to obtain modelled DP values

Hydraulic Conductivity File: STB120.hyc

```
program hydraulicconductivity_file_generator !use file STBspw
implicit none
integer nhpr !number of columns
integer nvpr !number of rows
integer file
character junk !character data type,
character*72 :: filename !character string data type, character holds a string of n characters
character*1610 :: currentRowString !this character number be x (x is number of characters in each digit) times the
number of horizontal pixels (find a way to allocate memory? Put in a subroutine?)
real, allocatable :: currentRowRealVector(:) !temporaraly storing floats in here between currentRowString and
greyscale matrix
real, allocatable :: greyscale(:,:)!real;approximation of a real number
integer l_filename
real plr !pixel length radiography
real hlr !length of x dimension in radiograph
real vlr !length of y dimension in radiograph
real mxl !model x-dimension length
real mzl !model z-dimension length
integer nxcvm !number of control volumes in x dimension
integer nzcvm !number of control volumes in y dimension
real z, y, x, hyc, reshyc,geolhyc, max_gsv, max_gsv1, tau, kyy
character*4 :: tauFormatString, postTauFormatString
character*12 :: tauOutputString
character*6 :: hycfilename
character*1 :: tauDigits, deltaTauDigits
integer :: i, j, k, xValue,yValue, n
reshyc = 1.0000000E-00
geolhyc = 1.0000000E-12
max_gsv = 40000 !maximum porosity (other files will have max gsv)
tau = 0.0
kyy = 1.0000000E-10
hycfilename = 'STB120'

write (*,'(a)') 'Welcome to ARRMCo'
```

```
write (*,'(a)') 'The AAMGP Radiography to MIN3P Converter'

write (*,'(a)') 'Input the file name if you want this program to work.' !*passed to a subprogram. a is an array of
characters
read (*,*) filename !this will be the .txt file with values processed from radiograph in visual studio

l_filename=index(filename,' ')-1 !!!Enter; STBspw


open (1,file = trim(filename(:l_filename))//'.txt',status='old',form='formatted',access='sequential')!open file stated above
write (*,*) 'opening ', filename(:l_filename), ' for processing'

write (*,*) 'What is the overall horizontal length of your radiograph in meters?' !ex:0.114925
read (*,*) hlr
write (*,*) 'Input the number of horizontal pixels in your radiograph;' !ex:161
read (*,*) nhpr

write (*,*) 'What is the overall vertical length of your radiograph in meters?' !ex:0.114925
read (*,*) vlr
write (*,*) 'Input the number of vertical pixels in your radiograph;' !ex:161
read (*,*) nvpr

write (*,*) 'What is the overall pixel length of your radiograph pixels in meters?' !ex:0.00071382
read (*,*) plr

write (*,*) nhpr,' columns!'
write (*,*) nvpr,' rows!'

!allocate an extra pixel at the top, bottom, left, and right for the min3p half cell boundaries
allocate (greyscale(nhpr+2,nvpr+2))

!this is for reading each number in a given row so we don't allocate extra space... border does not exist on image.
allocate (currentRowRealVector(nhpr))

!populate the entire matrix with gsv of 65536 to start, that will be the default value on the borders.
do i=1,nhpr+2
   do j=1,nvpr+2
```

```
        greyscale(i,j) = 65536 !this value is the default greyscale value for borders/margin (must be changed for every
file)
    end do
end do

!we're iterating over the vertical dimension of greyscale array, which is 2 greater than pixel number (half cell borders)
!but we're adding a 65536 value to the beginning and end so we skip those. we can only do <nhpr> number of reads!
do i=nvpr+1,2,-1
    read (1,*) currentRowString
    IF ((i < 24).OR.(i > 140)) THEN
        cycle
    END IF

    !parse single row of digit (& <.>) characters into a vector of floats, at intervals of 10 (reading from format:
0.0000.000, etc)
    do k=10,(10*nvpr),10
        read(currentRowString(k-9:k),*) currentRowRealVector(k/10)
    end do

    !now we have our greyscale values, corresponding to which pixel index they appear at in each row, so now we
store.
    !Would be faster but less semantic to do away with this loop and cram storing logic into the one above, but we
won't.
    do j=2,nhpr+1
        greyscale(i,j) = currentRowRealVector(j-1)!gsvs read from .txt file
    end do
end do

!now we write to a new or existing .hyc file of the same name
open(11,file=(hycfilename)//'.hyc',status='unknown',form='formatted')

write(11,'(a)') 'title = dataset stb120, hyc'
write(11,'(150a)') 'variables = "x", "y", "z", "kxx", "kyy", "kzz"'
write(11,'(a)') 'zone t= "T-j, initial", i = 163, j = 163, k = 1, f=point'

nxcvm = nhpr+2 !number of model control volumes x-dimension is equal to radiography number of horizontal pixels
plus 2 half cells
```

```
nzcvm = nvpr+2 !number of model control volumes z-dimension is equal to radiography number of vertical pixels plus
2 half cells

mxl = hlr+plr!total length in x dimension (m) !!!plus one hpl to add a half cell on both sides of model grid
mzl = vlr+plr!total length in z dimension (m) !!!plus one vpl to add a half cell on top and bottom of model grid

write (*,*) 'Hello, your min3p xmax value is ',mxl
write (*,*) 'and your min3p zmax value is ',mzl
write (*,*) 'The number of control volumes in the x direction is ',nxcvm
write (*,*) 'The number of control volumes in the z direction is ',nzcvm
write (*,*) 'The rest you will have to figure out yourself!'

do i=1,nzcvm
  z = (i-1)*plr !this (i-1) term indicates where the reading starts and increases; from 0
  y=0
  do j=1,nxcvm
    hyc = greyscale(i,j) !this replaces greyscale floats to real numbers
    x = (j-1)*plr !this (i-1) term indicates where the reading starts and increases; from 0
    write (11,"(ES13.7)", advance='no') x
    write (11, "(a3)", advance='no') ''
    write (11,"(ES13.7)", advance='no') y
    write (11, "(a3)", advance='no') ''
    write (11,"(ES13.7)", advance='no') z
    write (11, "(a3)", advance='no') ''
    IF (hyc >= max_gsv) THEN
      write (11,"(ES13.7)", advance='no') reshyc
    ELSE IF (hyc < max_gsv) THEN
      write (11,"(ES13.7)", advance='no') geolhyc
    END IF
    write (11, "(a3)", advance='no') ''
    write (11,"(ES13.7)", advance='no') kyy
    write (11, "(a3)", advance='no') ''
    IF (hyc >= max_gsv) THEN
      write (11,"(ES13.7)") reshyc
    ELSE IF (hyc < max_gsv) THEN
      write (11,"(ES13.7)") geolhyc
    END IF
```

```
    end do
end do

write (*,*)
write (*,*) 'Your hydraulic conductivity file is now ready - Good luck!'
write (*,*)

write (*,'(a)') 'Processing complete!'
write (*,'(a)') 'Goodbye!'

end program hydraulicconductivity_file_generator
```

Aqueous Totals File: STB120.aqt

```
program aqueoustotals_file_generator !use file STBspw
implicit none
integer nhpr !number of columns
integer nvpr !number of rows
integer file
character junk !character data type,
character*72 :: filename !character string data type, character holds a string of n characters
character*1610 :: currentRowString !this character number be x (x is number of characters in each digit) times the
number of horizontal pixels (find a way to allocate memory? Put in a subroutine?)
real, allocatable :: currentRowRealVector(:) !temporaraly storing floats in here between currentRowString and
greyscale matrix
real, allocatable :: greyscale(:,:)!real;approximation of a real number
integer l_filename
real plr !pixel length radiography
real hlr !length of x dimension in radiograph
real vlr !length of y dimension in radiograph
real mxl !model x-dimension length
real mzl !model z-dimension length
integer nxcvm !number of control volumes in x dimension
integer nzcvm !number of control volumes in y dimension
real z, y, x, aqt, resaqt, geolaqt, max_gsv, tau
character*4 :: tauFormatString, postTauFormatString
character*12 :: tauOutputString
```

```
character*6 :: aqtfilename
character*1 :: tauDigits, deltaTauDigits
integer :: i, j, k, xValue,yValue, n
resaqt = 1.0000000E+00
geolaqt = 1.0000000E-10
max_gsv = 40000 !maximum gsv
tau = 0.0
aqtfilename = 'STB120'

write (*,'(a)') 'Welcome to ARRMCo'
write (*,'(a)') 'The AAMGP Radiography to MIN3P Converter'

write (*,'(a)') 'Input the file name if you want this program to work.' !*passed to a subprogram. a is an array of
characters
read (*,*) filename !this will be the .txt file with values processed from radiograph in visual studio

l_filename=index(filename,' ')-1 !!!Enter; STBspw


open (1,file = trim(filename(:l_filename))//'.txt',status='old',form='formatted',access='sequential')!open file stated above
write (*,*) 'opening ', filename(:l_filename), ' for processing'

write (*,*) 'What is the overall horizontal length of your radiograph in meters?' !ex:0.114925
read (*,*) hlr
write (*,*) 'Input the number of horizontal pixels in your radiograph;' !ex:161
read (*,*) nhpr

write (*,*) 'What is the overall vertical length of your radiograph in meters?' !ex:0.114925
read (*,*) vlr
write (*,*) 'Input the number of vertical pixels in your radiograph;' !ex:161
read (*,*) nvpr

write (*,*) 'What is the overall pixel length of your radiograph pixels in meters?' !ex:0.00071382
read (*,*) plr

write (*,*) nhpr,' columns!'
write (*,*) nvpr,' rows!'
```

```
!allocate an extra pixel at the top, bottom, left, and right for the min3p half cell boundaries
allocate (greyscale(nhpr+2,nvpr+2))

!this is for reading each number in a given row so we don't allocate extra space... border does not exist on image.
allocate (currentRowRealVector(nhpr))

!populate the entire matrix with gsv of 65336 to start, that will be the default value on the borders.
do i=1,nhpr+2
   do j=1,nvpr+2
      greyscale(i,j) = 65536 !this value is the default greyscale value for borders/margin (must be changed for every
file)
   end do
end do

!we're iterating over the vertical dimension of greyscale array, which is 2 greater than pixel number (half cell borders)
!but we're adding a 65536 value to the beginning and end so we skip those. we can only do <nhpr> number of reads!
do i=nvpr+1,2,-1
   read (1,*) currentRowString
   IF ((i < 24).OR.(i > 140)) THEN
      cycle
   END IF

   !parse single row of digit (& <.>) characters into a vector of floats, at intervals of 10 (reading from format:
0.0000.000, etc)
   do k=10,(10*nvpr),10
      read(currentRowString(k-9:k),*) currentRowRealVector(k/10)
   end do

   !now we have our greyscale values, corresponding to which pixel index they appear at in each row, so now we
store.
   !Would be faster but less semantic to do away with this loop and cram storing logic into the one above, but we
won't.
   do j=2,nhpr+1
      greyscale(i,j) = currentRowRealVector(j-1)!gsv read from .txt file
   end do
end do
```

```
!now we write to a new or existing .aqt file of the same name
open(11,file=(aqtfilename)//'.aqt',status='unknown',form='formatted')

write(11,'(a)') 'title = "dataset stb120, aqt"'
write(11,'(150a)') 'variables = "x", "y", "z", "i-1"'
write(11,'(a)') 'zone t= "T-j, initial", i = 163, j = 163, k = 1, f=point'

nxcvm = nhpr+2 !number of model control volumes x-dimension is equal to radiography number of horizontal pixels
plus 2 half cells
nzcvm = nvpr+2 !number of model control volumes z-dimension is equal to radiography number of vertical pixels plus
2 half cells

mxl = hlr+plr!total length in x dimension (m) !!!plus one hpl to add a half cell on both sides of model grid
mzl = vlr+plr!total length in z dimension (m) !!!plus one vpl to add a half cell on top and bottom of model grid

write (*,*) 'Hello, your min3p xmax value is ',mxl
write (*,*) 'and your min3p zmax value is ',mzl
write (*,*) 'The number of control volumes in the x direction is ',nxcvm
write (*,*) 'The number of control volumes in the z direction is ',nzcvm
write (*,*) 'The rest you will have to figure out yourself!'

do i=1,nzcvm
   z = (i-1)*plr !this (i-1) term indicates where the reading starts and increases; from 0
   y=0
   do j=1,nxcvm
      aqt = greyscale(i,j) !this replaces greyscale floats with real numbers
      x = (j-1)*plr !does this (i-1) term indicate where the reading starts and increases from (0)
      write (11,"(ES13.7)", advance='no') x
      write (11, "(a3)", advance='no') ''
      write (11,"(ES13.7)", advance='no') y
      write (11, "(a3)", advance='no') ''
      write (11,"(ES13.7)", advance='no') z
      write (11, "(a3)", advance='no') ''
      IF (aqt >= max_gsv) THEN
         write (11,"(ES13.7)") resaqt
      ELSE IF (aqt < max_gsv) THEN
```

```
        write (11,"(ES13.7)") geolaqt
      END IF
   end do
end do

write (*,*)
write (*,*) 'Your aqueous totals file is now ready - Good luck!'
write (*,*)

write (*,'(a)') 'Processing complete!'
write (*,'(a)') 'Goodbye!'

end program aqueoustotals_file_generator
```

Porosity File: STB120.por

```
program porosity_file_generator!use file; 1.STBporosity2732 2.STBspw
implicit none
integer nhpr !number of columns
integer nvpr !number of rows
integer file
character junk !character data type,
character*72 :: filename !character string data type, character holds a string of n characters
character*1610 :: currentRowString, currentRowString2 !this character number be 5 times the number of horizontal
pixels (find a way to allocate memory? Put in a subroutine?)
real, allocatable :: currentRowRealVector(:), currentRowRealVector2(:) !temporaraly storing floats in here between
currentRowString and greyscale matrix
real, allocatable :: txtporval(:,:)!real;approximation of a real number
real, allocatable :: greyscale(:,:)!real;approximation of a real number
integer l_filename
integer m_filename
real plr !pixel length radiography
real hlr !length of x dimension in radiograph
real vlr !length of y dimension in radiograph
real mxl !model x-dimension length
real mzl !model z-dimension length
integer nxcvm !number of control volumes in x dimension
integer nzcvm !number of control volumes in y dimension
```

```
real z, y, x, porosity, max_porosity, tau, respor, unaltpor, tortuosity
character*4 :: tauFormatString, postTauFormatString
character*12 :: tauOutputString
character*6 :: porfilename
character*1 :: tauDigits, deltaTauDigits
integer :: i, j, k, xValue,yValue, n
max_porosity = 1.000 !maximum porosity
respor = 1.000
unaltpor = 0.015
tau = 0.0
porfilename = 'STB120'

write (*,'(a)') 'Welcome to ARRMCo'
write (*,'(a)') 'The AAMGP Radiography to MIN3P Converter'

write (*,'(a)') 'Input the file name if you want this program to work.' !*passed to a subprogram. a is an array of characters
read (*,*) filename !this will be the .txt file with values processed from radiograph in visual studio

l_filename=index(filename,' ')-1 !!!Enter; STBporosity2732


open (1,file = trim(filename(:l_filename))//'.txt',status='old',form='formatted',access='sequential')!open file stated above
write (*,*) 'opening ', filename(:l_filename), ' for processing'

write (*,*) 'What is the overall horizontal length of your radiograph in meters?' !ex:0.114925
read (*,*) hlr
write (*,*) 'Input the number of horizontal pixels in your radiograph;' !ex:161
read (*,*) nhpr

write (*,*) 'What is the overall vertical length of your radiograph in meters?' !ex:0.114925
read (*,*) vlr
write (*,*) 'Input the number of vertical pixels in your radiograph;' !ex:161
read (*,*) nvpr

write (*,*) 'What is the overall pixel length of your radiograph pixels in meters?' !ex:0.00071382
read (*,*) plr
```

```
write (*,*) nhpr,' columns!'
write (*,*) nvpr,' rows!'

!allocate an extra pixel at the top, bottom, left, and right for the min3p half cell boundaries.!add one row to bottom (all porval = 1.000), make first 119 (pixel row 0 to 118) rows porval = 1.000, make last 135 rows (pixel row 836 and lower) of .txt file porval = 1.000 and add one row to top (all gsv = 65536)
allocate (txtporval(nhpr+2,nvpr+2))

!this is for reading each number in a given row so we don't allocate extra space... border does not exist on image.
allocate (currentRowRealVector(nhpr))

!populate the entire matrix with porosity values of 1.000 to start, that will be the default value on the borders.
do i=1,nhpr+2
   do j=1,nvpr+2
      txtporval(i,j) = 1.000 !this value is the default porosity value for borders/margin (must be changed for every file)
   end do
end do

!we're iterating over the vertical dimension of the porosity_distribution_in_oxidized_rim_27_33.txt array, which is 2 greater than pixel number (half cell borders)
!but we're adding a 1.000 value to the beginning and end so we skip those. we can only do <nhpr> number of reads!
do i=nvpr+1,2,-1
   read (1,*) currentRowString
   IF ((i < 24).OR.(i > 140)) THEN
      cycle
   END IF

   !parse single row of digit (& <.>) characters into a vector of floats, at intervals of 10 (reading from format: 6553665536, etc)
   do k=10,(10*nvpr),10
      read(currentRowString(k-9:k),*) currentRowRealVector(k/10)
   end do

   !now we have our porosity values, corresponding to which pixel index they appear at in each row, so now we store from lowest row to highest, lowest to highest column.
```

```
    !Would be faster but less semantic to do away with this loop and cram storing logic into the one above, but we
won't.
    do j=2,nhpr+1
        txtporval(i,j) = currentRowRealVector(j-1)!porosity value read from .txt file
    end do
end do

write (*,'(a)') 'Input the file name used to distinguish reservoir from rock' !*passed to a subprogram. a is an array of
characters
read (*,*) filename !this will be the .txt file with values processed from radiograph in visual studio

m_filename=index(filename,' ')-1 !!!Enter; STBspw


open (2,file = trim(filename(:m_filename))//'.txt',status='old',form='formatted',access='sequential')!open file stated
above
write (*,*) 'opening ', filename(:m_filename), ' for processing'

!allocate an extra pixel at the top, bottom, left, and right for the min3p half cell boundary
allocate (greyscale(nhpr+2,nvpr+2))

!this is for reading each number in a given row so we don't allocate extra space... border does not exist on image.
allocate (currentRowRealVector2(nhpr))

!populate the entire matrix with gsv of 65536 to start, that will be the default value on the borders.
do i=1,nhpr+2
    do j=1,nvpr+2
        greyscale(i,j) = 65536 !this value is the default greyscale value for borders/margin (must be changed for every
file)
    end do
end do

!we're iterating over the vertical dimension of greyscale array, which is 2 greater than pixel number (half cell borders)
!but we're adding a 65536 value to the beginning and end so we skip those. we can only do <nhpr> number of reads!
do i=nvpr+1,2,-1
    read (2,*) currentRowString2
     IF ((i < 24).OR.(i > 140)) THEN
```

```
      cycle
   END IF

   !parse single row of digits (& <.>) characters into a vector of floats, at intervals of 10 (reading from format:
0.0000.000, etc)
   do k=10,(10*nvpr),10
      read(currentRowString2(k-9:k),*) currentRowRealVector2(k/10)
   end do

   !now we have our greyscale values, corresponding to which pixel index they appear at in each row, so now we
store.
   !Would be faster but less semantic to do away with this loop and cram storing logic into the one above, but we
won't.
   do j=2,nhpr+1
      greyscale(i,j) = currentRowRealVector2(j-1)!porosity value read from .txt file (other files will read greyscale)
   end do
end do

!now we write to a new or existing .por file of the same name
open(11,file=(porfilename)//'.por',status='unknown',form='formatted')

write(11,'(a)') 'title = "dataset stb120, por"'
write(11,'(150a)') 'variables = "x", "y", "z", "porosity"'
write(11,'(a)') 'zone t= "T-j, initial", i = 163, j = 163, k = 1, f=point'

nxcvm = nhpr+2 !number of model control volumes x-dimension is equal to radiography number of horizontal pixels
plus 2 half cells
nzcvm = nvpr+2 !number of model control volumes z-dimension is equal to radiography number of vertical pixels plus
2 half cells

mxl = hlr+plr!total length in x dimension (m) !!!plus one hpl to add a half cell on both sides of model grid
mzl = vlr+plr!total length in z dimension (m) !!!plus one vpl to add a half cell on top and bottom of model grid

write (*,*) 'Hello, your min3p xmax value is ',mxl
write (*,*) 'and your min3p zmax value is ',mzl
write (*,*) 'The number of control volumes in the x direction is ',nxcvm
write (*,*) 'The number of control volumes in the z direction is ',nzcvm
```

```
write (*,*) 'The rest you will have to figure out yourself!'

do i=1,nzcvm
   z = (i-1)*plr !this (i-1) term indicates where the reading starts and increases; from 0
   y=0
   do j=1,nxcvm
      porosity = txtporval(i,j) !!replaces whatever porosity is for a given txtporval value with a real number
      tortuosity = greyscale(i,j) !!replaces whatever porosity is for a given txtporval value with a real number
      x = (j-1)*plr !this (i-1) term indicates where the reading starts and increases; from 0
      write (11,"(ES13.7)", advance='no') x
      write (11, "(a3)", advance='no') ''
      write (11,"(ES13.7)", advance='no') y
      write (11, "(a3)", advance='no') ''
      write (11,"(ES13.7)", advance='no') z
      write (11, "(a3)", advance='no') ''
       IF (((i <= 123).AND.(i >= 36).AND.(j <= 95)).AND.(porosity <= 0.06))  THEN
         write (11,"(ES13.7)") unaltpor
       ELSE IF (((i >= 140).AND.(i <= 24)).OR.(tortuosity >= 40000))  THEN
         write (11,"(ES13.7)") respor
       Else
         write (11,"(ES13.7)") porosity
       END IF
   end do
end do

write (*,*)
write (*,*) 'Your porosity file is now ready - Good luck!'
write (*,*)

write (*,'(a)') 'Processing complete!'
write (*,'(a)') 'Goodbye!'

end program porosity_file_generator
```

Tortuosity File: STB120.tor

```
program tortuosity_file_generator !use file 1.STBspw, 2.STBporosity2732
implicit none
```

```
integer nhpr !number of columns
integer nvpr !number of rows
integer file
character junk !character data type,
character*72 :: filename !character string data type, character holds a string of n characters
character*1610 :: currentRowString !this character number be x (x is number of characters in each digit) times the
number of horizontal pixels (find a way to allocate memory? Put in a subroutine?)
character*1610 :: currentRowString2 !this character number be x (x is number of characters in each digit) times the
number of horizontal pixels (find a way to allocate memory? Put in a subroutine?)
real, allocatable :: currentRowRealVector(:) !temporaraly storing floats in here between currentRowString and
greyscale matrix
real, allocatable :: currentRowRealVector2(:) !temporaraly storing floats in here between currentRowString and
greyscale matrix
real, allocatable :: greyscale(:,:)!real;approximation of a real number
real, allocatable :: txtporval(:,:)!real;approximation of a real number
integer l_filename
integer m_filename
real plr !pixel length radiography
real hlr !length of x dimension in radiograph
real vlr !length of y dimension in radiograph
real mxl !model x-dimension length
real mzl !model z-dimension length
integer nxcvm !number of control volumes in x dimension
integer nzcvm !number of control volumes in y dimension
real z, y, x, torgsv, torpor, restor,oxtor, untor, max_gsv, tau
character*4 :: tauFormatString, postTauFormatString
character*6 :: torfilename
character*12 :: tauOutputString
character*1 :: tauDigits, deltaTauDigits
integer :: i, j, k, xValue,yValue, n
restor = 1.0000000E+00
oxtor = 8.0500000E-02
untor = 3.0500000E-04

max_gsv = 65537 !maximum gsv
tau = 0.0
torfilename = 'STB120'
```

```
write (*,'(a)') 'Welcome to ARRMCo'
write (*,'(a)') 'The AAMGP Radiography to MIN3P Converter'

write (*,'(a)') 'Input the file name used to distinguish reservoir from rock' !*passed to a subprogram. a is an array of
characters
read (*,*) filename !this will be the .txt file with values processed from radiograph in visual studio

l_filename=index(filename,' ')-1 !!!Enter; STBspw


open (1,file = trim(filename(:l_filename))//'.txt',status='old',form='formatted',access='sequential')!open file stated above
write (*,*) 'opening ', filename(:l_filename), ' for processing'

write (*,*) 'What is the overall horizontal length of your radiograph in meters?' !ex:0.114925
read (*,*) hlr
write (*,*) 'Input the number of horizontal pixels in your radiograph;' !ex:161
read (*,*) nhpr

write (*,*) 'What is the overall vertical length of your radiograph in meters?' !ex:0.114925
read (*,*) vlr
write (*,*) 'Input the number of vertical pixels in your radiograph;' !ex:161
read (*,*) nvpr

write (*,*) 'What is the overall pixel length of your radiograph pixels in meters?' !ex:0.00071382
read (*,*) plr

write (*,*) nhpr,' columns!'
write (*,*) nvpr,' rows!'

!allocate an extra pixel at the top, bottom, left, and right for the min3p half cell boundary
allocate (greyscale(nhpr+2,nvpr+2))

!this is for reading each number in a given row so we don't allocate extra space... border does not exist on image.
allocate (currentRowRealVector(nhpr))

!populate the entire matrix with gsv of 65536 to start, that will be the default value on the borders.
```

```
do i=1,nhpr+2
   do j=1,nvpr+2
      greyscale(i,j) = 65536 !this value is the default greyscale value for borders/margin (must be changed for every
file)
   end do
end do

!we're iterating over the vertical dimension of greyscale array, which is 2 greater than pixel number (half cell borders)
!but we're adding a 65536 value to the beginning and end so we skip those. we can only do <nhpr> number of reads!
do i=nvpr+1,2,-1
   read (1,*) currentRowString
   IF ((i < 24).OR.(i > 140)) THEN
      cycle
   END IF

   !parse single row of digits (& <.>) characters into a vector of floats, at intervals of 10 (reading from format:
0.0000.000, etc)
   do k=10,(10*nvpr),10
      read(currentRowString(k-9:k),*) currentRowRealVector(k/10)
   end do

   !now we have our greyscale values, corresponding to which pixel index they appear at in each row, so now we
store.
   !Would be faster but less semantic to do away with this loop and cram storing logic into the one above, but we
won't.
   do j=2,nhpr+1
      greyscale(i,j) = currentRowRealVector(j-1)!gsv read from .txt file
   end do
end do

write (*,'(a)') 'Input the image J porosity file name' !*passed to a subprogram. a is an array of characters
read (*,*) filename !this will be the .txt file with values processed from radiograph in visual studio

m_filename=index(filename,' ')-1 !!!Enter; STBporosity2732
```

```
open (2,file = trim(filename(:m_filename))//'.txt',status='old',form='formatted',access='sequential')!open file stated above
write (*,*) 'opening ', filename(:m_filename), ' for processing'

!allocate an extra pixel at the top, bottom, left, and right for the min3p half cell boundary
allocate (txtporval(nhpr+2,nvpr+2))

!this is for reading each number in a given row so we don't allocate extra space... border does not exist on image.
allocate (currentRowRealVector2(nhpr))

!populate the entire matrix with porosity values of 1.000 to start, that will be the default value on the borders.
do i=1,nhpr+2
   do j=1,nvpr+2
      txtporval(i,j) = 1.000 !this value is the default greyscale value for borders/margin (must be changed for every file)
   end do
end do

!we're iterating over the vertical dimension of greyscale array, which is 2 greater than pixel number (half cell borders)
!but we're adding a 1.000 value to the beginning and end so we skip those. we can only do <nhpr> number of reads!
do i=nvpr+1,2,-1
   read (2,*) currentRowString2
   IF ((i < 24).OR.(i > 140)) THEN
      cycle
   END IF

   !parse single row of digits (& <.>) characters into a vector of floats, at intervals of 10 (reading from format: 0.0000.000, etc)
   do k=10,(10*nvpr),10
      read(currentRowString2(k-9:k),*) currentRowRealVector2(k/10)
   end do

   !now we have our porosity values, corresponding to which pixel index they appear at in each row, so now we store.
   !Would be faster but less semantic to do away with this loop and cram storing logic into the one above, but we won't.
   do j=2,nhpr+1
      txtporval(i,j) = currentRowRealVector2(j-1)!porosity value read from .txt file
   end do
```

```
end do

!now we write to a new or existing .tor file of the same name
open(11,file=(torfilename)//'.tor',status='unknown',form='formatted')

write(11,'(a)') 'title = "dataset stb120, tor"'
write(11,'(150a)') 'variables = "x", "y", "z", "tortuosity"'
write(11,'(a)') 'zone t= "T-j, initial", i = 163, j = 163, k = 1, f=point'

nxcvm = nhpr+2 !number of model control volumes x-dimension is equal to radiography number of horizontal pixels
plus 2 half cells
nzcvm = nvpr+2 !number of model control volumes z-dimension is equal to radiography number of vertical pixels plus
2 half cells

mxl = hlr+plr!total length in x dimension (m) !!!plus one hpl to add a half cell on both sides of model grid
mzl = vlr+plr!total length in z dimension (m) !!!plus one vpl to add a half cell on top and bottom of model grid

write (*,*) 'Hello, your min3p xmax value is ',mxl
write (*,*) 'and your min3p zmax value is ',mzl
write (*,*) 'The number of control volumes in the x direction is ',nxcvm
write (*,*) 'The number of control volumes in the z direction is ',nzcvm
write (*,*) 'The rest you will have to figure out yourself!'

do i=1,nzcvm
   z = (i-1)*plr !this (i-1) term indicates where the reading starts and increases; from 0
   y=0
   do j=1,nxcvm
      torgsv = greyscale(i,j) !!this replaces greyscale floats with real numbers
      torpor = txtporval(i,j) !!this replaces greyscale floats with real numbers
      x = (j-1)*plr !this (i-1) term indicates where the reading starts and increases; from 0
      write (11,"(ES13.7)", advance='no') x
      write (11, "(a3)", advance='no') ''
      write (11,"(ES13.7)", advance='no') y
      write (11, "(a3)", advance='no') ''
      write (11,"(ES13.7)", advance='no') z
      write (11, "(a3)", advance='no') ''
      IF (((i <= 123).AND.(i >= 36).AND.(j <= 95)).AND.(torpor <= 0.06))  THEN
```

```
        write (11,"(ES13.7)") untor
      ELSE IF (torgsv >= 40000) THEN
        write (11,"(ES13.7)") restor
      ELSE
        write (11,"(ES13.7)") oxtor
      END IF
   end do
end do

write (*,*)
write (*,*) 'Your tortuosity model input file is now ready - Good luck!'
write (*,*)

write (*,'(a)') 'Processing complete!'
write (*,'(a)') 'Goodbye!'

end program tortuosity_file_generator
```

PEST Instruction File: STB120.ins

```
program PESTinstruction_file_generator !use file; STB120
implicit none
integer file
character junk !character data type,
character*72 :: filename !character string data type, character holds a string of n characters
character*13 :: tplval!value from 4th column in .tpl file
integer l_filename
real line, con, cont, prev, line2
character*13 :: conc
character*6 :: insfilename
character*4 ::  conFormatString, postconFormatString, lineFormatString, postlineFormatString
character*12 ::  conOutputstring, lineOutputstring
character*1 ::  conDigits, deltaconDigits, lineDigits, deltalineDigits
integer :: k, n, eof
real x, y, z, x1, x1a, z1, z1a, x2, x2a, z2, z2a, x3, x3a, z3, z3a, x4, x4a, z4, z4a, x5, x5a, z5, z5a, x6, x6a, z6, z6a
con = 0.0
```

```
line = 4.0
insfilename = 'STB120'
prev = 0.0

x1 = 1.5704039E-02
x1a = 1.7131679E-02
z1 = 8.6372219E-02
z1a = 9.5651880E-02
x2 = 7.9234019E-02
x2a = 8.0661662E-02
z2 = 6.4243801E-02
z2a = 8.2803115E-02
x3 = 8.6372219E-02
x3a = 1.0921445E-01
z3 = 5.0681219E-02
z3a = 5.2108858E-02
x4 = 6.9954358E-02
x4a = 7.1382001E-02
z4 = 2.1414600E-02
z4a = 3.8546279E-02
x5 = 2.2128420E-02
x5a = 2.3556059E-02
z5 = 1.9273140E-02
z5a = 2.4983700E-02

write (*,'(a)') 'Welcome to ARRMCo'
write (*,'(a)') 'The AAMGP Radiography to MIN3P Converter'

write (*,'(a)') 'Input the name of the template file you have generated for this time series "samplenamehour"' !*passed
to a subprogram. a is an array of characters
read (*,*) filename !this will be the .tpl file with values processed from c.co file & .otr file in visual studio & excel

l_filename=index(filename,' ')-1 !!!Enter; STB120.tpl

open (1,file = trim(filename(:l_filename))//'.tpl',status='old',form='formatted',access='sequential')!open file stated above
write (*,*) 'opening ', filename(:l_filename), ' for processing'
```

```
!now we write to a new or existing .ins file of the same name
open(11,file=(insfilename)//'.ins',status='unknown',form='formatted')

!Here the code skips to the 4th column and reads if the string has a $ as the first character
write(11,'(a)') 'pif $'

!read ptf (pest template file (.tpl)) file to 5th line where values reside
read (1,*)
read (1,*)
read (1,*)
read (1,*)

10  line = line+1
   read (1, '(ES13.7,3x,ES13.7,3x,ES13.7,3x,a13)', iostat=eof) x, y, z, tplval
! section of interest 1
   IF ((x >= x1).AND.(x <= x1a).AND.(z >= z1).AND.(z <= z1a)) THEN
      line2 = line - prev
      write(lineDigits, "(I1)") int(log10(line2))+1 !starts at 0+1 stored in space
      write(deltalineDigits, "(I1)") 6 - int(log10(line2))+1 !6 spaces minus amount of spaces above
      write (lineOutputString, "(I"//lineDigits//")") int(line2) !amount of digits line is ex 1
      lineFormatString = "(a"//lineDigits//")" !
      postlineFormatstring = "(a"//deltalineDigits//")"
      write (11, "(a1)", advance='no') 'l'
      write (11, lineFormatString, advance='no') lineoutputstring
      write (11, postlineFormatString, advance='no') ''
      write (11, "(a3)", advance='no') ''
      write (11,"(a)", advance='no') "!dum!   !dum!   !dum!"
      write (11, "(a3)", advance='no') ''
      con = con + 1
      write(conDigits, "(I1)") int(log10(con))+1
      write(deltaconDigits, "(I1)") 6 - int(log10(con))+1
      write (conOutputString, "(I"//conDigits//")") int(con)
      conFormatString = "(a"//conDigits//")"
      postconFormatstring = "(a"//deltaconDigits//")"
      write (11, "(a4)", advance='no') '!con'
      write (11, conFormatString, advance='no') conOutputString
      write (11, "(a1)") '!'
```

```
      prev = 0 + line
      go to 10
! section of interest 2
   ELSE IF ((x >= x2).AND.(x <= x2a).AND.(z >= z2).AND.(z <= z2a)) THEN
      line2 = line - prev
      write(lineDigits, "(I1)") int(log10(line2))+1 !starts at 0+1 stored in space
      write(deltalineDigits, "(I1)") 6 - int(log10(line2))+1 !6 spaces minus amount of spaces above
      write (lineOutputString, "(I"//lineDigits//")") int(line2) !amount of digits line is ex 1
      lineFormatString = "(a"//lineDigits//")" !
      postlineFormatstring = "(a"//deltalineDigits//")"
      write (11, "(a1)", advance='no') 'l'
      write (11, lineFormatString, advance='no') lineoutputstring
      write (11, postlineFormatString, advance='no') ''
      write (11, "(a3)", advance='no') ''
      write (11,"(a)", advance='no') "!dum!   !dum!   !dum!"
      write (11, "(a3)", advance='no') ''
      con = con + 1
      write(conDigits, "(I1)") int(log10(con))+1
      write(deltaconDigits, "(I1)") 6 - int(log10(con))+1
      write (conOutputString, "(I"//conDigits//")") int(con)
      conFormatString = "(a"//conDigits//")"
      postconFormatstring = "(a"//deltaconDigits//")"
      write (11, "(a4)", advance='no') '!con'
      write (11, conFormatString, advance='no') conOutputString
      write (11, "(a1)") '!'
      prev = 0 + line
      go to 10
! section of interest 3
   ELSE IF ((x >= x3).AND.(x <= x3a).AND.(z >= z3).AND.(z <= z3a)) THEN
      line2 = line - prev
      write(lineDigits, "(I1)") int(log10(line2))+1 !starts at 0+1 stored in space
      write(deltalineDigits, "(I1)") 6 - int(log10(line2))+1 !6 spaces minus amount of spaces above
      write (lineOutputString, "(I"//lineDigits//")") int(line2) !amount of digits line is ex 1
      lineFormatString = "(a"//lineDigits//")" !
      postlineFormatstring = "(a"//deltalineDigits//")"
      write (11, "(a1)", advance='no') 'l'
      write (11, lineFormatString, advance='no') lineoutputstring
```

```
      write (11, postlineFormatString, advance='no') ''
      write (11, "(a3)", advance='no') ''
      write (11,"(a)", advance='no') "!dum!   !dum!   !dum!"
      write (11, "(a3)", advance='no') ''
      con = con + 1
      write(conDigits, "(I1)") int(log10(con))+1
      write(deltaconDigits, "(I1)") 6 - int(log10(con))+1
      write (conOutputString, "(I"//conDigits//")") int(con)
      conFormatString = "(a"//conDigits//")"
      postconFormatstring = "(a"//deltaconDigits//")"
      write (11, "(a4)", advance='no') '!con'
      write (11, conFormatString, advance='no') conOutputString
      write (11, "(a1)") '!'
      prev = 0 + line
      go to 10
! section of interest 4
    ELSE IF ((x >= x4).AND.(x <= x4a).AND.(z >= z4).AND.(z <= z4a)) THEN
      line2 = line - prev
      write(lineDigits, "(I1)") int(log10(line2))+1 !starts at 0+1 stored in space
      write(deltalineDigits, "(I1)") 6 - int(log10(line2))+1 !6 spaces minus amount of spaces above
      write (lineOutputString, "(I"//lineDigits//")") int(line2) !amount of digits line is ex 1
      lineFormatString = "(a"//lineDigits//")" !
      postlineFormatstring = "(a"//deltalineDigits//")"
      write (11, "(a1)", advance='no') 'l'
      write (11, lineFormatString, advance='no') lineoutputstring
      write (11, postlineFormatString, advance='no') ''
      write (11, "(a3)", advance='no') ''
      write (11,"(a)", advance='no') "!dum!   !dum!   !dum!"
      write (11, "(a3)", advance='no') ''
      con = con + 1
      write(conDigits, "(I1)") int(log10(con))+1
      write(deltaconDigits, "(I1)") 6 - int(log10(con))+1
      write (conOutputString, "(I"//conDigits//")") int(con)
      conFormatString = "(a"//conDigits//")"
      postconFormatstring = "(a"//deltaconDigits//")"
      write (11, "(a4)", advance='no') '!con'
      write (11, conFormatString, advance='no') conOutputString
```

```
        write (11, "(a1)") '!'
        prev = 0 + line
        go to 10
! section of interest 5
    ELSE IF ((x >= x5).AND.(x <= x5a).AND.(z >= z5).AND.(z <= z5a)) THEN
        line2 = line - prev
        write(lineDigits, "(I1)") int(log10(line2))+1 !starts at 0+1 stored in space
        write(deltalineDigits, "(I1)") 6 - int(log10(line2))+1 !6 spaces minus amount of spaces above
        write (lineOutputString, "(I"//lineDigits//")") int(line2) !amount of digits line is ex 1
        lineFormatString = "(a"//lineDigits//")" !
        postlineFormatstring = "(a"//deltalineDigits//")"
        write (11, "(a1)", advance='no') 'l'
        write (11, lineFormatString, advance='no') lineoutputstring
        write (11, postlineFormatString, advance='no') ''
        write (11, "(a3)", advance='no') ''
        write (11,"(a)", advance='no') "!dum!   !dum!   !dum!"
        write (11, "(a3)", advance='no') ''
        con = con + 1
        write(conDigits, "(I1)") int(log10(con))+1
        write(deltaconDigits, "(I1)") 6 - int(log10(con))+1
        write (conOutputString, "(I"//conDigits//")") int(con)
        conFormatString = "(a"//conDigits//")"
        postconFormatstring = "(a"//deltaconDigits//")"
        write (11, "(a4)", advance='no') '!con'
        write (11, conFormatString, advance='no') conOutputString
        write (11, "(a1)") '!'
        prev = 0 + line
        go to 10
    ELSE IF (tplval /= '6.5336000E+04') THEN
        go to 10
    ELSE !!!MUST WRITE '6.5535000E+04' at last value in .tpl file
        go to 20
    END IF

20 write (11, '(a)') 'endd'

write (*,*)
```

```
write (*,*) 'Your PEST instruction file is now ready - Good luck!'

write (*,'(a)') 'Processing complete!'
write (*,'(a)') 'Goodbye!'

end program PESTinstruction_file_generator
```

PEST Control File: STB120.pst

```
program PESTcontrol_file_generator !use 1.stb120ff.tpl 2; c.co120aa
implicit none
integer file
character junk !character data type,
character*72 :: filename !character string data type, character holds a string of n characters
character*6 :: pcffilename !character string data type, character holds a string of n characters
character*1610 :: currentRowString !this character number be x (x is number of characters in each digit) times the
number of horizontal pixels (find a way to allocate memory? Put in a subroutine?)
character*1610 :: currentRowString2 !this character number be x (x is number of characters in each digit) times the
number of horizontal pixels (find a way to allocate memory? Put in a subroutine?)
real, allocatable :: currentRowRealVector(:) !temporaraly storing floats in here between currentRowString and
greyscale matrix
real, allocatable :: currentRowRealVector2(:) !temporaraly storing floats in here between currentRowString and
greyscale matrix
real, allocatable :: greyscale(:,:)!real;approximation of a real number
real, allocatable :: txtporval(:,:)!real;approximation of a real number
integer l_filename, m_filename, k_filename
real plr !pixel length radiography
real hlr !length of x dimension in radiograph
real vlr !length of y dimension in radiograph
real mxl !model x-dimension length
real mzl !model z-dimension length
integer nxcvm !number of control volumes in x dimension
integer nzcvm !number of control volumes in y dimension
integer nhpr !number of columns
integer nvpr !number of rows
integer :: i, j, k, xValue,yValue, n
real x, z, y, line, con, con_, cco, tau, tau_
real  torpor, restor,oxtor, untor, max_gsv, tau2
```

```
real x1, x1a, z1, z1a, x2, x2a, z2, z2a, x3, x3a, z3, z3a, x4, x4a, z4, z4a, x5, x5a, z5, z5a, x6, x6a, z6, z6a
character*4 ::  conFormatString, postconFormatString, tauFormatString, posttauFormatString, con_FormatString, &
postcon_FormatString, tau_FormatString, posttau_FormatString
character*12 ::  conOutputstring, tauOutputstring, con_Outputstring, tau_Outputstring
character*1 ::  conDigits, deltaconDigits, tauDigits, deltatauDigits, con_Digits, deltacon_Digits, tau_Digits,
deltatau_Digits, l
character*13 ::  tplval
integer :: m, eof
con = 0.0
tau = 0.0
pcffilename = 'STB120'

x1 = 1.5704039E-02
x1a = 1.7131679E-02
z1 = 8.6372219E-02
z1a = 9.5651880E-02
x2 = 7.9234019E-02
x2a = 8.0661662E-02
z2 = 6.4243801E-02
z2a = 8.2803115E-02
x3 = 8.6372219E-02
x3a = 1.0921445E-01
z3 = 5.0681219E-02
z3a = 5.2108858E-02
x4 = 6.9954358E-02
x4a = 7.1382001E-02
z4 = 2.1414600E-02
z4a = 3.8546279E-02
x5 = 2.2128420E-02
x5a = 2.3556059E-02
z5 = 1.9273140E-02
z5a = 2.4983700E-02

write (*,'(a)') 'Welcome to ARRMCo'
write (*,'(a)') 'The AAMGP Radiography to MIN3P Converter'
```

```
write (*,'(a)') 'Input the file name used to distinguish reservoir from rock' !*passed to a subprogram. a is an array of characters
read (*,*) filename !this will be the .txt file with values processed from radiograph in visual studio

l_filename=index(filename,' ')-1 !!!Enter; STB120ff.tpl


open (1,file = trim(filename(:l_filename))//'.tpl',status='old',form='formatted',access='sequential')!open file stated above
write (*,*) 'opening ', filename(:l_filename), ' for processing'


!now we write to a new or existing .pcf file of the same name
open(11,file=(pcffilename)//'.pst',status='unknown',form='formatted')

! write pcf input parameters up to line 13
write(11,'(a)') 'pcf'
write(11,'(a)') '* control data'
write(11,'(a)') 'norestart   estimation'
write(11,'(a)') 'NPAR   NOBS   1   0   1'
write(11,'(a)') '1   1   single   point   1   0   0'
write(11,'(a)') '10.0   2.0   0.3   0.01   10'
write(11,'(a)') '5.0   5.0   0.05'
write(11,'(a)') '0.1'
write(11,'(a)') '30   0.005   4   3   0.01   3'
write(11,'(a)') ' 0   0   0'
write(11,'(a)') '* parameter groups'
write(11,'(a)') 'tau   relative   0.015   0.0   switch   2.0   best_fit'
write(11,'(a)') '* parameter data'

!read the .tpl file to 5th line where x,y,z,tor statements reside
   read (1,*)
   read (1,*)
   read (1,*)
   read (1,*)

10  read (1, '(ES13.7,3x,ES13.7,3x,ES13.7,3x,a13)', iostat=eof) x, y, z, tplval
   IF  (tplval(1:4) == '$tau') THEN
```

```
        tau = tau+1
        write(tauDigits, "(I1)") int(log10(tau))+1
        write(deltatauDigits, "(I1)") 6 - int(log10(tau))
        write (tauOutputString, "(I"//tauDigits//")") int(tau)
        tauFormatString = "(a"//tauDigits//")"
        posttauFormatstring = "(a"//deltatauDigits//")"
        write (11, "(a3)", advance='no') 'tau'
        write (11, tauFormatString, advance='no') tauOutputString
        write (11, "(a3)", advance='no') ''
        write (11,'(a)') 'log factor 8.04e-2   1.0e-06   1.0e-0  tau 1.0 0.0 1'
        go to 10
    ELSE IF (tplval == '3.0499999E-04') THEN
        go to 10
    ELSE IF (tplval == '8.0499999E-02') THEN
        go to 10
    ELSE IF (tplval == '1.0000000E+00') THEN
        go to 10
    ELSE IF (tplval == '6.5336000E+04') THEN
        go to 15
15  END IF

    write(11,'(a)') '* observation groups'
    write(11,'(a)') 'obvsgp'
    write(11,'(a)') '* observation data'

    write (*,'(a)') 'Input the name of the relative concentration_hour "c.co120aa" file that has been created by PEST for
the PEST control file' !*passed to a subprogram. a is an array of characters
    read (*,*) filename !this will be the .txt file with c.co radiograph values processed

    m_filename=index(filename,' ')-1 !!!Enter; c.co120aa

    open (2,file = trim(filename(:m_filename))//'.txt',status='old',form='formatted',access='sequential')!open file stated
above
    write (*,*) 'opening ', filename(:m_filename), ' for processing'

    !read .pft file to 5th line where tau staements reside in the .ins file
    read (2,*)
```

```
   read (2,*)
   read (2,*)
   read (2,*)

20  read (2, '(ES13.7,3x,ES13.7,3x,ES13.7,3x,ES13.7)', iostat=eof) x, y, z, cco
!Section1
IF  (((x >= x1).AND.(x <= x1a).AND.(z >= z1).AND.(z <= z1a))) THEN
      con = con+1
      write(conDigits, "(I1)") int(log10(con))+1
      write(deltaconDigits, "(I1)") 6 - int(log10(con))
      write (conOutputString, "(I"//conDigits//")") int(con)
      conFormatString = "(a"//conDigits//")"
      postconFormatstring = "(a"//deltaconDigits//")"
      write (11, "(a3)", advance='no') 'con'
      write (11, conFormatString, advance='no') conOutputString
      write (11, "(a3)", advance='no') ''
      write (11,"(ES13.7)", advance='no') cco/2
      write (11, "(a3)", advance='no') ''
      write (11,'(a)') '1.0   obvsgp'
      go to 20
!Section2
   ELSE IF(((x >= x2).AND.(x <= x2a).AND.(z >= z2).AND.(z <= z2a))) THEN
      con = con+1
      write(conDigits, "(I1)") int(log10(con))+1
      write(deltaconDigits, "(I1)") 6 - int(log10(con))
      write (conOutputString, "(I"//conDigits//")") int(con)
      conFormatString = "(a"//conDigits//")"
      postconFormatstring = "(a"//deltaconDigits//")"
      write (11, "(a3)", advance='no') 'con'
      write (11, conFormatString, advance='no') conOutputString
      write (11, "(a3)", advance='no') ''
      write (11,"(ES13.7)", advance='no') cco/2
      write (11, "(a3)", advance='no') ''
      write (11,'(a)') '1.0   obvsgp'
      go to 20
!Section3
   ELSE IF(((x >= x3).AND.(x <= x3a).AND.(z >= z3).AND.(z <= z3a))) THEN
```

```
        con = con+1
        write(conDigits, "(I1)") int(log10(con))+1
        write(deltaconDigits, "(I1)") 6 - int(log10(con))
        write (conOutputString, "(I"//conDigits//")") int(con)
        conFormatString = "(a"//conDigits//")"
        postconFormatstring = "(a"//deltaconDigits//")"
        write (11, "(a3)", advance='no') 'con'
        write (11, conFormatString, advance='no') conOutputString
        write (11, "(a3)", advance='no') ''
        write (11,"(ES13.7)", advance='no') cco/2
        write (11, "(a3)", advance='no') ''
        write (11,'(a)') '1.0   obvsgp'
        go to 20
!Section4
    ELSE IF(((x >= x4).AND.(x <= x4a).AND.(z >= z4).AND.(z <= z4a))) THEN
        con = con+1
        write(conDigits, "(I1)") int(log10(con))+1
        write(deltaconDigits, "(I1)") 6 - int(log10(con))
        write (conOutputString, "(I"//conDigits//")") int(con)
        conFormatString = "(a"//conDigits//")"
        postconFormatstring = "(a"//deltaconDigits//")"
        write (11, "(a3)", advance='no') 'con'
        write (11, conFormatString, advance='no') conOutputString
        write (11, "(a3)", advance='no') ''
        write (11,"(ES13.7)", advance='no') cco/2
        write (11, "(a3)", advance='no') ''
        write (11,'(a)') '1.0   obvsgp'
        go to 20
!Section5
    ELSE IF(((x >= x5).AND.(x <= x5a).AND.(z >= z5).AND.(z <= z5a))) THEN
        con = con+1
        write(conDigits, "(I1)") int(log10(con))+1
        write(deltaconDigits, "(I1)") 6 - int(log10(con))
        write (conOutputString, "(I"//conDigits//")") int(con)
        conFormatString = "(a"//conDigits//")"
        postconFormatstring = "(a"//deltaconDigits//")"
        write (11, "(a3)", advance='no') 'con'
```

```
        write (11, conFormatString, advance='no') conOutputString
        write (11, "(a3)", advance='no') ''
        write (11,"(ES13.7)", advance='no') cco/2
        write (11, "(a3)", advance='no') ''
        write (11,'(a)') '1.0   obvsgp'
        go to 20
    ELSE IF (cco /= 6.5336000E+04) THEN
        go to 20
    ELSE
        go to 30
30  END IF

write(11,'(a)') '* model command line'
write(11,'(a)') 'MIN3P_THCm_x64d_seq.exe < STB120.inp'
write(11,'(a)') '* model input/output'
write(11,'(a)') 'STB120.tpl   STB120.tor'
write(11,'(a)') 'STB120.ins   STB120_2.gst'

write (*,*)
write (*,*) 'Your PEST control file is now ready - Good luck with MIN3P & PEST!'
write (*,'(a)') 'Go through the PEST control file you have generated and enter the appropriate NPAR and NOBS
values & tau & con statements'

write (*,'(a)') 'Processing complete!'
write (*,'(a)') 'Goodbye!'

end program PESTcontrol_file_generator
```

D_P distribution in image J format – Step 1 Tortuosity (τf)output formatting

```
program PESTcontrol_file_generator !use 1.stb120modeloutputtor
implicit none
integer file
character junk !character data type,
character*72 :: filename !character string data type, character holds a string of n characters
character*8 :: Dpfilename !character string data type, character holds a string of n characters
integer l_filename, m_filename
integer :: i, j, k, xValue,yValue, n
```

```
real x, z, y, torval, porval, torval2, zero, tormax
real  torpor, restor,oxtor, untor, max_gsv, tau2
integer :: m, eof
zero = 0.0000000E+00
tormax = 6.5336000E+04

Dpfilename = 'STB120preppedmodeloutputtor'

write (*,'(a)') 'Welcome to ARRMCo'
write (*,'(a)') 'The AAMGP Radiography to MIN3P Converter'

write (*,'(a)') 'Input the filename holding final tortuosity values' !*passed to a subprogram. a is an array of characters
read (*,*) filename !this will be the .txt file with values processed from radiograph in visual studio

l_filename=index(filename,' ')-1 !!!Enter; STB120modeloutputtor


open (1,file = trim(filename(:l_filename))//'.tor',status='old',form='formatted',access='sequential')!open file stated
above
write (*,*) 'opening ', filename(:l_filename), ' for processing'


!now we write to a new or existing .txt file of the same name
open(11,file=(Dpfilename)//'.txt',status='unknown',form='formatted')

!header that is MIN3P formatted
write(11,'(a)') 'Prepped model output tor values'
write(11,'(a)') 'title = stb120'
write(11,'(150a)') 'variables = "x", "y", "z", "preppedmodeloutputtor"'
write(11,'(a)') 'zone t= "T-j, initial", i = 163, j = 163, k = 1, f=point'

!read .tor file to 4th line where x,y,z,tor statements reside
   read (1,*)
   read (1,*)
   read (1,*)

10  read (1, '(ES13.7,3x,ES13.7,3x,ES13.7,3x,ES13.7)', iostat=eof) x, y, z, torval
```

```
   IF (torval == 6.5336000E+04) THEN
    write (11,"(ES13.7,3x,ES13.7,3x,ES13.7,3x,ES13.7)") x, y, z, tormax
      go to 15
   ELSE IF (torval == 3.0499999E-04) THEN
      write (11,"(ES13.7,3x,ES13.7,3x,ES13.7,3x,ES13.7)") x, y, z, zero
      go to 10
   ELSE IF (torval == 8.0499999E-02) THEN
       write (11,"(ES13.7,3x,ES13.7,3x,ES13.7,3x,ES13.7)") x, y, z, zero
      go to 10
   ELSE IF (torval == 1.0000000E+00) THEN
       write (11,"(ES13.7,3x,ES13.7,3x,ES13.7,3x,ES13.7)") x, y, z, zero
      go to 10
   ELSE
       write (11,"(ES13.7,3x,ES13.7,3x,ES13.7,3x,ES13.7)") x, y, z, torval
      go to 10
15  END IF

write (*,*)
write (*,*) 'Your processed MIN3P .txt file is now ready - Good luck with MIN3P & PEST!'
write (*,'(a)') 'Next, run the STB120Dp2.f90 file to create array of Dp values in MIN3p format'

write (*,'(a)') 'Processing complete!'
write (*,'(a)') 'Goodbye!'

end program PESTcontrol_file_generator
```

D_P distribution in image J format – Step 2 Calculating D_P values

```
program PESTcontrol_file_generator !use 1; STB120preppedmodeloutputtor
implicit none
integer file
character junk !character data type,
character*72 :: filename !character string data type, character holds a string of n characters
character*9 :: Dpffilename !character string data type, character holds a string of n characters
integer l_filename, m_filename
integer :: i, j, k, xValue,yValue, n
real x, z, y, torval, porval, torval2, zero, Dl, dpmax
real  torpor, restor,oxtor, untor, max_gsv, tau2
```

```
integer :: m, eof
zero = 0.0000000E+00
DI = 0.00000000188
dpmax = 6.5336000E+04

Dpffilename = 'STB120PESTdp'

write (*,'(a)') 'Welcome to ARRMCo'
write (*,'(a)') 'The AAMGP Radiography to MIN3P Converter'

write (*,'(a)') 'Input the filename containing porosity values in fpoint format' !*passed to a subprogram. a is an array of
characters
read (*,*) filename !this will be the .love file with c.co radiograph values processed

m_filename=index(filename,' ')-1 !!!Enter; STB120preppedmodeloutputtor

open (2,file = trim(filename(:m_filename))//'.txt',status='old',form='formatted',access='sequential')!open file stated
above
write (*,*) 'opening ', filename(:m_filename), ' for processing'

!now we write to a new or existing .txt file of the same name
open(11,file=(Dpffilename)//'.txt',status='unknown',form='formatted')

!header that is tecplot formatted
write(11,'(a)') 'Final Dp values-MIN3P formatted'
write(11,'(a)') 'title = stb120'
write(11,'(150a)') 'variables = "x", "y", "z", "PESTDp"'
write(11,'(a)') 'zone t= "T-j, initial", i = 163, j = 163, k = 1, f=point'

  !read .txt file to 5th line where tau staements reside in the .ins file
  read (2,*)
  read (2,*)
  read (2,*)
  read (2,*)

20  read (2, '(ES13.7,3x,ES13.7,3x,ES13.7,3x,ES13.7)', iostat=eof) x, y, z, torval2
  IF (torval2 == 6.5336000E+04) THEN
```

```
      write (11,"(ES13.7,3x,ES13.7,3x,ES13.7,3x,ES13.7)") x, y, z, dpmax
      go to 30
   ELSE IF (torval2 == 0.0000000E+00) THEN
      write (11,"(ES13.7,3x,ES13.7,3x,ES13.7,3x,ES13.7)") x, y, z, zero
      go to 20
   ELSE
      write (11,"(ES13.7,3x,ES13.7,3x,ES13.7,3x,ES13.7)") x, y, z, (torval2 * DI)
      go to 20
30  END IF


write (*,*)
write (*,*) 'Your .txt file with Dp values in MIN3p format is now ready - Good luck with MIN3P & PEST!'
write (*,'(a)') 'Next, run the STB120txttotiffdp.f90 file to create array of Dp values in a format Image J can read create
a .tiff with'

write (*,'(a)') 'Processing complete!'
write (*,'(a)') 'Goodbye!'

end program PESTcontrol_file_generator
```

D_P distribution in image J format – Step 3 Formatting D_P values

```
program PESTcontrol_file_generator !use 1.STB120PESTdp
implicit none
integer file
character junk !character data type,
character*72 :: filename !character string data type, character holds a string of n characters
character*10 :: Dpfilename !character string data type, character holds a string of n characters
integer l_filename, m_filename
integer :: i, j, k, xValue,yValue, n
real x, z, y, torval, porval, torval2, zero, demax, dpval
real  torpor, restor,oxtor, untor, max_gsv, tau2
integer :: m, eof
zero = 0.0000000E+00
demax = 6.5336000E+04
```

```
Dpfilename = 'STB120PESTdpf'

write (*,'(a)') 'Welcome to ARRMCo'
write (*,'(a)') 'The AAMGP Radiography to MIN3P Converter'

write (*,'(a)') 'Input the filename holding final tortuosity values' !*passed to a subprogram. a is an array of characters
read (*,*) filename !this will be the .txt file with values processed from radiograph in visual studio

l_filename=index(filename,' ')-1 !!!Enter; STB120PESTdp


open (1,file = trim(filename(:l_filename))//'.txt',status='old',form='formatted',access='sequential')!open file stated above
write (*,*) 'opening ', filename(:l_filename), ' for processing'


!now we write to a new or existing .txt file of the same name
open(11,file=(Dpfilename)//'.txt',status='unknown',form='formatted')

!read .txt file to 5th line where x,y,z,tor statements reside
   read (1,*)
   read (1,*)
   read (1,*)
   read (1,*)

10  read (1, '(ES13.7,3x,ES13.7,3x,ES13.7,3x,ES13.7)', iostat=eof) x, y, z, dpval
   IF (dpval == 6.5336000E+04) THEN
    write (11,"(ES13.7)") zero
      go to 15
   ELSE IF (x /= 1.1563884E-01) THEN
      write (11,"(ES13.7,3x)", advance='no') dpval
      go to 10
   ELSE IF (x == 1.1563884E-01) THEN
       write (11,"(ES13.7,3x)", advance='yes') dpval
       go to 10
15  END IF

write (*,*)
```

```
write (*,*) 'Your .txt file with Dp values in grid (imageJ ready) format is now ready - Good luck with MIN3P & PEST!'
write (*,'(a)') 'Next, creat a .tiff in imageJ and proceed with anaylsing the data'


write (*,'(a)') 'Processing complete!'
write (*,'(a)') 'Goodbye!'


end program PESTcontrol_file_generator
```